Ida Ådnebergli

Effects of Supersaturation Build-Up on the Crystal Properties and Filtration Performance of an Aromatic Amine

Master's thesis in Chemical Engineering and Biotechnology
Supervisor: Seniz Ucar
Co-supervisor: Torfinn Håland
June 2021

Master's thesis

NTNU
Norwegian University of Science and Technology
Faculty of Natural Sciences
Department of Chemical Engineering

NTNU
Norwegian University of
Science and Technology

Ida Ådnebergli

Effects of Supersaturation Build-Up on the Crystal Properties and Filtration Performance of an Aromatic Amine

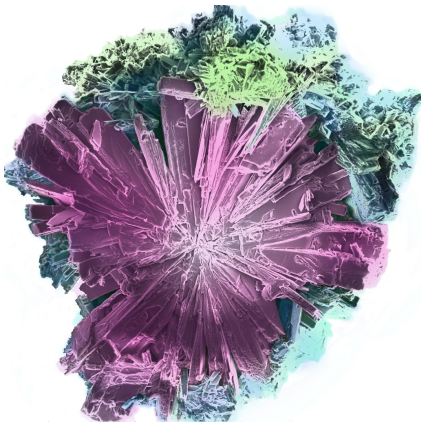

Master's thesis in Chemical Engineering and Biotechnology
Supervisor: Seniz Ucar
Co-supervisor: Torfinn Håland
June 2021

Norwegian University of Science and Technology
Faculty of Natural Sciences
Department of Chemical Engineering

NTNU
Norwegian University of
Science and Technology

Abstract

The manufacture of active pharmaceutical ingredients (APIs) in the pharmaceutical industry is often achieved by crystallization and subsequent filtration process, where the filtration process is commonly referred to as the major process bottleneck. This thesis comprises a study of crystallization of an aromatic amine (AA), which is an intermediate in the manufacturing of the X-ray contrast agent iohexol. The crystallization process was carried out as a neutralization reaction by acid addition followed by cooling crystallization in both synthetic and real process systems. The aim was to vary the supersaturation build-up by different acid addition procedures and investigate the accompanying effect on filtration performance and final crystal characteristics. Experiments with single-step, multi-step and continuous addition of the acid were conducted from the synthetic system, and single-step and continuous addition of the acid experiments were performed from the real process system. Highly crystalline and pure precipitates of AA was established, verified by XRD and FTIR analyses for both systems, and HPLC analysis for real process system. Additionally, the precipitates gave high yields and fast filtration rates, indicating robust crystallization systems. Filtration experiments showed similar trends in synthetic and real process systems where semi-batch experiments resulted in improved filterability, and continuous addition of the acid experiments offered the best results. Furthermore, size data showed the same trends where precipitates from continuous addition of the acid experiments resulted in higher sedimentation velocities, hence, larger particles. Investigations of the particle morphology via LM and SEM imaging revealed differences in particle populations produced via different acid addition procedures. The difference in the establishment of supersaturation profiles for the acid addition procedures was explained by theoretical supersaturation profiles. In experiments via single-step addition of the acid an onset of precipitation occur, due to high initial supersaturation levels and high initial nucleation rates, resulting in smaller particles. In multi-step experiments, the supersaturation is gradually built up by the addition of acid in portions, and point towards growth-dominated mechanisms with additional nucleation mechanisms, resulting in wider size distribution. In continuous addition of the acid experiments, a more smooth supply of acid is

added to the system at a lower supersaturation level, without shocking the system and growth-dominated crystallization was presumed, resulting in larger particles.

From observing similar trends in both systems in terms of filtration performance, size analysis, and similarities in structures, it was concluded that the synthetic system is a good representation of the real process system. Investigations in this thesis pointed out that semi-batch crystallization systems yield better filtration results and should be selected to minimize energy consumption in the filtration process.

Sammendrag

Produksjonen av aktive farmasøytiske ingredienser i farmasøytisk industri oppnås ofte ved krystallisering og påfølgende filtreringsprosess, der filtreringsprosessen vanligvis blir ansett som den viktigste prosessflaskehalsen. Denne oppgaven omfatter studier angående krystallisering av et aromatisk amin (AA), som er et mellomprodukt i fremstillingen av røntgenkontrastmidlet iohexol. Krystalliseringssprosessen ble utført som en nøytraliseringsreaksjon ved syretilsetning, etterfulgt av avkjølings krystallisering i både et syntetisk og reelt prosessystem. Målet var å variere oppbygning av overmetningen ved forskjellige syretilsetnings prosedyrer, og undersøke den medfølgende effekten på filtreringsytelse og endelige krystallegenskaper. Eksperimenter med enkelttrinns, flertrinns og kontinuerlig tilsetning av syren ble utført fra det syntetiske systemet. Eksperimenter med enkelttrinns og kontinuerlig tilsetning av syren ble utført fra det reelle prosess systemet. Høyt krystallinske og rene produkter av AA ble etablert, bekreftet av XRD- og FTIR-analyser for begge systemene, og HPLC-analyser for det reelle prosessystemet. I tillegg ga utfellingene høye utbytter og raske filtreringshastigheter, som indikerer robuste krystalliseringssystemer. Filtreringseksperimenter viste lignende trender i det syntetiske og reelle prosessystemet, der semi-batch eksperimenter resulterte i forbedret filtrerbarhet, og eksperimenter med kontinuerlig tilsetning av syren ga de beste resultatene. Videre viste størrelsesdata de samme trendene der produktet fra eksperimenter med kontinuerlige tilsetning av syren ga høyere sedimenteringshastigheter, derav større partikler. Undersøkelser av partikkelmorfologien via LM- og SEM-avbildning avslørte forskjeller i partikkelpopulasjoner produsert via forskjellige syretilsetnings prosedyrer. Forskjellene i etablering av overmettingsprofiler for syretilsetnings prosedyrene ble forklart med teoretiske overmettingsprofiler. I eksperimenter med enkelttrinns tilsetning av syren oppstår bunnfall grunnet høye innledende overmettningsnivåer og høye innledende nukleeringshastigheter, som resulterer i mindre partikler. I eksperimenter med flertrinns tilsetning av syren blir overmetningen gradvis etablert ved tilsetning av syre i porsjoner, og peker mot vekst dominerende mekanismer med ytterligere nukleerings mekanismer, som resulterer i bredere størrelsesfordeling. I eksperimenter med kontinuerlige tilsetning av syren er det en jevnere tilførsel av syre til systemet

ved et lavere overmettningsnivå, uten å sjokkere systemet, og en vekst dominert krystallisering ble antatt, som resulterer i større partikler.

Fra observasjoner av like trender i begge systemene relatert til filtreringsytelse, størrelsesanalyser og likheter i strukturer ble det konkludert at det syntetiske systemet er en god representasjon for det reelle prosessystemet. Undersøkelser i denne oppgaven påpekte at semi-batch krystalliseringssystemer gir bedre filtreringsresultater og bør velges for å minimere energiforbruket i filtreringsprosessen.

Preface

This master thesis was written in spring 2021 within the specialization Environmental Engineering and Reactor Technology at the Department of Chemical Engineering. It is a cooperation project between NTNU and GE Healthcare AS Lindesnes, where the research topic and objective is related to the industrial production of active pharmaceutical ingredients. The laboratory and research work was mostly conducted at the Department of Chemical Engineering at NTNU, experiments were also carried out on-site at Lindesnes.

I would like to give a special thanks to my supervisor Seniz Ucar. I appreciate your patience, motivating words, and scientific and experimental discussions and guidance throughout the thesis. I am grateful for the opportunity given to me by GE Healthcare Lindesnes to work on this project. Thanks to my co-supervisors from GE Healthcare Lindesnes, for your interest in my work and help on-site; Torfinn Håland, Arne Askildsen, and Inger Dagny Saanum. Thanks to the people that trained me in different characterization apparatus, specially Zeshaan Ali, for guidance with LUMiSizer. I am thankful to my classmates at K4-230, for lots of fun and Monday meetings. The love and support from my friends and family have also meant a lot. And of course, my roommates in "Nonna", that always cheer on me.

I, Ida Ådnebergli, hereby declare that this is independent work according to the exam regulations of the Norwegian University of Science and Technology.

Trondheim, June 14, 2021

Table of Contents

1 Background **1**

2 Introduction **1**

3 Theory **5**

3.1 Fundamentals 5

3.1.1 Supersaturation 5

3.1.2 Nucleation 7

3.1.3 Crystal Growth 9

3.2 Crystallization in the Pharmaceutical Industry 11

3.2.1 Considerations for Enhanced Systems 11

3.2.2 Reactive Crystallization and Neutralization Reactions 12

3.2.3 Cooling Crystallization 13

3.3 Filtration 14

3.3.1 Particle and Liquid Properties 14

3.3.2 Compressible Filter Cake Formation 16

3.3.3 Pressure Filtration and Filterability 16

4 Experimental **19**

4.1 Chemicals 19

4.2 Experimental Design 21

4.2.1 Synthetic Solution Setup 21

4.2.2 Real Process Solution Setup 22

4.3 Crystallization from Synthetic Solution 24
4.3.1 Dissolution of AA in Solvent 24
4.3.2 Neutralization and Cooling Crystallization 25
4.3.3 Pressure Filtration 26
4.4 Crystallization from Real Process Solution 27
4.4.1 Synthesis Steps 27
4.4.2 Neutralization and Cooling Crystallization 28
4.4.3 Pressure Filtration 29
4.5 Characterization Apparatus 29
4.5.1 UV-Vis Spectrophotometry at NTNU 29
4.5.2 UV-Vis Spectrophotometry at GE Healthcare Lindesnes . . . 30
4.5.3 X-ray Powder Diffraction 30
4.5.4 Fourier-Transform Infrared Spectroscopy 31
4.5.5 Scanning Electron Microscopy 31
4.5.6 Light Microscope 31
4.5.7 LUMiSizer 32
4.5.8 High-Performance Liquid Chromatography 34

5 Results and Discussion **35**

5.1 Synthetic Solution Studies 35
5.1.1 Filtration Performance 35
5.1.2 Precipitation of AA via Different Acid Addition Procedures . 37
5.1.3 Supersaturation Profile and Crystal Characteristics 44

5.2 Real Process Solution Studies 47
5.2.1 Filtration Performance 47
5.2.2 Precipitation of AA from RPS via different Acid Addition Procedures 48
5.2.3 Supersaturation Profile and Crystal Characteristics 54
5.3 Comparison of the Synthetic and Real Process System 55
5.3.1 Level of Control in the Systems 56
5.3.2 Filtration Performance and Crystal Characteristics 56
5.3.3 Concluding Remarks 60

6 Conclusion **63**

7 Future Outlooks **65**

Bibliography **66**

A Molar Mass of Compounds **i**

B Calibration Curve for Experiments at NTNU **i**

B.1 Calculations i
B.2 Establishment of Calibration Curve ii
B.3 Concentration of AA in Reaction Solution iii
B.4 Discussion on Uncertainty in Concentration Measurements iv

C Solubility Curve and Reaction Time of Neutrtralization Reaction of AA **v**

C.1 Discussion on Solubility Curve of AA v

C.2 Reaction Time of Neutralization Reaction of AA vii

D FTIR Analysis viii

E Calculation of Moisture Content ix

F Calculation of Yield x

G Filtration Experiments and Calculations of Specific Filter Cake Resistance x

H LUMiSizer xiv

H.1 Analyses from Suspension of AA xiv

H.2 LUMiSizer Analysis for Each Experiment xvi

H.3 LUMiSizer - Analysis Summary xviii

I Additional SEM Images xxiii

J Additional LM Images xxvii

K HPLC Analyses of RPS Studies xxviii

L In-situ Images with EasyViewer xxix

List of Symbols and Abbreviations

Table 1: An overview of the symbols used with associated unit and description.

Symbol	Unit	Description
A	cm^2	Filter area
Abs	nm	Absorbance
c	g/cm^3	Solids concentration
c	mol/L	Solution concentration
c*	mol/L	Solubility concentration
d	-	Dilution factor
h	cm	Height of filter cake
M	wt%	Moisture content
Mm	g/mol	Molar mass
m	g	Mass
m_s	g	Mass of dry cake
n	mol	Mol
p	Pa	Applied pressure
p_0	Pa	Atmospheric pressure
R	s/cm^3	Filter medium resistance
R^2	-	Coefficient of determination
S	-	Supersaturation ratio
s	-	Mass fraction of solids in suspension
T	°C	Temperature
t	s	Time
V	m^3	Volume
Y	%	Yield

Table 2: An overview of the Greek symbols used with associated unit and description.

Symbol	Unit	Description
α	s/cm^6	Specific cake resistance
ϵ	1/cm	Porosity
μ	mPas	Viscosity
ρ_l	g/cm^3	Density of filtrate
ρ_s	g/cm^3	Density of solid in suspension

Table 3: An overview of the abbreviations used.

AA	Aromatic amine
API	Active pharmaceutical ingredient
CSD	Crystal size distribution
FTIR	Fourier transform infrared
HPLC	High-performance liquid chromatography
LM	Light microscope
PAT	Process analytical technology
RPS	Real process solution
SEM	Scanning electron microscopy
SOP	Standard operating procedure
SS	Synthetic solution
UV-Vis	Ultraviolet-visible
XRD	X-ray powder diffraction

1 Background

GE Healthcare AS Lindesnes manufacture active pharmaceutical ingredients (APIs); X-ray contrast agents to be used in contrast media in X-ray imaging. The factory holds 40% of the world's use of contrast agents, and every second there are three patients all over the world being examined with products from GE Healthcare Lindesnes. The industrial production of contrast agents contains several syntheses and crystallization steps, followed by downstream processes like filtration, washing, and drying. The efficiency of these downstream processes is highly dependent on the final crystal properties like crystal purity, crystal size, crystal size distribution (CSD), and morphology.

Recently, investigations have been initiated for developing a new crystallization process of an aromatic amine, which is an intermediate in the manufacturing of the X-ray contrast agent iohexol. Crystallization of the product is carried out as a neutralization reaction with the addition of acid in a methanol-water solvent medium, and subsequent cooling crystallization. Investigations should be conducted to understand the crystallization step for further optimization and control, aiming to obtain a high yield process with crystals that are easy to handle during filtration and drying.

2 Introduction

Crystallization is regarded as one of the most important separation and purification unit operations throughout the history of the pharmaceutical industry and is used in the manufacture cascade of active pharmaceutical ingredients. There is a high demand for a continuous supply of APIs of high and reproducible quality. This requires an efficient and robust crystallization process to meet time and supply constraints, as well as scalability from laboratory to industrial production and limitation of batch-to-batch variations throughout all phases of drug development [1, 2]. Therefore, the main objective of industrial crystallization processes is to produce a controlled population of crystals in terms of structure, habits, crystal size, and crystal size

distribution. Understanding the fundamentals of supersaturation, nucleation, and growth rates play a decisive role in determining the final crystal properties [3]. These characteristics influence downstream processes like filtration, washing, and drying, and problems associated with these operations are often considered as the major bottleneck in the industrial crystallization operations [4].

Crystallization is often followed by filtration, which is used to separate the product crystals from the mother liquor. Changes in crystal shape and variations in size and crystal size distribution due to changes in initial supersaturation, temperature, and mixing conditions in crystallization processes will affect the filterability in the subsequent filtration process. For example, crystals with a narrow size distribution, large crystal size, and spherical morphology are often advantageous in these terms [4]. The specific cake resistance is often used as a measure to characterize the filterability of crystal suspensions [5].

Most commonly, industrial-scale pharmaceutical crystallization is performed in batch reactors and carried out as cooling, evaporation of the solvent, the addition of antisolvent, or by reactive crystallization [6]. Batch crystallization may also include semi-batch systems, where the difference between the two mentioned is that in a batch crystallizer the feed is added at time zero, while in a semi-batch unit, one or more feed streams is added during the time course of a round. Semi-batch systems serve a variety of operating modes, for example, the feed can be added in portions or continuously during the crystallization. The product is removed, for both cases, at a determined endpoint [7]. Research upon these batch systems is well developed, but there are still significant issues connected to batch-to-batch variability.

More rigorous requirements for improved efficiency and properties of drugs have started a shift in recent years for pharmaceutical manufacturing, from batch to continuous processes [2]. Examples of continuous systems are suspension mixed product removal (MSMPR) and plug flow reactors, these systems are beneficial in terms of economics, control, and reproducibility [8]. The main differences between batch and continuous processes are continuity and yield. Continuous crystallization processes tend to give consistent product thanks to operating at steady-state and uninterrupted production. On the other hand, it is difficult to obtain as high yields

as in a batch system which can go to an equilibrium state [2].

Along with these considerations, an ongoing research project is established at GE Healthcare AS Lindesnes, regarding X-ray contrast agent production. The presented work is a part of this initiative and focuses on providing knowledge concerning important crystallization conditions to obtain an effective and controlled production. Investigations on the crystallization process of aromatic amine as a function of supersaturation build-up with resulting crystal properties should be carried out in order to evaluate its accompanying effect on the subsequent filtration process.

3 Theory

3.1 Fundamentals

Crystallization operations offer strategies to obtain and separate high-purity products, and the objective of industrial crystallization is to produce crystals with controlled properties. In order to control the products of crystallization operations, understanding the fundamentals of crystal formation becomes crucial. The predominant factor that regulates crystallization reactions is supersaturation, which defines the thermodynamic driving force for crystallization and affects the final crystal properties. [6, 9, 10].

3.1.1 Supersaturation

A solution in thermodynamic equilibrium with a solid phase, at a given temperature, is saturated. The required amount of solute to reach this saturated solution is defined as the solubility concentration or the equilibrium concentration, c^*. However, when more solid than the solubility concentration is dissolved, thus exceeding the solubility line, the solution is said to be supersaturated [6, 9]. The state of supersaturation is an essential requirement for all spontaneous crystallization operations, and for industrial applications, it can be defined in terms of concentration differences of a solute between a given state and at equilibrium, as shown in Equation 1 [11]. Supersaturated systems strive to reach equilibrium. In order to do so the supersaturated solution move towards equilibrium by crystallization. Supersaturation value can be used as a quantification of the driving force towards precipitation, and the supersaturation is relieved by a combination of nucleation and crystal growth [12].

$$S = \left(\frac{c}{c^*}\right) > 1. \tag{1}$$

Supersaturation is classified in the metastable zone, where the solution can persist for a time. The metastable zone width is where nucleation and crystal growth occur, thus investigations and the understanding of this zone can reveal the effect of

different factors on the nucleation and crystal growth processes. The metastable zone width is therefore intimately related to the efficiency of industrial crystallization processes and the control of shape and size of final crystalline products, and is often a good choice of a zone to obtain controlled crystallization reactions [13]. In the labile zone, precipitation occurs instantaneously and explains an unstable and supersaturated solution. A third zone is a stable and unsaturated zone, where crystallization is impossible. The relationship between the three terms is schematically explained in a solubility-supersolubility diagram in Figure 1. In the figure, at the starting point A, a saturated solution is achieved by decreasing the temperature to point B. Crystallization will occur when cooling to point C, where the solution is supersaturated. Also, starting from point A, increasing the solution concentration to point D will result in a saturated system, and further reaching point E to a supersaturated system [9].

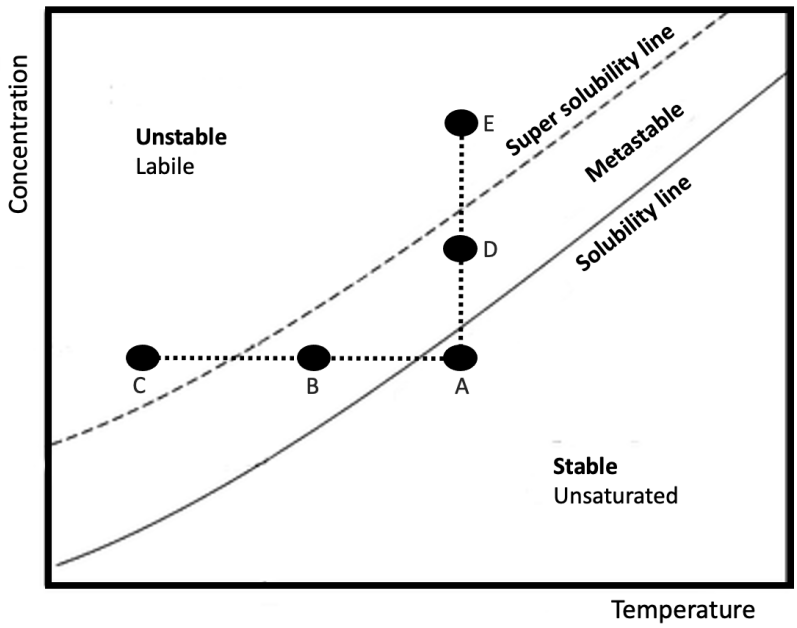

Figure 1: The solubility-supersolubility diagram explained in terms of zones; stable, metastable, and labile zone and with points A, B, C, D, and E explaining the situation when exceeding the solubility and supersolubility lines.

In reactive crystallization, if the system is isothermal and the solvent has a constant composition, supersaturation can be created only as a species is formed by a chemical

reaction. When the system operates as a batch unit, where reactants are added at the beginning of the process, the concentration of the product, c, would typically increase from an initial value of zero. When exceeding c^*, the supersaturation ratio, S, becomes greater than one and the system has a tendency to precipitate and crystallization can begin to occur and proceed as long as the reaction maintains supersaturated [11].

3.1.2 Nucleation

The first step of a crystallization process is nucleation, a phase separation in which new crystals, nuclei, are "born". The formation of nuclei occurs via a dynamic and stochastic association of monomeric units to form larger and larger entities until a stable nucleus is produced. These units exceed a free energy barrier at a critical size, at the metastable limit, and phase separation occurs in the system. The supersaturated solution is at higher free energy than at equilibrium, to relieve this a combination of nucleation and crystal growth arises. The system moves towards an energetically more favorable place, towards equilibrium [9, 11, 14].

Primary nucleation mechanisms refer to the primal formation of nuclei of interest in a system and can be divided into homogeneous and heterogeneous primary nucleation. In homogeneous primary nucleation, nuclei form on their own accord. The occurrence of homogeneous nucleation is rare, however, the basis of several nucleation theories builds on it. The system has to overcome the activation energy barrier for nucleation to occur and to further form stable nuclei. At this point, the nucleus bulk energy balances the energetic costs of creating a surface. In heterogeneous nucleation, the presence of foreign solid surfaces affects the nucleation process. The heterogeneous nucleation may occur at a lower supersaturation than at homogeneous nucleation. This is because a foreign substance gives the availability of a solid surface, which reduces both the interfacial free energy and the activation energy barrier [15].

Seeding is intentionally adding preexisting crystals with desired properties into the system to get the desired product crystals. This is a common controlling practice

and is associated with uncertainties with primary nucleation. This explains a shift from primary to secondary nucleation and is specially used in the industry to increase reproducibility. Secondary nucleation is referred to as any mechanism that involves the presence of crystals in the suspension and uses these parent crystals as a site and source in the generation of new crystals. With parent crystals present in the solution, there already exists a solid-liquid interface, hence secondary nucleation requires less energy thus a lower supersaturation to nucleate compared to primary nucleation [9, 11].

Primary nucleation is typically the dominant mechanism at the beginning of crystal formation when starting with a clear solution in a batch operation. Once a sufficient number of crystals have formed these crystals originating from primary nucleation often grow and then serve as stimuli for secondary nucleation. The supersaturation drop within the metastable regime, and secondary nucleation becomes the dominant mechanism in the formation of nuclei. This is often the case in industrial crystallization processes operating at high crystal slurry density and supersaturation in the metastable zone [16, 17]. This was investigated in the work of Li *et al*, where paracetamol was crystallized from a clear solution in ethanol. Results from careful in situ observation during several cooling crystallization experiments implied that crystals produced in an industrial crystallizer originate all from one single crystal and are formed by secondary nucleation. Results also indicated that this mechanism was not limited to paracetamol but occurred more generally [18]. However, due to the small length and time scales involved in nucleation, the fundamental understanding of crystal nucleation from solution still remains unclear. An overview of the research regarding secondary nucleation and its fundamentals and applications in the past 30 years was written by Xu *et al.* In this paper, the sources of secondary nuclei and mechanisms of secondary nucleation are explained among other things like the secondary nucleation threshold from the perspective of the metastable zone widths associated with nucleation mechanisms [19].

3.1.3 Crystal Growth

The second step of a crystallization process is crystal growth. In this stage, the stable nuclei from the nucleation are to grow larger. The fundamental driving force for both steps is lowering the chemical potential of the system. However, the nucleation step must surpass a higher activation energy barrier than for crystal growth. When a certain amount of nuclei is formed, supersaturation is consumed further by growth. For growth to occur both monomer addition of units on the crystal surfaces and their incorporation into the lattice sites must overcome. This requires two steps; (1) transport, by diffusion or convection, of growth units from the solution to the crystal face, and (2) a surface reaction in which growth units are incorporated into the crystal lattice. The growth can either be diffusion-controlled or reaction-controlled based on their relative rates. Growth scales with supersaturation, temperature, and the characteristics of the solid-liquid interface. These factors cause different growth mechanisms resulting in different morphologies of the final crystals. An illustration of the growth rate as a function of the driving force is presented in Figure 2. The figure consists of spiral growth (A) and 2-dimensional nucleation (B), in which both are reaction-controlled, and rough growth (C) which is diffusion-controlled. Spiral growth and 2D nucleation create well-defined crystals with smooth faces. Dendritic growth is when some parts of the crystal will access a higher driving force and become self-enforcing. The crystal then starts branching in the directions of the higher supersaturation, and monocrystals are produced. The branching mechanism will change to non-crystallographic branching via surface nucleation at even higher supersaturation, which will produce polycrystalline crystals. This mechanism is called spherulitic growth [9, 15, 20]. Spherulite formation mechanism can be formed in two ways depending on where the growth front starts. For the first type the spherulite form via central multidirectional growth and the second form from a single crystal in a folded-chain and develop further to a dumbbell-like structure via unidirectional growth and low angle branching [21, 22].

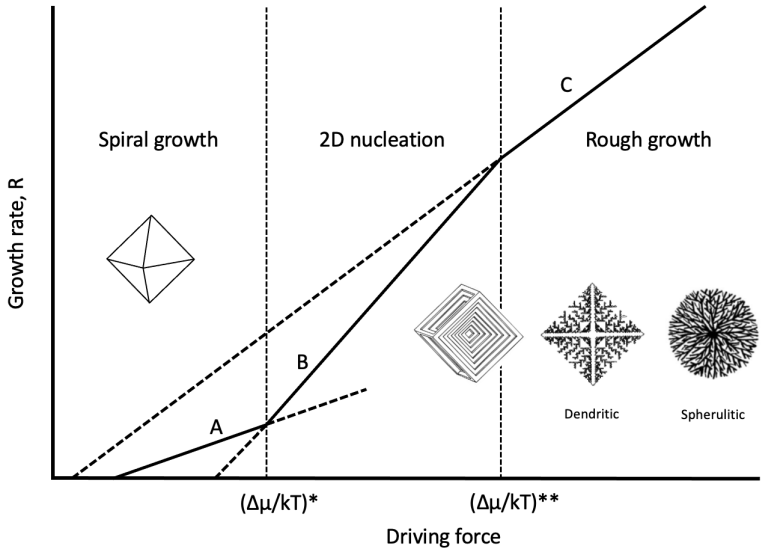

Figure 2: The growth rate as a function of driving force, divided in regions; spiral growth (A), 2D nucleation (B), and rough growth (C).

When two or more particles collide it might result in a permanent attachment via enlargement or growth of the particles together to form one entity. This is a common phenomenon in systems with a high number of particles and high supersaturation [23]. These entities that are formed might be a result of agglomeration or aggregation, which are difficult to distinguish by using visual techniques. In agglomeration, the entities are formed by cementation of individual growth, where a bridge is formed between the particles. Aggregation is a reversible process, where the aggregates contain more loosely bound mixtures of individual particles and agglomerates [7]. It can be difficult to distinguish between particles formed by spherulitic growth and aggregation or agglomeration by visual analysis on the final particles only. However, understanding the growth mechanisms can be of importance in the control of crystal size and morphology in crystallization processes [22].

3.2 Crystallization in the Pharmaceutical Industry

3.2.1 Considerations for Enhanced Systems

Crystallization in the pharmaceutical industry is an important unit operation for manufacturing, separating, and purifying crystalline drug substances. Research upon crystallization processes is often about developing a control scheme of the system, which depends on the nature of the species with its desired characteristics. Different reaction parameters can dictate the final crystal characteristics to varying degrees depending on the system. Crystal characteristics often investigated are for example morphology, crystal size distribution, and purity profile, which can independently or collectively impact the efficiency of the crystallization process and subsequent processes. Therefore, the understanding of these processes, regardless of batch or continuous systems, is key to their control to achieve an optimized and efficient process. However, the issue with these systems is their complex multifactorial being, which requires new technologies to aid in their understanding and to achieve process control. To improve this, advances in the understanding of the crystallization mechanisms and the advent of process analytical technology (PAT) are crucial. PAT is a broad topic with a multidisciplinary nature, but in general, PAT aims to ensure final product quality by monitoring, analyzing, and controlling critical quality and performance attributes during the crystallization process [24, 25, 26]. The development of PAT in recent years is reviewed in the work of Gao and colleagues, including monitoring methods and control strategies and not to mention a summary of commonly used PAT tools with its applications [27]. Several studies analyze reactive crystallization processes using PAT [24, 28, 29].

Another important consideration in the research and development of the pharmaceutical industry is the 2030 Agenda for Sustainable Development with its seventeen Sustainable Development Goals, specifically goal number 9; "build resilient infrastructure, promote inclusive and sustainable industrialization and foster innovation" [30], with emphasis on the sustainable industrialization. Also, the twelve principles of green chemistry and engineering should be considered. The 6^{th} principle of green chemistry underlines the necessity of considerations about energy efficiency;

"energy requirements should be recognized for their environmental and economic impacts and should be minimized" [31]. The 3^{rd} and 4^{th} principle of green engineering are also relevant; "separation and purification operations should be designed to minimize energy consumption and materials use" and "products, processes, and systems should be designed to maximize mass, energy, space, and time efficiency" [32].

3.2.2 Reactive Crystallization and Neutralization Reactions

Reactive crystallization denotes processes, where a chemical reaction generates the driving force that is necessary to produce a crystalline product. A review of the current state and future directions for reactive crystallization is given by the work of McDonald *et al.* In this review, PAT is promoted, this is also seen in the work of Cote *et al*, who gives a brief review of the perspectives on the current state, challenges, and opportunities in pharmaceutical crystallization process development [33].

In the literature, for inorganic systems, the focus of investigation tends to be on specific crystallization phenomenon. For example investigations regarding crystallization kinetics to develop models for nucleation and growth kinetics [34, 35], and/or predict characteristics like size, CSD [36], morphology, and polymorphism [37]. For organic systems equilibrium modification and intermediate isolation are more common areas of investigation. These reactive crystallization reactions are termed neutralization reactions due to the removal of either an acid or a base. In other words, a subset of ionic reactions occurs, that contain either the addition or removal of a proton from a proton-labile functional group such as an amine, acid, or alcohol [11]. Reactive crystallization is widely used in the production of organic crystalline pharmaceuticals. It is a field with significant research throughout history. Yet, there is always room for improvement, and this area of research keeps evolving and diversifying in response to among other things, the rapid development of various analytical and measurement techniques. The aim is often further optimizing the system towards higher yields, energy efficiency, product quality, successful scale-up, etc. [38, 39, 40]. The area of research is wide-ranging due to the diversity of compounds,

and because these systems often are meant to produce intermediates or products in the industry, with the goal to enhance the process for economical reasons. Nevertheless, there exist typical themes and difficulties with such systems. The dynamic behavior of such a system is governed by chemical reaction, nucleation, and crystal growth, which are interrelated to the supersaturation profile. Meaning, supersaturation control has a great impact on crystal properties like CSD and morphology [11]. However, the reaction rate of neutralization reactions is often considered instantaneous [9, 41]. With this, it can be difficult to obtain tight control due to high supersaturation levels. Here, one can manipulate the supersaturation indirectly by varying the reaction rate through the supply of reactants, adjusting pH, adjusting solvent composition, or by adding seed crystals [22, 42, 43, 44, 45]. Fast kinetics and the formation of practically insoluble compounds make the mixing strategy have a remarkable effect on process attributes such as morphology and CSD [3, 46, 47]. In summary, the goal is often to optimize a robust production in terms of desired crystal characteristics, which is usually obtained by supersaturation control via reactant flow rate or addition of seed-crystals [11].

3.2.3 Cooling Crystallization

A cooling crystallization for a batch reactor provides the advantage to control the supersaturation profile easily by controlling the temperature profile. In order to obtain supersaturation and a sufficient yield, it requires the solubility to have a sufficient dependence on temperature. It is a preferred and commonly used option in batch crystallization as it is the most simple and flexible controlled technique [15, 48]. There are multiple studies where the aim is to develop a controlled and optimized cooling crystallization by investigating for example the effect of cooling rates and profiles [49, 50], feed flow rates [51] and seeding strategies [52, 53] and enables controlling final crystal properties [54, 55]. Cooling crystallization is an often utilized mode of crystallization in pharmaceutical production, as for many compounds the solubility decreases with decreasing temperature. Also, there are many APIs that require cooling crystallization due to thermal sensitivity [7, 26, 56].

3.3 Filtration

In the industry, a crystallization operation is often followed by a filtration step, and it is commonly referred to as the major process bottleneck. Therefore, determining the filtration performance is essential to develop an efficient and economically viable filtration process. A filtration process phase separates the slurry, here the crystallized suspension, of a solid and liquid phase. The aim is to recover the solid component, thus the product crystals, from the mother liquor. There are several techniques and equipment available and any system design must consider all stages of the separation process to reduce industrial costs. These stages include pre-treatment, solids concentration, solids separation, and post-treatment. Pre-treatment and solids concentration are applied to get a better filtration performance. The solid separation step involves a filter media, which is the permeable member where the filtrate passes, and on which the filtered solids accumulate. Regarding the filter, the solids can either form a cake on the filter medium, or particles can be captured in the depth of the filter medium. The former mentioned is named cake filtration and is the most common case in industrial filtration processes. Post-treatment includes washing soluble impurities and removal of excess liquid from cake voids to reduce the cake moisture content, and thermal drying as the final stage to remove liquid from the solids that are discharged from a filter as a cake. Another post-treatment is blowing, termed cake deliquoring, which is applied for desaturation of the filter cake and to reduce the moisture content. Here, the filtrate flow ceases, and air flows through the cake void [5, 57].

3.3.1 Particle and Liquid Properties

A completely described solid-liquid system contains the primary properties, the state of the system, and macroscopic properties. Solid and liquid physical properties such as crystal size, particle size distribution, morphology, and surface properties are the primary properties that can be measured independently of the other components of the system. The state of the system includes the porosity or concentration, homogeneity, and the extent of dispersion of the particles. These factors combined

with the primary properties control the macroscopic properties which are measured to investigate the application of a particular separation method. The specific cake resistance, terminal settling velocity, or settling rate of particles in a suspension are examples of macroscopic properties which are of importance when investigating filterability. The crystallization conditions, and thus the operating conditions of the particle production process affect the particle size, crystal size distribution, and shape in the slurry fed to the filtration unit, and can have a profound effect on the characteristics of separation.

Desired crystal properties from a filtration point of view would most commonly be to obtain large, monosized, and spherical crystals. Large crystals minimize the interactions at the particle-liquid interface due to reduced specific surface area and thus particle-liquid interfacial surface area [5]. Fine crystals should be avoided as these might enable bleeding through the filter cloth and contribute significantly to the specific cake resistance, having a slowing effect on filtration rate, washing, and deliquoring, and tend to cause higher moisture contents [58]. Differences in size, CSD, and morphology of calcium carbonate were obtained by variations in temperature, supersaturation, seeding procedure, etc. and their effect on pressure filtration was investigated in the work of Beck and Andreassen. Results revealed that spherical particles with a larger size show better filterability than spheres with wider size distribution. Wider size distribution was due to high supersaturation and nucleation which resulted in higher average cake resistance values [59]. A uniform size or narrow size distribution increases the voidage between the crystals and decreases the tortuosity, thus improve the filterability. Andreassen *et al.* varied the initial supersaturation ratio, temperature, and crystallization time of both L-glutamic acid and an aromatic amine derivative to produce different morphologies and sizes, and investigate its effect on porosity, cake resistance, and compressibility. For this study, it was found that supersaturation should be kept at moderate levels to avoid spherulites explained by high cake resistances associated with their formation [4]. This work shows that spherical shapes might not always give improved filtration performance. Bourcier and colleagues studied cake filterability and compressibility of calcium carbonate and uranium oxalate as a function of the shape and CSD, where the latter had the strongest effect on cake resistance and compressibility [60].

3.3.2 Compressible Filter Cake Formation

Introductory in cake filtration, the particles from the suspension are retained at the surface of the filter medium and are termed surface filtration [61]. Further, the particles deposit on the already deposited particles resulting in filter cake formation. Cake filtration is the most common case of filtration in the industry and can be performed with pressure, vacuum, centrifugal, or gravity operations. Filter cakes that are quite insensitive to an increase in applied pressure to the surface of the cake are said to be incrompessible. On the other hand, when the permeability of the cake is dependent on the applied pressure, the filter cake is said to be compressible. The occurrence of incrompessible or compressible cakes depends on the physicochemical properties of the particles and liquids forming the suspension. In several filtration operations, the case is often more complex, non-uniform, compressible cakes rather than uniform and incompressible ones. However, the basic laws that govern the flow of liquids through these more simple beds develop the basis for these more complex cakes [5].

3.3.3 Pressure Filtration and Filterability

The performance of pressure filtration is evaluated by the filterability of the system which can be described by the specific cake resistance, α. For estimations of α and filter resistance, R, when the pressure is kept constant Equation 2 can be used [5]. This equation has been derived under several assumptions which are of importance for understanding its limitations. The assumptions are; (a) the pressure difference is assumed kept constant during the filtration process, (b) the feed suspension is assumed to be constant with no sedimentation, (c) the liquid is assumed to flow through the incompressible cake in a laminar way, (d) all particles are assumed to deposit on the surface of the filter cloth or the top of the developing cake [59]. Also, there is a probability of filter medium compression and particle penetration into its pores causing increased resistance. Despite this, (e) the medium resistance is

assumed to remain constant during filtration [5].

$$\frac{t - t_0}{V - V_0} = \frac{\alpha c \mu}{2A^2 \Delta p} V + \frac{\mu R}{A \Delta p} \tag{2}$$

The pressure difference, Δp, is the difference between the applied pressure to the system, p, and the atmospheric pressure, p_0. The filtration time, t, and the volume of the filtrate, V, is recorded during a pressure filtration process. μ is the viscosity of the filtrate, A is the area of the filter medium, and c is the solids concentration in the suspension given by,

$$c = \frac{\rho_l}{\frac{1}{s} - \frac{\rho_l}{\rho_s} \frac{\epsilon}{(1-\epsilon)}}, \tag{3}$$

where s is the mass fraction of solids in the feed suspension, ρ_l is the density of the filtrate and ρ_s the density of the solid. The porosity, ϵ, can be calculated from

$$\epsilon = \frac{Ah - \frac{m_s}{\rho_s}}{Ah} \tag{4}$$

where m_s is mass of dry cake and h is the height of the filter cake [5].

4 Experimental

Investigations on the crystallization of aromatic amine (AA) were carried out in two systems as described below:

1. Synthetic model system

   Crystallization experiments at NTNU were conducted from synthetic solutions (SS). The SS was prepared by dissolving the pure product of AA in the solvent of choice with sodium hydroxide. Further, hydrochloric acid was added for crystallizing the aromatic amine.

2. Real process system

   Additional experiments were conducted on-site at GE Healthcare Lindesnes, by using the real process solution (RPS). The RPS was prepared from synthesis steps before the crystallization, and will contain significant amounts of the amine reagent which will be crystallized to AA upon addition of hydrochloric acid. It will also, from synthesis steps contain impurities from side reactions and raw materials.

In both systems, crystallization experiments were performed in batch reactors, followed by pressure filtration. Liquid and solid phases were characterized by different characterization apparatuses to obtain information about the concentration of the suspension, and intermediate and final crystal properties, respectively.

4.1 Chemicals

Synthetic Solution

AA, which is an aromatic amine, was provided from GE Healthcare AS Lindesnes in the form of a white crystalline powder. The organic solvent used consisted of high purity methanol and water in a 95:5vol% ratio. Sodium hydroxide pellets and 3M HCl in methanol (methanolic HCl) were used for the dissolution and recrystallization of AA salt, respectively. Technical grade methanol was used for washing in the

following filtration step, and for redispersion of dry crystals for characterization of samples. Trizma base was used to prepare a 10mM Tris buffer solution of pH 8 that was used for diluting the samples for UV-Vis measurements.

Table 4: An overview of all the chemicals used in the SS experiments.

Chemical	Formula	Supplier	Purity [%]
AA	-	Ge Healthcare Lindesnes	-
Methanol ACS reagent	CH_3OH	Sigma-Aldrich	$\geq$99
Technical Methanol	CH_3OH	VWR Chemicals	$\geq$98.5
Methanolic HCl	HCl	Merck	-
Sodium hydroxide pellets	NaOH	Merck	>99
Trizma base	-	Sigma	$\geq$99.9
Distilled water	H_2O	NTNU	100

Real Process Solution

The real process solution of AA was prepared by GE Healthcare Lindesnes in synthesis steps prior to the crystallization step. The initial methanol-water solvent ratio of the RPS was 92:8vol%. Higher water content compared to the synthetic solution was to prevent precipitation in synthesis steps. The methanol used in the solvent was recovered from the Lindesnes site and was also used for washing in the filtration step. Recovered 35wt% aqueous hydrochloric acid was used in the neutralization crystallization of AA, as methanolic acid was not available. The acid was diluted in methanol to reach the same volume ratio between suspension and total amount of acid as for the synthetic solution. When using aqueous acid diluted in methanol the water content will increase during acid addition, and the final methanol-water solvent ratio resulted in an 89:11vol% in the suspension. This should be kept in mind when comparing results from synthetic and real process systems as a higher water content can affect the supersaturation level in the system. Distilled water was used for UV-Vis sample preparation. All chemicals used in the crystallization experiments are listed in Table 5.

Table 5: An overview of all the chemicals used in the RPS experiments.

Chemical	Formula	Supplier	Purity [%]
AA RPS	-	Ge Healthcare Lindesnes	-
Methanol	CH_3OH	Recovered from GE Healthcare Lindesnes	-
Aqueous HCl	HCl	Recovered from GE Healthcare Lindesnes	35wt
Distilled water	H_2O	GE Healthcare Lindesnes	100

4.2 Experimental Design

The experiments were conducted in batch reactors and filtrated by pressure filtration units for both synthetic and real process solutions. The experimental setups are explained in detail in the sections below.

4.2.1 Synthetic Solution Setup

Batch Reactor Setup

The synthetic solution recrystallization experiments of AA were carried out in a 1L double-jacketed glass reactor, either as batch or semi-batch experiments. The experimental setup used for all experiments are illustrated in Figure 3. The reactor was equipped with two baffles to maintain a homogeneous solution. A mechanical stirrer with a four-bladed propeller of 6cm diameter was used to keep a constant stirring speed. The temperature was controlled by a Julabo F33 refrigerated/heating circulator. The reactor top contained six ports for injection of reactants and removal of products. A condenser was outfitted to one of the ports and was used to prevent the solvent from evaporating to the surroundings and for reflux of potential condensate. For experiments where the acid was added continuously, a Masterflex pump or a Chemyx syringe pump was used and connected via one of the ports. The outlets not used were sealed with plastic stoppers.

Filtration Unit

The filtration process was performed with a 1L BHS Sonthofen pressure filtration unit shown in Figure 4. Temperature control was achieved by a Julabo F33 water bath. Whatman filter papers ashless, with a diameter of 55mm were used as filter media. Constant pressure was achieved by applying nitrogen gas. The weight of filtrate was recorded as a function of time by LabVIEW software.

Figure 3: Batch reactor setup used in the synthetic solution experiments.

Figure 4: 1L BHS Sonthofen pressure filtration setup used for synthetic solution experiments.

4.2.2 Real Process Solution Setup

Batch Reactor Setup

The RPS crystallization experiments of AA were carried out in a 0.5L double-jacketed glass reactor, shown in Figure 5, either as batch or semi-batch experiments. A mechanical stirrer with a three-bladed propeller of 7cm diameter was used to keep a constant stirring speed. The temperature was controlled by a Julabo F25 refrig-

erated/heating circulator. The reactor top contained three ports for injection of reactants and removal of products. A condenser was outfitted to one of the ports and was used to prevent the solvent from evaporating to the surroundings and for reflux of potential condensate. The outlets not used were sealed with glass stoppers. For experiments where the acid was added continuously, a Cole-Parmer dual-syringe infusion/withdrawal pump was used and connected via one of the ports.

Filtration Unit

The filtration process was performed with a 0.35L BHS Sonthofen pressure filtration unit imaged in Figure 6, without temperature control. As the filtration process was performed immediately after the crystallization process was completed and was rapidly done, the final crystals were assumed not to be affected by temperature differences between the slurry and surroundings. Whatman filter papers ashless, with a diameter of 55mm were used as filter media. Constant pressure was achieved by applying nitrogen gas. The weight of filtrate was recorded as a function of time by filming with an iPhone XR.

Figure 5: Batch reactor setup used in the real process solution experiments.

Figure 6: 0.35L BHS Sonthofen pressure filtration setup used for real process solution experiments.

4.3 Crystallization from Synthetic Solution

All experiments performed of SS crystallization consisted of three main steps; dissolution of AA in the solvent, neutralization and cooling crystallization, and pressure filtration. The three main steps were followed by washing, blowing, and drying. The neutralization crystallization was achieved by the addition of acid in different procedures; single-step addition of the acid, multi-step addition of the acid, and continuous addition of the acid. The procedure in its entirety is illustrated in Figure 7.

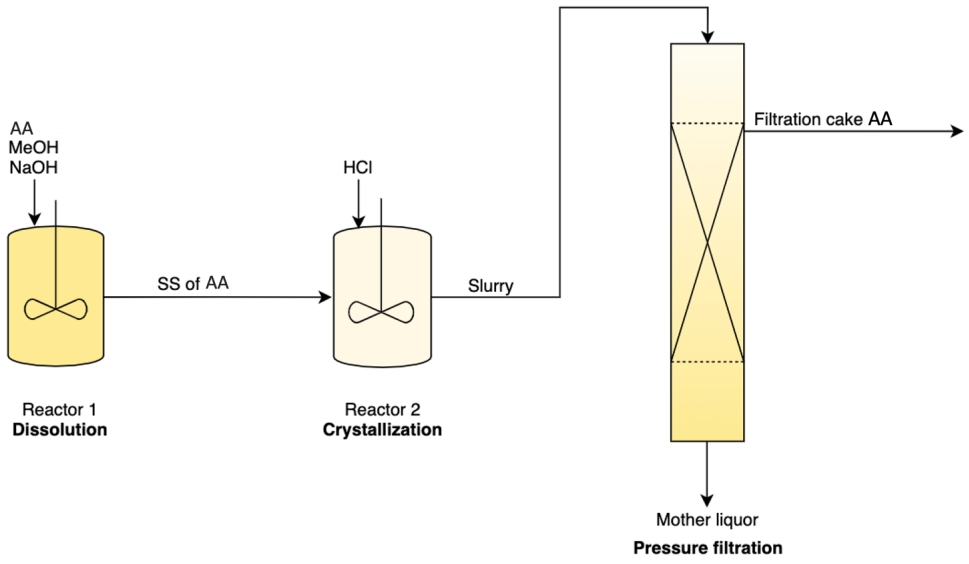

Figure 7: An overall illustration of the synthetic solution (SS) procedure consisting of dissolution of AA, neutralization and cooling crystallization, and pressure filtration.

4.3.1 Dissolution of AA in Solvent

A higher initial concentration is desirable to ensure high yields in the production of AA. However, previous work showed that it is difficult to dissolve all AA in the solvent and reach a higher concentration than 0.3M [20]. The initial goal of SS studies was to modify the preparation procedure to reach a higher concentration. The procedure is explained below and was successfully modified to reach a concentration

of 0.5M, and further used in SS studies.

AA was weighted out with digits 0.0001 to reach a 0.5±0.05M initial concentration. The AA salt and 475mL of methanol were added to reactor 1, 500-700rpm of stirring was applied and the temperature was set to 50°C. 1.2 equivalents sodium hydroxide pellets compared to the concentration of AA were weighed out and dissolved in 25mL water. This basic solution was added to reactor 1 to dissolve the AA and to reach a 95:5vol% ratio of methanol-water solvent. The temperature was further increased to 80°C to dissolve the AA salt and then reduced to 50°C. The pH was measured and the concentration of the dissolved salt was monitored by spectrometric measurements. When the desired concentration was reached at 50°C, the stirring was stopped to let the undissolved solids settle. 350mL of the clear solution was decanted to a volumetric flask to measure the volume, then the clear solution was added to reactor 2 for crystallization, and a sample for concentration measurements was withdrawn.

4.3.2 Neutralization and Cooling Crystallization

The total amount of methanolic hydrochloric acid to reach 100% neutralization, thus 1.2 equivalents compared to the concentration of AA, was prepared. Water was added to the acid to get the same ratio as the solvent; 95:5vol% methanol to water. The reaction crystallization was carried out as a neutralization reaction by adding acid to the solution in one of the three different acid addition procedures explained in the list below, at the fixed values of 50°C and 500rpm. After all the acid was added the suspension was left for 1h, then cooling crystallization was applied by decreasing the temperature to 20°C and left for 1h to reach steady-state. The solubility limits of the neutralization reaction of AA at equivalents of acid together with determination and discussion on 1h reaction time are found in the Appendix, Section C. At the end of the experiments, the pH was measured and the final concentration of the AA salt in the solution was determined by UV-Vis spectrometry.

1. **Single-step Addition of the Acid**

   The experiments were carried out as a single-step addition of the acid, thus as batch experiments. The acid solution was heated to reach 50°C in the Julabo water bath prior to the addition, then added to the suspension in one portion. The suspension was left for 1h after the addition.

2. **Multi-step Addition of the Acid**

   The experiments were carried out as a multi-step addition of the acid, thus as semi-batch experiments. The acid was added in five equal amounted portions and the reaction was left to proceed for 1h after each addition.

3. **Continuous Addition of the Acid**

   The experiments were carried out as continuous addition of the acid, thus as semi-batch experiments. The acid was added continuously by a pump at a fixed feed rate of 0.5mL/min and left for 1h after all acid was added.

4.3.3 Pressure Filtration

Firstly, the filtration unit was tested for leakage, and the desired pressure was established. After reaching steady-state in the crystallization step, pressure filtration was performed at 20°C and Δp = 1bar. The slurry was filtrated in 3x100mL portions to determine porosity and cake height, or as "full rounds", meaning approximately the whole suspension (300ml), in order to calculate the specific cake resistance. The specific cake resistance was calculated according to Equation 2 for each experiment. α were determined by the slope from plotting $\frac{t-t_0}{V-V_0}$ as a function of the filtrate volume, V (explained in detail in Appendix, Section G) [5]. The filter cake was washed with methanol, in a 1:1 volume ratio compared to the filtered suspension, and was blown for 10s per 100mL of suspension. The height of the filter cake was measured from three places to get a more accurate measurement. The moisture content was determined by measuring the weight of the filter cake prior to and after drying at 30°C overnight. The viscosity of the filtrate was assumed to be similar to methanol; 0.59mPas [62]. The density of the filtrate was assumed to be equal for all experiments and was calculated from three repeats by weighing 50mL of filtrate.

4.4 Crystallization from Real Process Solution

All experiments performed with RPS consisted of these main steps; synthesis steps to prepare the real process solution, neutralization and cooling crystallization, and pressure filtration. The neutralization crystallization was achieved by the addition of acid in different procedures; single-step addition of the acid and continuous addition of the acid. The filtration process was followed by washing, blowing, and drying. The overall procedure is illustrated in Figure 8.

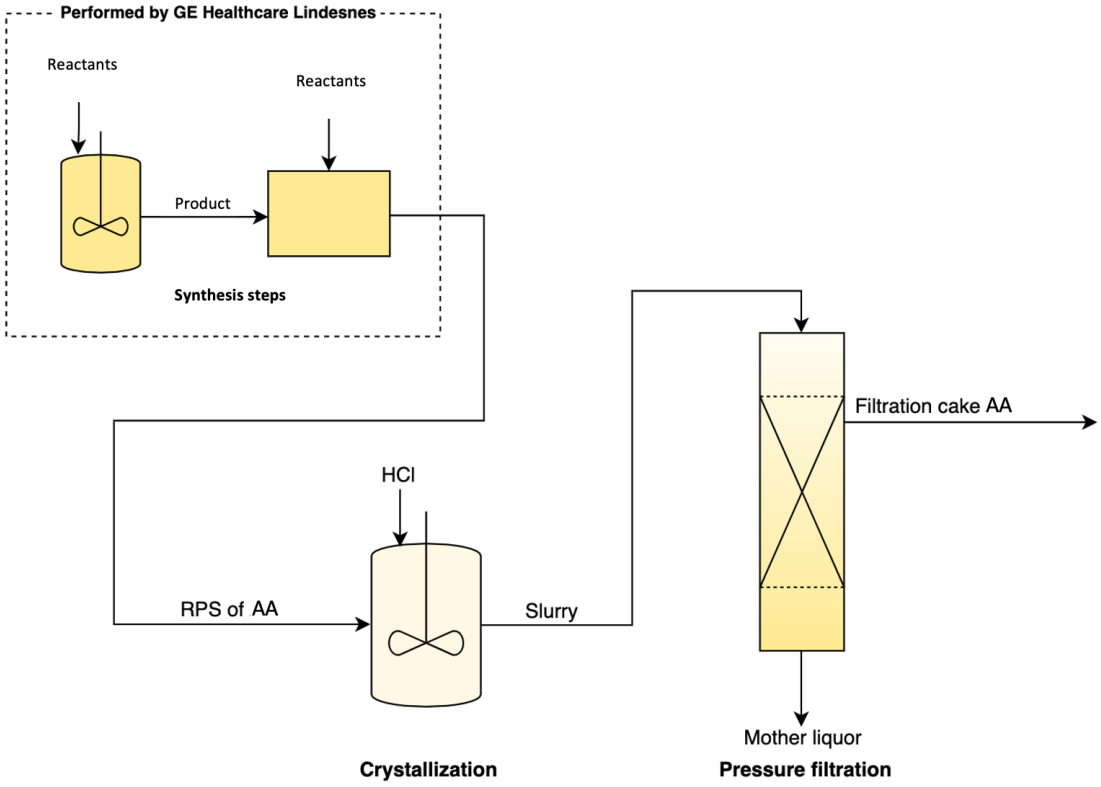

Figure 8: An overall illustration of the real process solution (RPS) procedure, including synthesis steps performed by GE Healthcare Lindesnes, neutralization and cooling crystallization, and pressure filtration.

4.4.1 Synthesis Steps

The real process solution was provided by GE Healthcare Lindesnes and was prepared by synthesis steps prior to crystallization experiments. The most important to notice from the synthesis steps are what is left of raw material and by-products

from side reactions, which constitute impurities in the final precipitate. This is the main difference between the synthetic and real process systems and can affect the final crystal properties.

4.4.2 Neutralization and Cooling Crystallization

The total amount of aqueous hydrochloric acid to reach 100% neutralization, thus 1.2 equivalents compared to the concentration of AA, was prepared. The acid was diluted with methanol to get a similar acid:suspension volume ratio as in SS. The reaction crystallization was carried out as a neutralization reaction by adding acid to the solution in one of the two different acid addition procedures explained in the list below, at the fixed values of 50°C and 500rpm. After all the acid was added the suspension was left for 1h, then cooling crystallization was applied by decreasing the temperature to 20°C and left for 1h to reach steady-state. The pH was measured by pH strips prior to and after crystallization. The initial and final concentration of the AA salt in the solution was determined by UV-Vis spectrometry. High-performance liquid chromatography (HPLC) was used prior to and at the endpoint of crystallization in order to quantify the components in suspension and the purification of the crystallization process.

1. **Single-step Addition of the Acid**

   The experiments were carried out as a single-step addition of the acid, thus as batch experiments, meaning the acid was added in one portion. The suspension was left for 1h after the addition.

2. **Continuous Addition of the Acid**

   The experiments were carried out as continuous addition of the acid, thus as semi-batch experiments. The acid was added continuously by a pump at a fixed feed rate of 0.5mL/min and left for 1h after all acid was added.

4.4.3 Pressure Filtration

Firstly, the filtration unit was tested for leakage, and the desired pressure was established. After reaching steady-state in the crystallization step, pressure filtration was performed at room temperature and $\Delta p = 1$bar. The slurry was filtrated as "full rounds", meaning 200mL suspensions, in order to determine porosity and cake height, and calculate the specific cake resistance. The same method for filtration measurements was performed for the real process solution as for the synthetic solution explained above in Section 4.3.3. The filter cake was further washed with 200mL methanol and blown for 20s. The height of the filter cake was measured from three places to get a more accurate average height. The moisture content was determined by measuring the weight of the filter cake prior to and after drying at 30-40°C overnight. The viscosity of the filtrate was assumed to be similar to methanol; 0.59mPas [62]. The density was calculated from the average of three different experiments with three repeats of each by weighing 50mL of filtrate.

4.5 Characterization Apparatus

Different analysis apparatuses were used for the characterization of both liquid and solid phases of AA. The apparatuses used were ultraviolet-visible (UV-Vis) spectroscopy, scanning electron microscopy (SEM), X-ray powder diffraction (XRD), Fourier-transform infrared spectroscopy (FTIR), light microscope (LM), LUMiSizer, and high-performance liquid chromatography (HPLC).

4.5.1 UV-Vis Spectrophotometry at NTNU

The absorbance, *Abs*, of liquid phase samples of SS was measured by a UV-Vis spectrophotometer (Thermo Helio γ) at a wavelength of 320nm. The absorbance was further used for determining AA concentration in samples of the reaction solution. A calibration curve was established as a linear regression model of absorbance and concentration, expressed by Equation 5, and further used to calculate the concentration of AA in liquid phases by the average of three absorbance measurements.

Tris buffer at pH 8 was used for dilutions with AA solutions since the UV-Vis measurements should be conducted at a constant basic pH value due to the sensitivity of the system to pH. The establishment of the calibration curve, procedure on concentration measurements of AA, and the discussion upon the uncertainty in these measurements can be found in the Appendix, Section B.

$$C_{\mathrm{AA}}[\mathrm{mol/L}] = \frac{Abs - 0.0006349}{9.9031746} \tag{5}$$

4.5.2 UV-Vis Spectrophotometry at GE Healthcare Lindesnes

The absorbance of liquid phase samples of RPS was measured by GE Healthcare Lindesnes using a UV-Vis spectrophotometer (UV-1900) at a wavelength of 320nm. The samples, 2-5mL, were withdrawn from the reactor by a syringe coupled with a tube and filtered through a 0.2μm syringe filter (WWPTFE ACRODISC) to remove solid crystals. Further, the sample was diluted with water. The absorbance values were measured from 2 parallels for each sample and displayed with four digits. The concentration of AA was calculated by Equation 6, where d is the dilution factor.

$$\%\mathrm{AA}\ [\mathrm{g/100mL}] = 0.01471 \cdot Abs \cdot d \tag{6}$$

4.5.3 X-ray Powder Diffraction

In order to determine the crystalline phase of filtered and dried precipitated AA a D8 Focus XRD system was used. Sample preparations were performed by adding solids to sample holders, making the surface flat and smooth and with the same height as the sample's holder edges. The experimental parameters included a 0.2mm divergence slit with a step size of 0.02 and step time 0.08s over a 2θ range of 5-60 degrees. Limitations with XRD analysis, in this case, is that if amorphous phases are present in the samples they could easily be lost in the background due to the crystals present with well-defined peaks. XRD analysis is only used to check if different solids are present and to confirm the consistency of final crystals.

4.5.4 Fourier-Transform Infrared Spectroscopy

FTIR (Nicolet iS50) analysis was used for compound identifications of final crystals and to verify the consistency of final crystals. Solid samples were placed on a sample position and IR radiation passed through the sample and radiation was transmitted. The resulting signal at the detector is a spectrum representing the molecular "fingerprint" of the sample. The samples were analyzed with Smart Golden Gate Accessory, ZnSe lenses (100 scans with 0.2 resolution). The analysis of FTIR spectra of recrystallized AA is shown in the Appendix, Section D.

4.5.5 Scanning Electron Microscopy

To investigate particle morphology and sizes of filtered and dried crystals from the experiments, SEM APREO was used. Solid samples were either placed directly on SEM stubs with carbon tape or dispersed with a magnetic stirrer in methanol and placed on stubs with carbon tape and silica wafer. Initial trials were performed and showed that redispersed crystals showed dissolution on the crystal surfaces, the preferred method was therefore to use dry powder. Gold layers of different thicknesses were tested. 5, 10, and 15nm thickness resulted in indistinct images. Therefore, the samples were coated with 20nm gold layers in a Sputter Coater before the analysis. The coated stubs were placed in the SEM APREO chamber and analyzed with the secondary electrons (SE) technique at a high voltage of 4-10.00kV and a beam current of 50pA. The magnification varied between 150-3500.

4.5.6 Light Microscope

Both light microscopes, Zeiss Imager A1m and Olympus BH2-UMA were used at NTNU and GE Healthcare Lindesnes, respectively, to observe changes in crystals during experiments at a magnification of x5, x10, x20, and x40. One droplet was collected directly from the suspension, placed on a glass plate, and analyzed immediately. For the single-step addition of the acid experiments, images with a light microscope were taken for the final crystals. For the multi-step addition of the acid

experiments, images from 1h after each addition and of the final crystals were withdrawn. For the continuous addition of the acid experiments, images from halfway and final crystals were collected.

4.5.7 LUMiSizer

LUMiSizer and the associated software "SEPview" were used in order to obtain information about the cumulative velocity distribution as a function of sedimentation velocity. Analysis of sedimentation velocities of the particles in suspension would further elucidate differences in crystal sizes and crystal size distributions for the final crystals produced at different supersaturation build-ups, and shed light on characteristics that were crystallized from synthetic solution and real process solution.

Sedimentation Theory

Sedimentation theory is based on differences in density between a continuous and dispersed phase for a suspension of colloidal particles. The density of the continuous phase must be lower than the density of the dispersed phase. When this is the case, sedimentation of the dispersed phase may occur due to gravity. The sedimentation phase separates the continuous and dispersed phase which results in the formation of a particle sediment bed. Sedimentation proceeds until all of the dispersed phase have settled in the sedimentation bed, and there is only a clear solution above. The particles in the suspension will not sediment by themselves, and their motions will be affected by the surrounding particles, where this effect increases with increasing concentration [63]. In general, the size, shape, and density of the particles affect the settling rate. Larger particles will settle more quickly than smaller particles and rounder and more spherical particles settle faster than angular or irregularly shaped particles, and denser particles settle faster [64].

Optimization of Preparation and Analyzing Method

To achieve an optimized and repeatable method of the usage of LUMiSizer and SEPview trials and errors were performed of the preparation and analyzing procedures. Different solid dispersion concentrations were tested, where 0.05M gave a desirable transmission profile with a 30-60% initial transmission, representing the interface position [65]. Also, different standard operating procedures (SOPs) containing different profiles, intervals, and centrifuge rotation speeds were tested. A higher number of profiles and lower speeds, at least for the beginning of the analysis had the best fit allowing larger particles to settle slower such that the instrument could recognize it. 2mm cells (LUMiSizer cell type 2) were tested first, but to ensure that the larger and fast settled particles were monitored by the instrument, by giving longer residence time to settle, 10mm cells (LUMiSizer cell type 6) were used instead. In the first trials of data analysis, a volume-weighted particle size distribution was used. However, since AA showed a wide size distribution in SEM images and uncertain density it is difficult to accurately determine size and crystal size distribution. Therefore, the samples were analyzed based on the velocity-based distribution which is independent of the density of the particles. As the main point of these investigations is to distinguish the particle characteristics between different acid addition procedures, this was concluded to be a good way of representing the different particle populations.

Established Preparation and Analyzing Method

Filtered and dried crystals were redispersed in methanol to reach a concentration of 0.05M. The suspension was stirred for 5min at 300-500rpm, then the solution was transferred to three small glass vials. These glass vials were stirred for 10s immediately before 10mm cells were filled with 1.5mL of suspension, reaching a filling height of 23mm, then sealed with a lid before it was placed horizontally inside the instrument. Samples directly from the crystallization suspension were withdrawn and diluted with methanol (1:1 volume ratio). The same procedure was used for these analyses. In these samples the concentration is unknown. Three repeats of

each sample were measured to establish the standard uncertainty of repeatability. Normalization was performed before the analysis. The instrument monitors the transmission through each sample in time in the centrifuge. Each sample was analyzed at centrifuge rotation speeds of 200-3200rpm at a temperature of 25°C. The sedimentation velocity was determined in "particle characterization" in the analysis module of SEPview. Here, the analysis is based on velocity; distribution of the separation velocity of the individual classes, and sedimentation; profiles propagate from left to right. The starting position of particles corresponds to the filling height. Further, three nodes at constant positions were placed between positions 115-125mm in the transmission profile, and from this SEPview calculates the cumulative velocity distribution as a function of sedimentation velocity. No distribution fit was used for the cumulative velocity distribution graph, but three points moving average for analyzing smoothing was applied. An example of a sample's summary analysis with its specifications is given in Section H.3 in Appendix. The summary contains the sample's SOP, transmission profile, the cumulative velocity distribution curve, and the results of the average distribution, the latter is the data used to calculate size data.

4.5.8 High-Performance Liquid Chromatography

The purity of the final precipitate and impurity content, thus remaining raw materials and by-products from side reactions in the preparation of real process solution were analyzed by GE Healthcare Lindesnes, using HPLC. The stationary phase used was a C18 column. The mobile phase consisted of eluent A; water with 0.1 formic acid, and eluent B; 100% acetonitrile. 5-20μL of the sample was initiated in the column in order to analyze the composition of different components prior to and after crystallization.

5 Results and Discussion

The crystallization process of aromatic amine was investigated as a function of supersaturation build-up, with the resulting filtration performance. The filterability was evaluated in terms of specific cake resistance and further discussed with the associated final crystal properties. Studies of both synthetic and real process systems were discussed and compared to understand the different outcomes.

5.1 Synthetic Solution Studies

Initially, studies of recrystallization of AA were investigated, with emphasis on optimizing the system in a controlled, repeatable, and consistent manner. In the synthetic solution studies, the supersaturation was built up in three different procedures; single-step, multi-step and continuous addition of the acid.

5.1.1 Filtration Performance

The filtration performance of slurry obtained from neutralization and cooling crystallization of AA was evaluated as a measure of specific cake resistance and the moisture content was determined. The specific cake resistance, α, remarks the time and ease with which the fluid will flow through or permeate its voids in the solid-liquid separation. α is a result of the interplay between crystal size ranges and particle surface properties, which affect the capillary retention forces holding the liquor in the pores of the cake. Investigations on the specific cake resistance are of importance to achieve efficient industrial operation times and decreased energy demands. The moisture content may reflect the filtration, washing, and blowing performance, and have impacts on the final solid product weight, handling of filter cake, and impurity content. To minimize the energy consumption related to drying, the moisture content of filter cakes should be kept at a low level. Also, reduced moisture content lowers the risk of trapped impurities in the voids of the filter cake [5, 66, 67].

In general, rapid filtration times were observed in the filtration of AA precipitates obtained by different acid addition procedures. Results exhibit filtration times varying from 26-50s for full round (300mL slurry) filtration experiments. The shortest filtration times give the lowest specific cake resistances, while the longest times correspond to the highest. Figure 9 show that single-step addition of the acid results in the highest specific cake resistance. Semi-batch crystallization procedures resulted in lower α and improved filterability, where continuous addition of the acid gave the best results. Single-step addition of the acid shows 4.8 times higher specific cake resistance compared to the continuous addition of acid, while multi-step addition of the acid gives 1.7 times higher cake resistance. These differences might seem small in lab-scale, where 300mL of suspension is filtered. However, when scaling up to pilot scale and industrial scale, these differences in filterability might lead to significant differences in the time and energy demand of the filtration step. The clear differences observed in specific cake resistance for different acid addition procedures were not seen in the moisture content of the cakes shown in Figure 10. Here, the values fall in the same range. These results may be a consequence of constant washing amounts and blowing times with slightly different volumes of slurry filtered.

The standard deviations are below 10% for both the specific cake resistance and moisture contents, with a slightly higher variation in moisture contents. These results imply good consistency in crystallization and filtration experiments due to highly controlled systems. The different acid addition procedures exert considerable effects on the filtration performance, with the most prominent impact on the specific cake resistance. Depending on these results, improved filterability can be achieved by employing semi-batch crystallization systems for AA production.

The filtration performance is strongly connected to the properties of the accumulated filter cake on the filter medium, which in turn is affected by the individual crystal characteristics. In this study, the supersaturation profile was varied by using different acid addition procedures, which can significantly affect the characteristics of the precipitates. How the different reaction conditions; single-step, multi-step and continuous addition of the acid correlate with the resulting crystal properties will be enlightened in the following section.

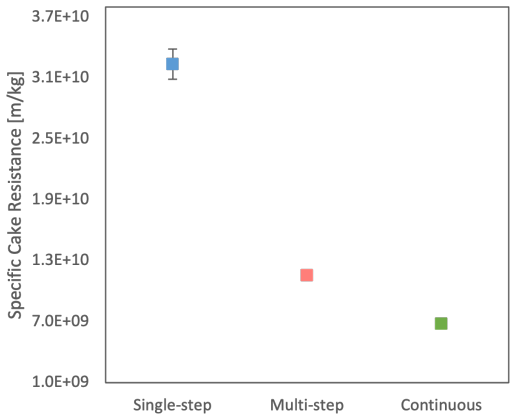

Figure 9: Specific cake resistance of precipitates formed upon different acid addition procedures from synthetic solution.

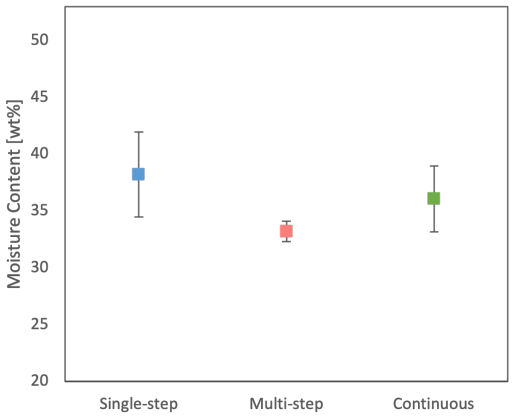

Figure 10: Moisture content of precipitates formed upon different acid addition procedures from synthetic solution.

5.1.2 Precipitation of AA via Different Acid Addition Procedures

The final crystal properties exert considerable effects on their following filtration performance. Concomitantly, the solution supersaturation is the driving force of nucleation and growth kinetics. Thus, the establishment of supersaturation in the system determines the precipitation pathway and nucleation and growth mechanisms which further contribute to the final outcome of crystal properties in terms of sizes, crystal size distribution, morphologies, and crystalline phases [15]. High supersaturation levels are typical in neutralization reactions, which causes difficulties in direct control of the supersaturation profile. In this work, the supersaturation profile was evaluated indirectly by varying the acid addition procedure in the reaction medium, and by quantifying and observing differences in final crystal properties; crystal size with cumulative velocity distribution as a function of sedimentation velocity, and morphology with SEM, respectively. High yields above 95% were obtained in all experiments, and to confirm the consistency of the crystal product, XRD and FTIR analyses were conducted. The Figures 11 and 12 show that the same highly crystalline and pure compounds are established during precipitation of AA.

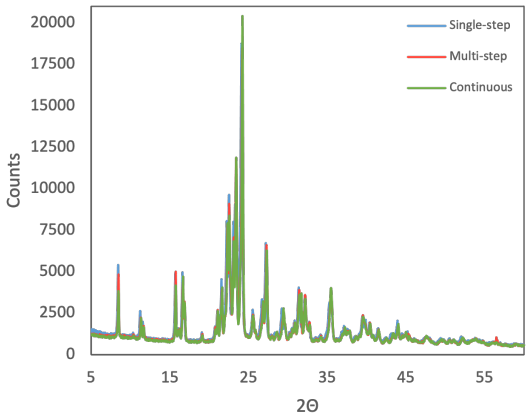

Figure 11: XRD spectra of precipitates from different acid addition procedures in synthetic solution studies.

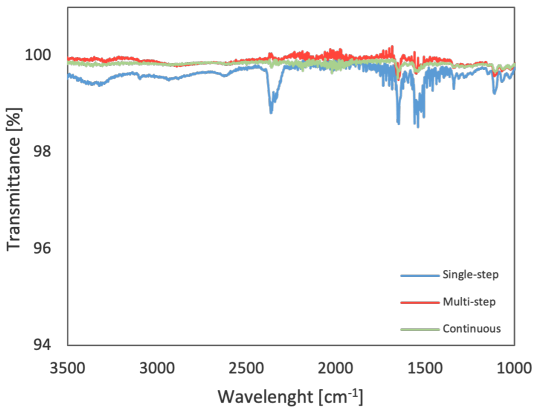

Figure 12: FTIR spectra of precipitates from different acid addition procedures in synthetic solution studies.

LUMiSizer analysis was performed to get a quantitative measure of size, which can help us explain the filterability results and support the data collected by SEM imaging of precipitates. Figure 13 show that precipitates from semi-batch experiments resulted in higher sedimentation velocities. Single-step addition of the acid resulted in precipitates with lower sedimentation velocity, shown by the blue bars. Sedimentation velocities from multi-step precipitates are between sedimentation velocities from single-step and continuous addition of the acid precipitates, where the latter resulted in higher sedimentation velocities. This correlates well with the aforementioned filtration data, as higher sedimentation velocities indicate larger particle sizes or more dense particles due to faster settling [63]. Larger particles result in lower filter cake resistance as they provide a lower interface area between the particles in the filter cake and the liquid flowing through, and smaller particles can accumulate near the filter cloth and interact more with the liquid flowing through resulting in a slower filtration rate, hence higher specific cake resistance [5, 67]. Although the absolute crystal sizes cannot be determined by the LUMiSizer measurements and the differences in crystal size distribution are difficult to read, these results show a clear trend in relative particle size in precipitates obtained by different acid addition procedures.

The standard deviations are similar for all experiments in each cumulative velocity distribution bar and are between 5-12% confirming that this method is reliable and consistent. The standard deviations are calculated from a combined mean with accompanying standard deviations from three replicates in each experiment. The cumulative velocity distribution from each experiment is given in H.2 and gives the basis of the average cumulative velocity distribution from each acid addition procedure. LUMiSizer analysis directly from suspension was also conducted and is given in Section H.1 in the Appendix. These analyses did not undergo optimization, and it is difficult to conclude something from the results.

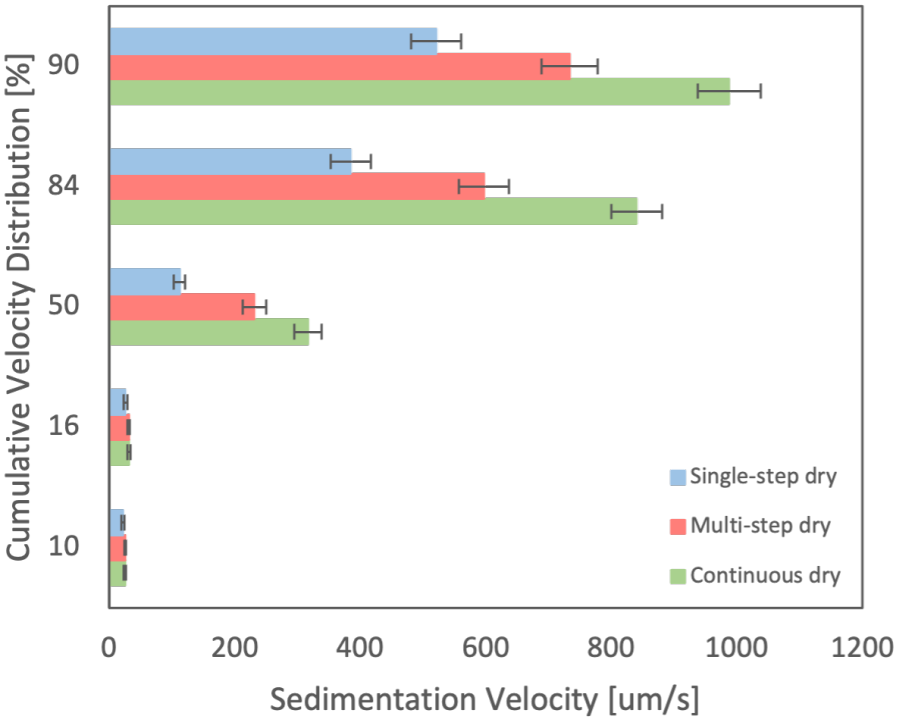

Figure 13: Cumulative velocity distribution of filtered and dried crystals from experiments conducted from the synthetic system. The distributions ranges like this example; 10% of distribution $\leq 23\mu$m/s etc.

Single-step Addition of the Acid

In the single-step addition of the acid experiments, all acid was added at once, creating a high thermodynamic driving force in the system, which can induce a high

nucleation rate at the beginning of the crystallization. As observed from the single-step addition of the acid experiments, the precipitation occurs almost instantly after adding the acid to the system. A high initial supersaturation onset a fast and high nucleation rate. This could indicate chaotic precipitation creating a particle population of smaller crystals. From SEM images in Figures 14 and 15 the crystals are seen from a lower and higher magnitude, respectively. In Figure 14 both smaller and larger sphere-like clusters are observed. Also, tiny clusters consisting of a few crystals and individual crystals are observed next to the larger sphere-like clusters. In Figure 15 thin plate-like crystals covering the outside of the sphere-like clusters are observed.

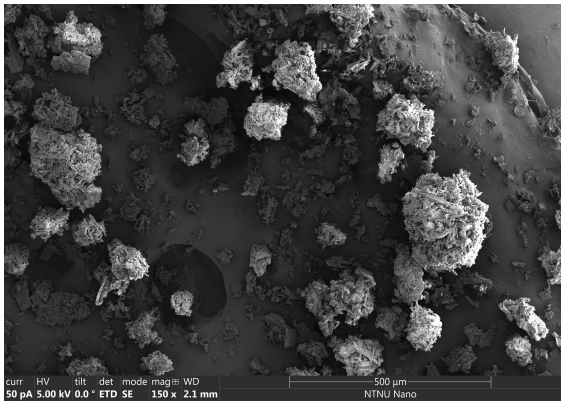

Figure 14: SEM image of final crystals from single-step addition of the acid, in the synthetic system.

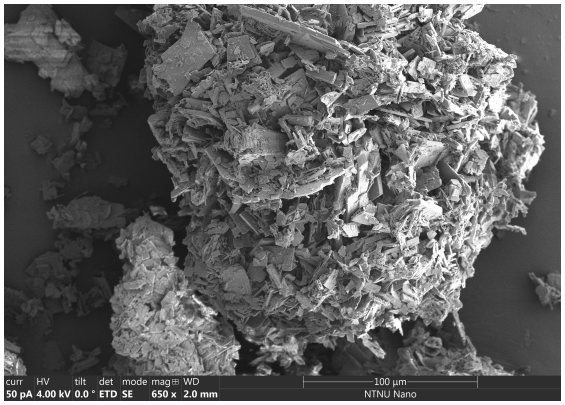

Figure 15: SEM image of final crystals from single-step addition of the acid, in the synthetic system.

Multi-step Addition of the Acid

In multi-step addition of the acid experiments, the precipitation occurs more gradually. From the addition of the first portion of the acid, there are small changes that can be detected visually, but burst precipitation was not observed immediately. This can be explained by the neutralization of the excess base in the suspension by the acid, happening first. This is confirmed by a small decrease in UV measurements with AA concentrations from 0.50±0.02M to 0.45±0.02M and a high decrease in pH measurements from pH 11-13 to pH 6. Precipitation at this point are confirmed from crystals seen in LM images in Figure 16 and 17. When adding several portions to

the suspension the supersaturation profile will at some point reach a high supersaturation level, precipitating a large number of crystals, but at a lower level compared to single-step addition of the acid. In this acid addition procedure, there will be competition over time between supersaturation consumed for the growth of earlier created crystals and additional nucleation mechanisms creating smaller crystals. In Figure 18, like in single-step addition of the acid experiments, both smaller and larger sphere-like clusters of particles are seen. However, seen in the higher magnitude image in Figure 19, quite a different population seems to develop or cover these clusters. The plate-like particles look thicker and more brick-like and these crystals seem more protruding of the sphere-like cluster compared to the crystals seen at higher magnitude from single-step precipitations. These protruding crystals look slanted with well-defined and smooth faces. Also, there seems to be a wider size distribution with many larger brick-like crystals that are tightly covered by tiny crystals. These observations of crystals with significantly different particle sizes support the theory that this system is prone to additional nucleation mechanisms.

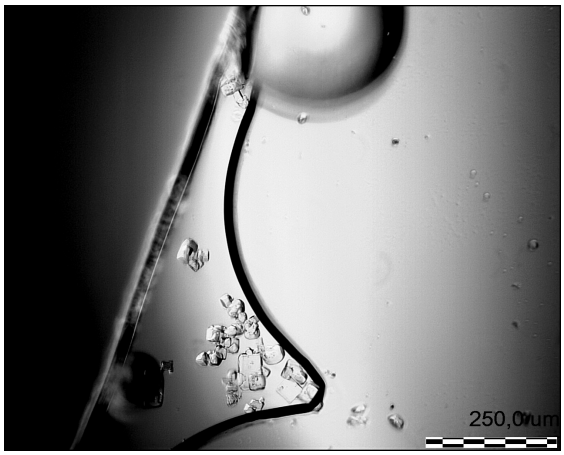

Figure 16: LM image of crystals from 1h after 1^{st} acid addition in multi-step addition of the acid, in the synthetic system.

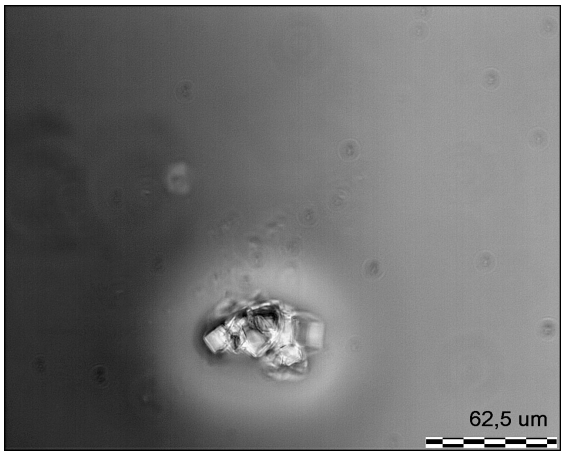

Figure 17: LM image of crystals from 1h after 1^{st} acid addition in multi-step addition of the acid, in the synthetic system.

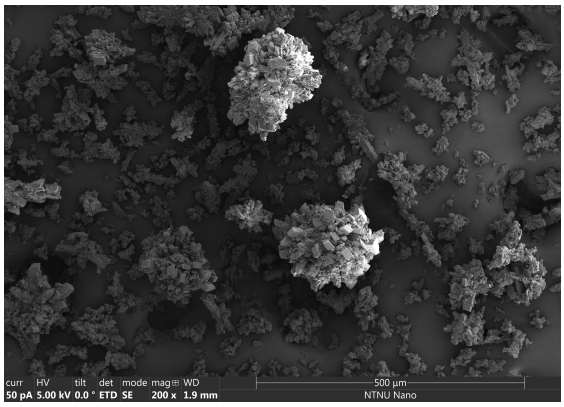

Figure 18: SEM image of final crystals from multi-step addition of the acid, in the synthetic system.

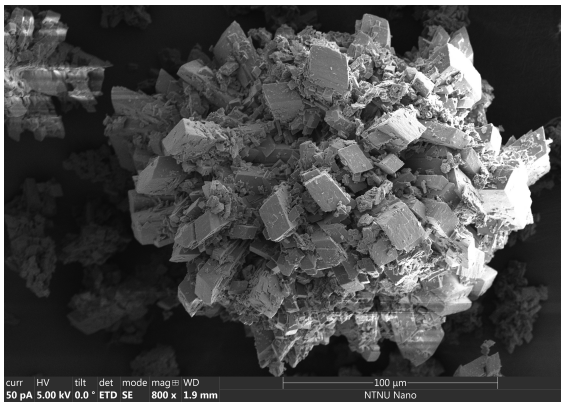

Figure 19: SEM image of final crystals from multi-step addition of the acid, in the synthetic system.

Continuous Addition of the Acid

In continuous addition of the acid experiments, the precipitation occurs at a lower supersaturation level evenly throughout the crystallization. This was observed by precipitation evoked at a later time point of the crystallization process. After half of the amount of acid was added to the reactor medium, the AA concentration had changed from 0.52±0.03M to 0.30±0.03M. The pH decreased from pH 11-12 to pH 4-6. LM images from this time point are shown in Figure 20 and 21. For these experiments there is no shocking of the system with high supersaturation like in single-step and multi-step addition of the acid experiments. These statements might point towards a growth-dominated precipitation resulting in larger crystals and with a more narrow CSD compared to multi-step addition of the acid experiments. Larger particles obtained from the supersaturation build-up coheres well with the aforementioned size data and specific cake resistance. In Figure 22 sphere-like clusters varying in size and more elongated clusters are observed. In Figure 23 thicker plate-like crystals are protruding from the clusters. From SEM images it looks like the thickness of these plate-like particles are intermediate between the thickness of plate-like particles in single-step addition of the acid experiments and brick-like particles in multi-step addition of the acid experiments. Also, it looks like a lower number of fine particles are covering these plate-like crystals compared to

multi-step addition of the acid experiments, which supports the earlier mentioned theory regarding the establishment of supersaturation in this acid addition procedure experiments. Additional LM images from experiments conducted from the synthetic system is presented in Section J in Appendix.

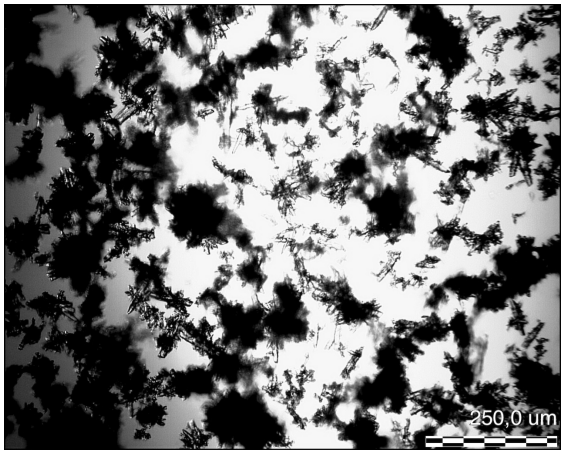

Figure 20: LM image of crystals from half way of the acid addition in continuous addition of the acid, in the synthetic system.

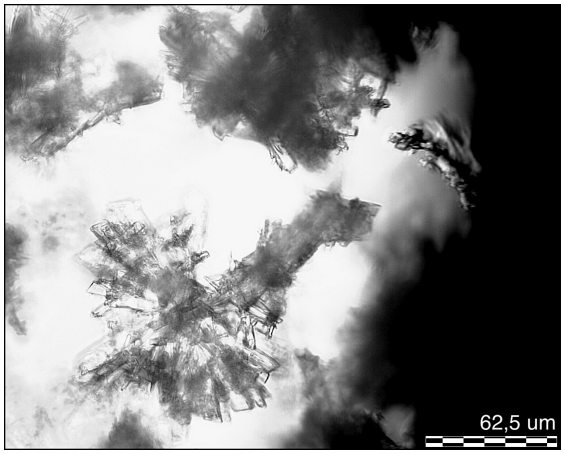

Figure 21: LM image of crystals from half way of the acid addition in continuous addition of the acid, in the synthetic system.

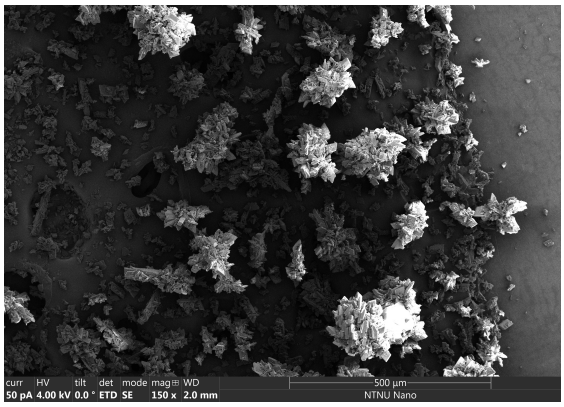

Figure 22: SEM image of final crystals from continuous addition of the acid, in the synthetic system.

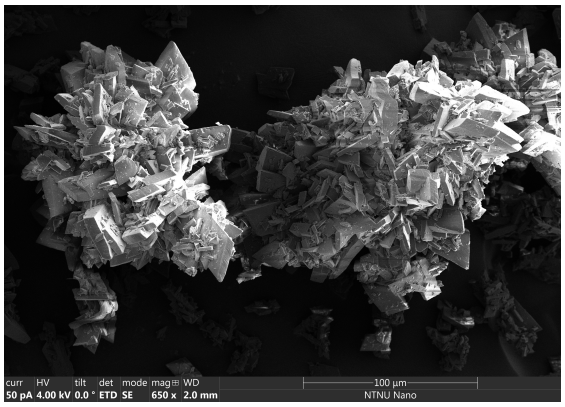

Figure 23: SEM image of final crystals from continuous addition of the acid, in the synthetic system.

5.1.3 Supersaturation Profile and Crystal Characteristics

Starting from a clear solution, with no seed crystals present, a higher free energy barrier for precipitation exists in the system. To exceed this barrier a sufficiently high supersaturation is required. Initially, if a very high supersaturation is generated in the system, the free energy barrier is easily exceeded and might result in rapid precipitation with a generation of a large number of fine particles due to the system being dominated by nucleation. Because of the high supersaturation level in the system, homogeneous primary nucleation is usually dominant, and followed by rough growth mechanisms, resulting in irregular crystal surfaces. If a lower supersaturation is generated in the system, which is just high enough to exceed the energy barrier, a few critical nuclei might be formed in the suspension, with a low probability to aggregate to each other. Further, the supersaturation can gradually be increased by adding more reactants to the system. At this point, the energy barrier for precipitation is lower compared to the initial situation, and if there are enough crystal surfaces, the dominating mechanism will in most cases be growth. By gradually increasing the supersaturation level in the system one would also expect that at some point the system would be prone to secondary nucleation mechanisms. However, primary nucleation could also occur at this point if the supersaturation level is high enough. It is difficult to distinguish between primary and secondary nucleation mechanisms without further investigations. Therefore, these nucleation mechanisms will be referred to as additional nucleation mechanisms. Precipitation dominated by growth with additional nucleation mechanisms present, one would expect larger particles due to growth, but also a wider crystal size distribution due to nuclei formed by additional nucleation [9, 68, 69].

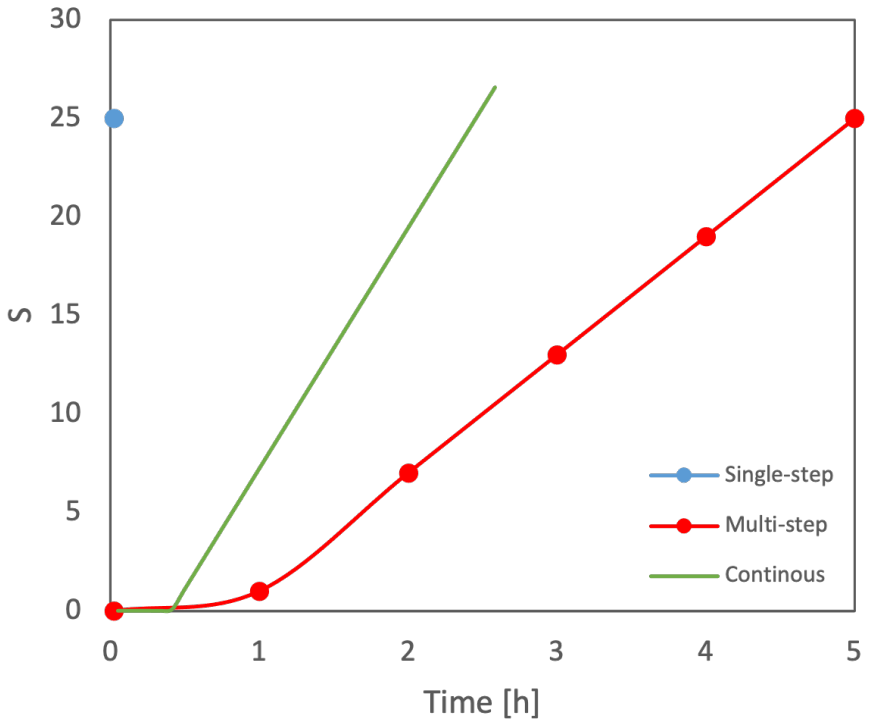

Figure 24: Theoretical illustration of the supersaturation profiles in single-step, multi-step and continuous addition of the acid experiments as a function of time [h].

In Figure 24 a theoretical illustration of the supersaturation profiles in single-step, multi-step and continuous addition of the acid as a function of time is shown. In this illustration it is assumed that no precipitation occurs in the systems during acid addition, the initial concentration of AA is 0.5M, and volume changes with acid addition are neglected. As stated above, the single-step addition of the acid experiments induce a high initial supersaturation in the system illustrated by the blue dot. What is interesting and most similar to reality is the difference in the developed supersaturation profiles at the beginning of multi-step and continuous addition of the acid experiments. First, acid is consumed for neutralization of excess base in both systems, subsequently, the supersaturation is developed by additional acid. In the multi-step addition of the acid experiments, the acid is added in portions, illustrated by 5 red dots. Here, most of the acid in the first portion is used to neutralize the base, and the rest generates supersaturation. The continuous addition of the acid experiments have a continuous supply of acid, illustrated by the green line, and use more time to neutralize the excess base as the acid is slowly added

to the system. However, when the base is neutralized, supersaturation is generated simultaneously as precipitation occurs if the supersaturation level is high enough to exceed the energy barrier for nucleation and growth. As seen from the illustration the semi-batch experiments develop at a significantly lower initial supersaturation level compared to single-step addition of the acid experiments, and there is more time and probability for supersaturation to be consumed for growth of crystals. As a summary of these statements, one anticipates that single-step addition of the acid would produce smaller crystals compared to the multi-step and continuous addition of the acid experiments. Multi-step addition of the acid might result in a wider crystal size distribution compared to the two other procedures due to acid added in portions inducing higher supersaturation levels several times during the crystallization. These hypotheses correlate very closely with the particle characteristics observed via LUMiSizer measurements and SEM images. It should be noted that at time points after the onset of precipitation, the semi-batch supersaturation profiles will deviate remarkably from reality due to consumption of supersaturation.

From these crystallization theories, one would expect that inducing a very high initial supersaturation, like in single-step addition of the acid, would evoke high nucleation rates and result in fast precipitation. Single-step addition of the acid experiments would most probably be dominated by nucleation and result in a smaller particle population. As the supersaturation is being consumed by nucleation, eventually the supersaturation level will decrease and the nuclei formed will further consume the supersaturation for growth. With a multi-step addition of the acid procedure, one would gradually build up the supersaturation level in the system over time. If the supersaturation is high enough it might be consumed for primary nucleation and further growth of these nuclei. Then when adding a new portion of acid, a higher supersaturation is created instantly in the system and might be susceptible to additional nucleation mechanisms and growth of earlier produced crystals, creating a wide size distribution in the system. As the portions in multi-step are one-fifth of the portion in the single-step addition of the acid one might expect that a high supersaturation level would last for a shorter period of time, giving more possibilities for growth. Continuous addition of the acid gives a more smooth and even supply of acid to the system, without shocking it like in single-step and multi-step addition

of the acid. This might indicate less pronounced additional nucleation mechanisms, and more time and prerequisite for growth as the overall crystallization is carried out at a lower supersaturation level compared to single-step and multi-step addition of the acid.

5.2 Real Process Solution Studies

In order to obtain an insight into how the crystallization of AA would behave in industrial production it is necessary to get information about the real process solution with its filtration behavior and final crystal properties. The most distinct and known difference between SS and RPS systems is the presence of impurities from side reactions and raw materials in RPS.

In the real process solution studies addition of acid was conducted in two different procedures; single-step and continuous addition of the acid. These two procedures were chosen due to larger differences in the filtration data in the synthetic system, and because multi-step addition of the acid is time demanding. An additional experiment with continuous addition of the acid was conducted at 20°C. Due to limited time and resources, a single round of experiment was performed at 20°C, whereas the other two conditions were repeated three times and twice for single-step and continuous addition of the acid, respectively.

5.2.1 Filtration Performance

The filtration performance of slurry obtained from neutralization and cooling crystallization of RPS was evaluated in terms of specific cake resistance, and the moisture content was determined. The filtration times in the real process system varied from 23-70s for full round (200mL slurry) filtration experiments. The results in Figure 25 show that continuous addition of the acid experiment at 20°C resulted in higher specific filter cake resistance, with 3.4 times and 5.9 times higher α than single-step and continuous addition of the acid experiments, respectively. This significantly higher specific cake resistance for operation temperature at 20°C compared to 50°C

is evidence that elevated temperatures is advantageous in the neutralization crystallization of AA. Single-step experiments show 1.8 times higher α than continuous addition of the acid experiments, hence continuous addition of the acid experiments give improved filtration performance. Figure 26 show small variations in moisture content for real process solution studies, with values in the same range. The standard deviations of specific cake resistance and moisture content for single-step and continuous addition of the acid experiments are up to 10% and imply consistency in filterability of all precipitates formed via different acid addition procedures.

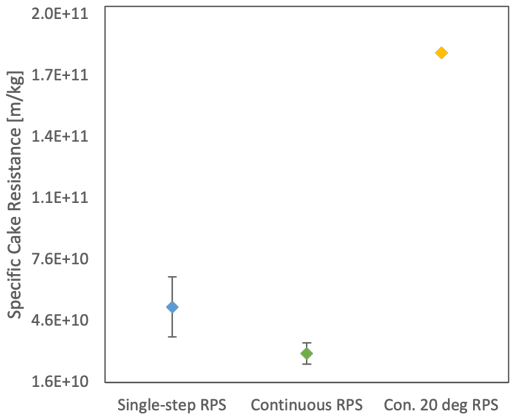

Figure 25: Specific cake resistance of precipitates formed upon different acid addition procedures from real process solution.

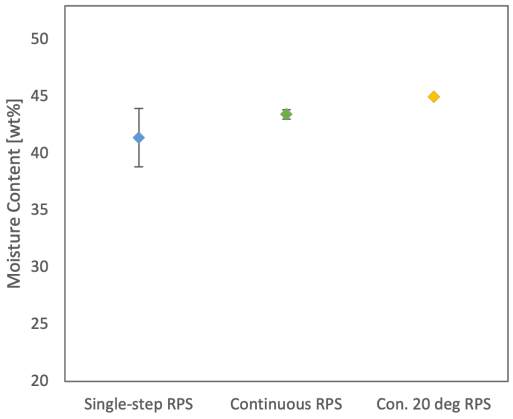

Figure 26: Moisture contents of precipitates formed upon different acid addition procedures from real process solution.

5.2.2 Precipitation of AA from RPS via different Acid Addition Procedures

The final crystal properties, affect the RPS system like in SS system, the filtration performance. The theory and statements regarding the build-up of supersaturation in different acid addition procedures apply to the real process solution as well. Still, in the real process solution impurities from side reactions and raw materials from the preparation of the real process solution are present and can affect the final crystal characteristics. However, XRD and FTIR analysis presented in Figure 27 and 28, verify the same highly crystalline and pure product of AA. Also, HPLC

analysis shows a high purity of AA above 98% for all experiments, and high yields above 96% were obtained in all experiments. The results from HPLC analyses are described and discussed in more detail in Section K in the Appendix.

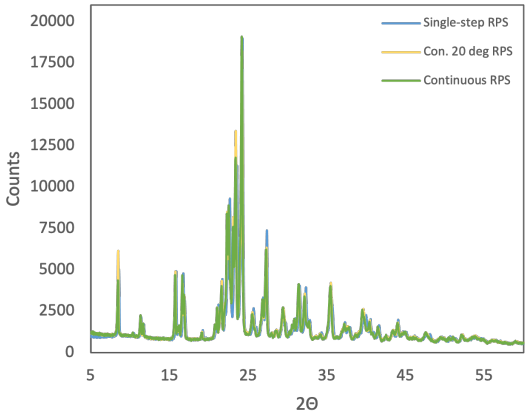

Figure 27: XRD spectra of precipitates from different acid addition procedures in real process solution studies.

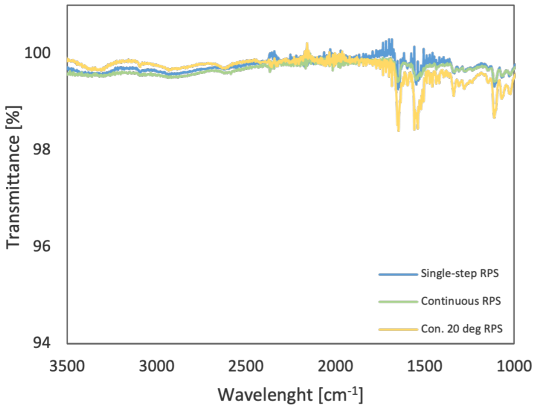

Figure 28: FTIR spectra of precipitates from different acid addition procedures in real process solution studies.

As seen from the sedimentation velocities in Figure 29, continuous addition of the acid experiments give higher sedimentation velocities indicating a larger particle population compared to single-step experiments and continuous addition of the acid at 20°C. The graph shows similar trends as the filtration data, as one would expect that smaller particles would give higher specific cake resistance and larger particles lower specific cake resistance due to their interactions between the particles and the liquid flowing through the filter cake [67]. The figure shows small standard deviations between 2-15% for all procedures, with variations in standard deviations between them. One explanation for the variations in standard deviations might be that single-step addition of the acid experiment were performed 3 times, while continuous addition of the acid experiment 2 times, and the continuous addition of the acid experiment at 20°C was performed once. The standard deviations in single-step and continuous addition of the acid experiments are calculated from a combined mean with accompanying standard deviations from three replicates in each experiment. The continuous acid addition experiment at 20°C is calculated from three replicates.

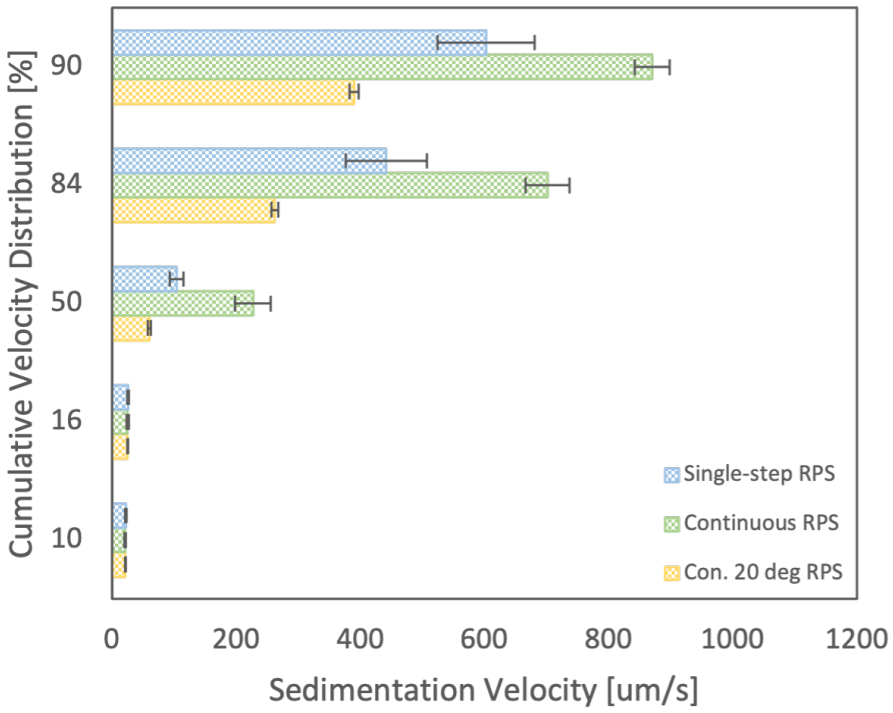

Figure 29: Cumulative velocity distribution of filtered and dried crystals from experiments in the real process system. The distributions ranges like this example; 10% of distribution $\leq 23\mu$m/s etc.

Single-step Addition of the Acid

SEM images of precipitates formed via single-step acid addition showed both sphere-like clusters and more open structures with plate-like morphology, seen in Figure 31 and 30. Figure 32 reveals a combination of thicker plate-like crystals and brick-like crystals covering the surface of these sphere-like clusters. In Figure 33, some of the smaller particles on the surface of the larger ones seem to be a part of the larger crystals and some seem to be individual crystals laying on top of the larger ones.

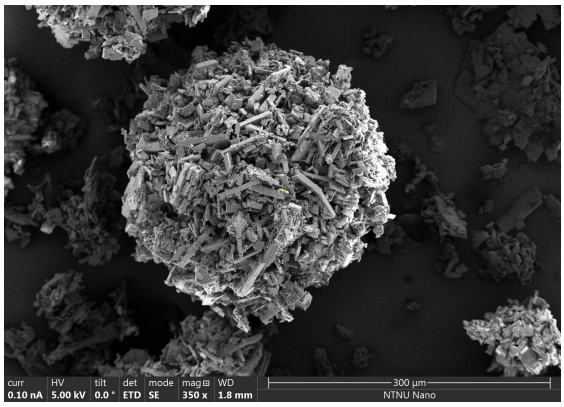

Figure 30: SEM image of final crystals from single-step addition of the acid, in the real process system.

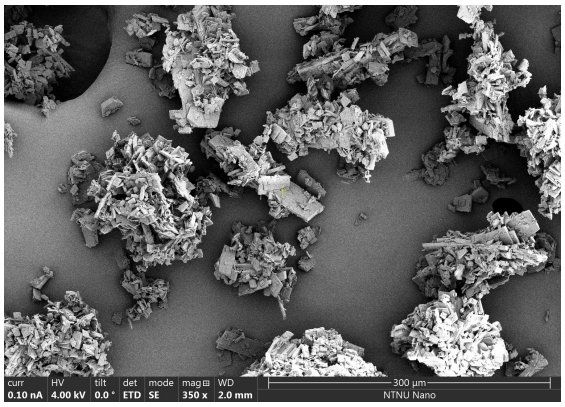

Figure 31: SEM image of final crystals from single-step addition of the acid, in the real process system.

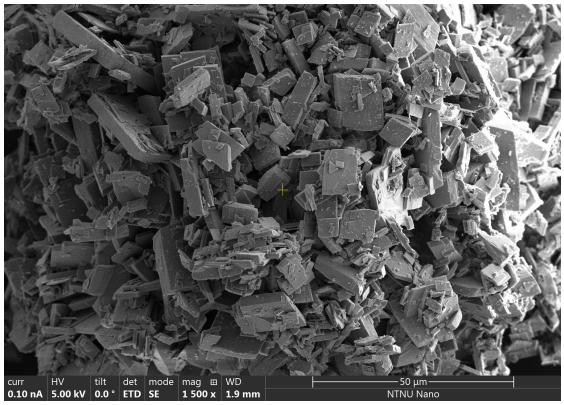

Figure 32: SEM image of final crystals from single-step addition of the acid in the real process system.

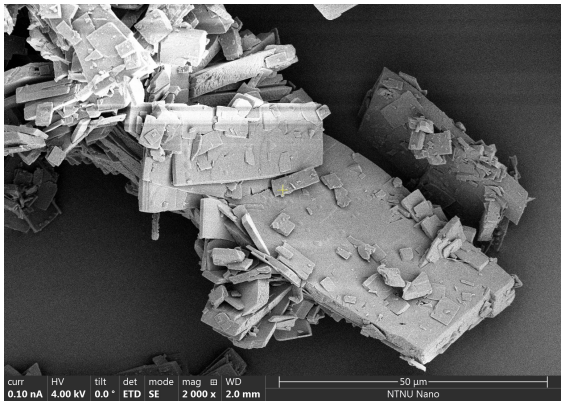

Figure 33: SEM image of final crystals from single-step addition of the acid, in the real process system.

Under single-step procedure, at uncertain conditions in terms of solvent ratio and reaction time, a sphere-like cluster was observed, shown in Figure 34. The cross-section of this larger cluster reveals what looks like a spherulite. High supersaturation can cause rough growth under a diffusion-controlled growth regime, showed by the crystals emerging from the center. The surface of the crystal is covered by smaller crystals, which could point towards secondary nucleation mechanisms. Sphere-like clusters are present in SEM images for the different acid addition procedures both in SS and RPS studies. Observations of the cross-section suggest that they could be explained by spherulite formation mechanism via central multidirectional growth.

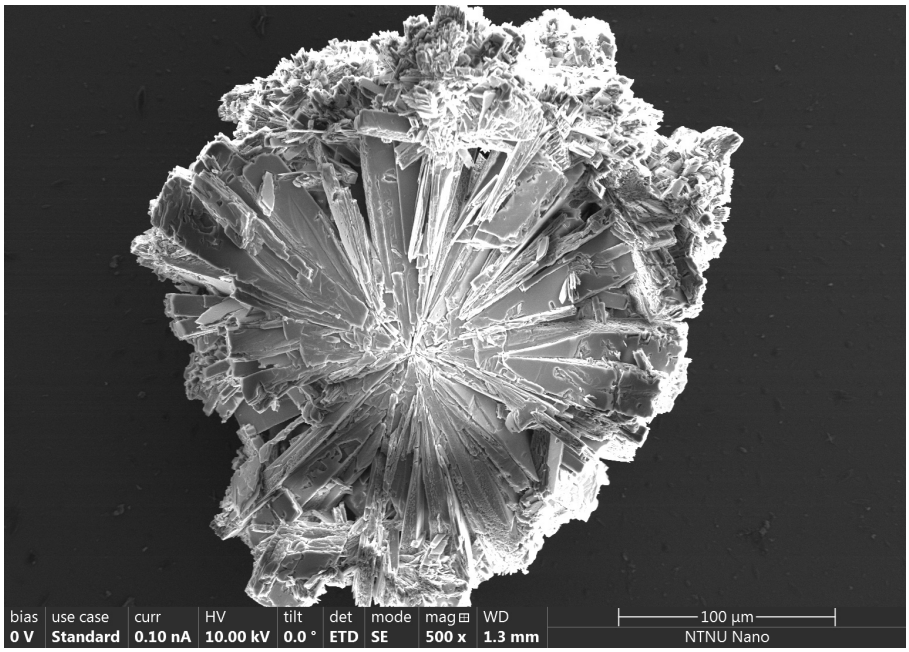

Figure 34: Cross-section of a sphere-like crystal from an RPS experiment formed via single-step addition of the acid procedure.

Continuous Addition of the Acid at 50°C

SEM images of precipitates via continuous addition of the acid showed both sphere-like clusters and elongated brick-like crystals with their surface covered with smaller particles, seen in Figure 35-38. In these images, one can also see a wide size distribution seen from larger elongated crystals with smaller individual crystals surrounding.

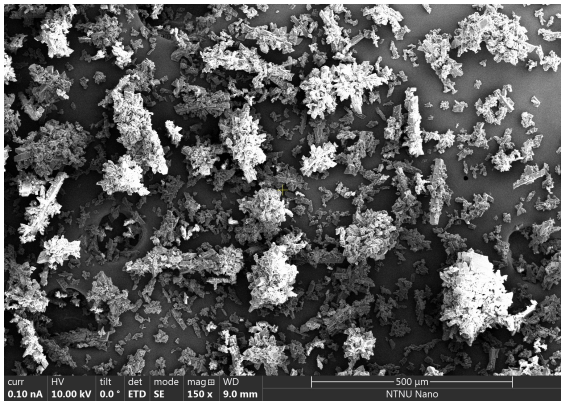

Figure 35: SEM image of final crystals from continuous addition of the acid, in the real process system.

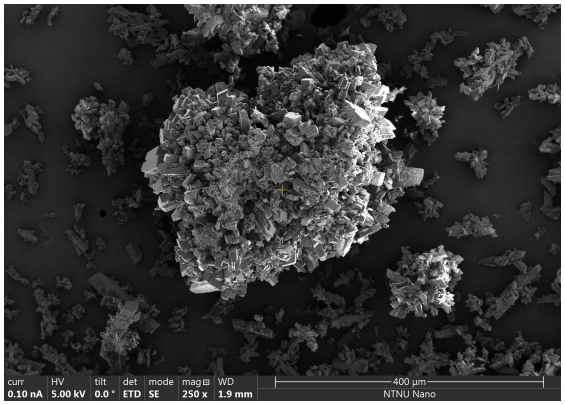

Figure 36: SEM image of final crystals from continuous addition of the acid, in the real process system.

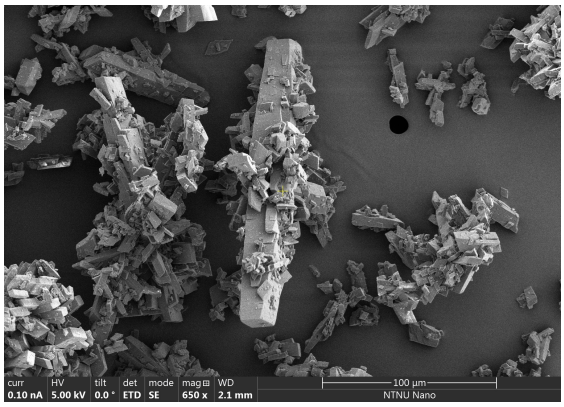

Figure 37: SEM image of final crystals from continuous addition of the acid, in the real process system.

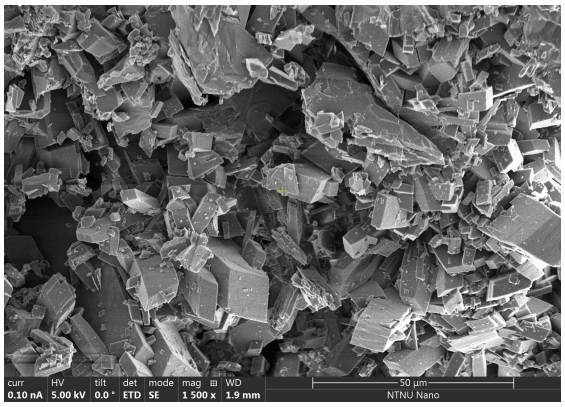

Figure 38: SEM image of final crystals from continuous addition of the acid, in the real process system.

Continuous Addition of the Acid at 20°C

Continuous addition of the acid at a temperature of 20°C give a higher supersaturation than the aforementioned procedures due to lower temperature, thus lower solubility and higher supersaturation. Crystals from precipitation with this aid addition procedure shows a drastic difference in particle size and shape shown in Figure 39 and 40. From the images smaller and more open sphere-like crystals are observed. Figure 41 and 42 show that these sphere-like clusters consist of long and thin needle-like structures. These characteristics can explain the big difference in its filterability, as smaller particles indicate higher surface area and larger solid-liquid interface resulting in higher specific cake resistance [5]. Additionally, an EasyViewer 100 was used in this experiment which provides the opportunity for in-situ images (shown in Section L in the Appendix).

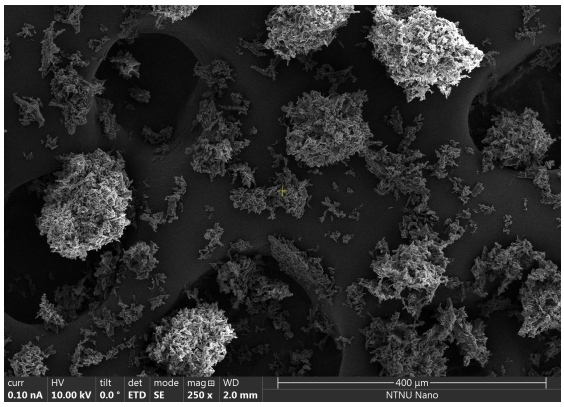

Figure 39: SEM image of final crystals from continuous addition of the acid at 20°C, in the real process system.

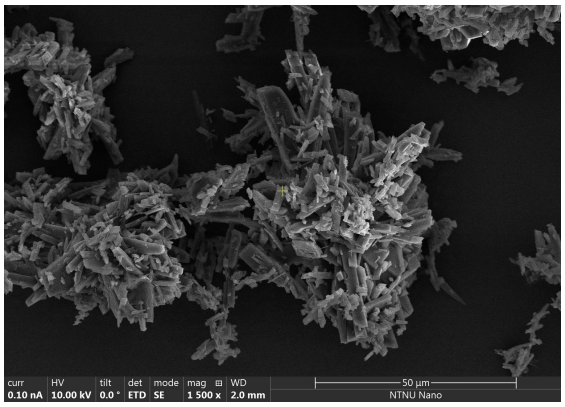

Figure 40: SEM image of final crystals from continuous addition of the acid at 20°C, in the real process system.

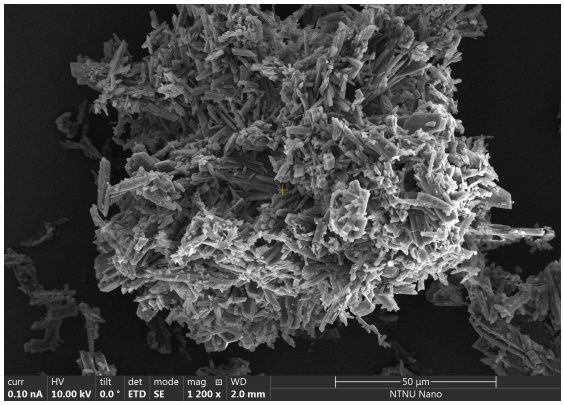

Figure 41: SEM image of final crystals from continuous addition of the acid at20°C, in the real process system.

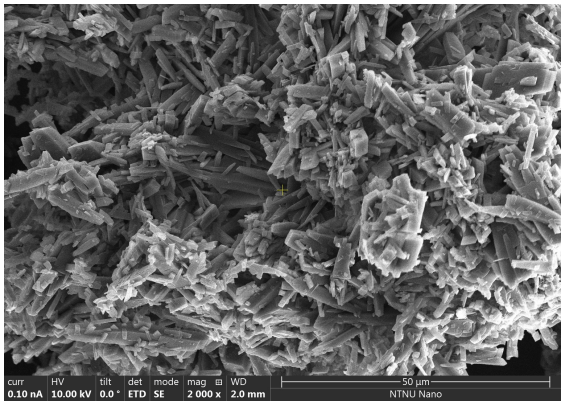

Figure 42: SEM image of final crystals from continuous addition of the acid at 20°C, in the real process system.

5.2.3 Supersaturation Profile and Crystal Characteristics

The same theories regarding how the supersaturation profile is established for single-step and continuous addition of the acid apply for the real process solution. Single-step induces a high initial supersaturation level, which can result in the emergence of smaller particles. Continuous addition of the acid will operate at a lower and more moderate supersaturation level, which could result in a growth-dominated crystallization resulting in larger particles. For continuous addition of the acid at 20°C, a higher supersaturation level is expected, as a decrease in the temperature

decreases the solubility, thus increase the supersaturation level. Even though the acid is added continuously, the supersaturation in the system is significantly high, which in turn prevalence smaller particles. Seen from SEM images and size data these particles are smaller than the single-step addition of the acid and coincide with filtration data as well.

The real process solution contains low levels of impurities seen from the aforementioned HPLC data. Even at relatively small impurity concentrations, they can have a significant effect on the crystal habit in crystallization processes. These impurities can stem from raw materials, or be formed as by-products from side reactions during the synthesis of the real process solution. Impurities can have similar effects as additives in crystallization processes, which often have the ability to act upon the crystal surface, rather than impact the supersaturation level in the system explained by inefficient capacity because of low concentration. They can act as growth inhibitors or habit modifiers, for example by changing the growth mechanism of the most dominated faces [7]. However, in systems with high supersaturation levels and rough growth rates, it is difficult for these impurities to inhibit the growth rate. In most cases, the majority of the impurity is rejected by the growing crystals, and separated together with the mother liquor in the filtration step [70, 71].

Also, in these experiments, the methanol-water solvent ratio is increasing during the acid addition because an aqueous acid was used. A higher water content might decrease the supersaturation level in these systems as the aromatic amine is more soluble in water compared to methanol. Further investigations should be conducted to determine the effect of the methanol-water solvent ratio.

5.3 Comparison of the Synthetic and Real Process System

Synthetic and real process solution studies were both carried out and compared to point out possible trends and differences between the results and to evaluate if the synthetic system is a good representation of the real process system. If the outcome is that the synthetic studies are representative of the real process system, the synthetic system can further be optimized and used to provide new knowledge

regarding the crystallization of AA. It is advantageous to conduct experiments from the synthetic system as it requires fewer steps of preparation before crystallization compared to the real process system, and the experiments can be performed in a more controlled manner.

5.3.1 Level of Control in the Systems

The synthetic solution system enables strict control as the preparation steps and reactants used are few. The real process solution undergo several synthesis steps prior to crystallization, where the extent of impurities vary and provides multiple steps for uncertainties and variations, confirmed by higher standard deviations and larger batch-to-batch variations. The synthetic system went through several optimization experiments, where this was not feasible for the real process system, which causes less insurance of consistency of the final product in the real process system. Other factors such as differences in methanol-water solvent ratio, differences in density and viscosity, with and without the use of baffles, small differences in propellers, different purity grades of chemicals, and different lengths of the filtration units might also have small effects on the results. Despite these statements, the results of SS and RPS studies show similarities of filtration trends and final crystal characteristics, and the studies in both cases indicate robustness. This will be discussed further in the following section.

5.3.2 Filtration Performance and Crystal Characteristics

As explained above, there are several differences in experimental setups and some differences in reaction conditions between the synthetic and real process systems. This makes it difficult to compare quantitative data. Still, it is useful to compare trends and similarities in the systems. The filtration performance in terms of specific cake resistance for both systems is presented in Figure 43. Continuous addition of the acid at 20°C is given in an inset graph in the same figure since it gives a substantial difference compared to the other procedures. The real process solution studies show the same trend as the synthetic solution studies, meaning that semi-

batch experiments show improved filtration performance. Single-step addition of the acid experiments does in both cases give higher specific cake resistance compared to the continuous addition of the acid experiments in the same system. However, there is a difference regarding how significant these differences are. In SS studies single-step experiments give 4.8 times higher α than continuous addition of the acid experiments, while in RPS studies single-step experiments show 1.8 times higher α. This indicates that the real process system is less affected by variations in acid addition procedures. In Figure 44 the moisture contents are given, and small differences are seen between the SS system and the RPS system, where the RPS system shows slightly higher moisture contents. The standard deviations are higher in RPS studies for specific cake resistance, while in the same range for the moisture contents. In Section G in the Appendix, all filtration curves with associated trend lines and R^2 values are presented and show high linearity. However, the real process system shows slightly lower R^2 values in some experiments, explained by a less accurate recording method of the weight of filtrate as a function of time, and can help explain the higher standard deviations in specific cake resistance in this system. As there are similar trends in the systems it indicates that synthetic system is a good representation of the real process system.

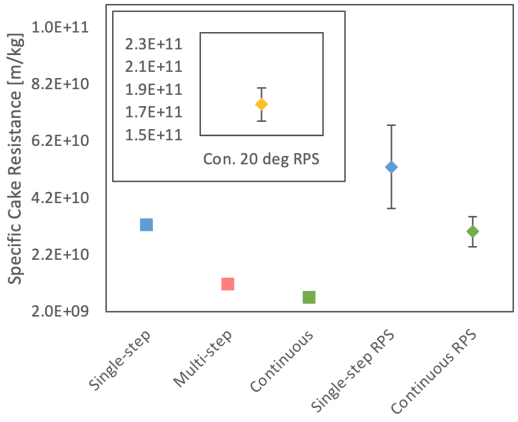

Figure 43: Specific cake resistance of acid addition procedures in the SS and RPS studies with input graph.

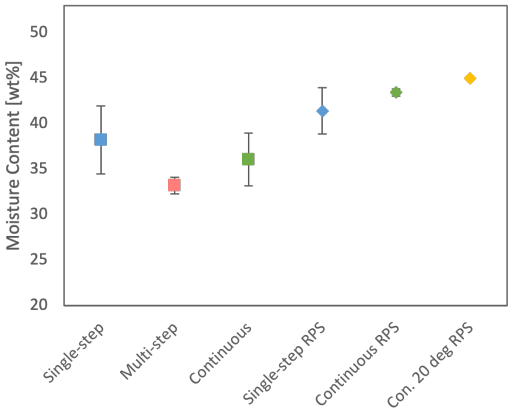

Figure 44: Specific cake resistance of acid addition procedures in the synthetic and real process solution studies.

In Figure 45 the sedimentation velocities of different acid addition procedures in both systems are given. These results coincide well with filtration data. The experiments from acid addition procedures with associated systems show similar trends as for the specific cake resistances; continuous addition of the acid experiments have higher sedimentation velocities than single-step experiments in both cases. Also, the sedimentation velocities are closer to each other for the real process solution experiments, which is also seen in the filtration data. These results amplify that the synthetic system is representative of the real process system and that the real process system seems more robust to changes in acid addition procedures. With some exceptions, the RPS studies show slightly higher standard deviations, which can be explained by the aforementioned variations in different parameters.

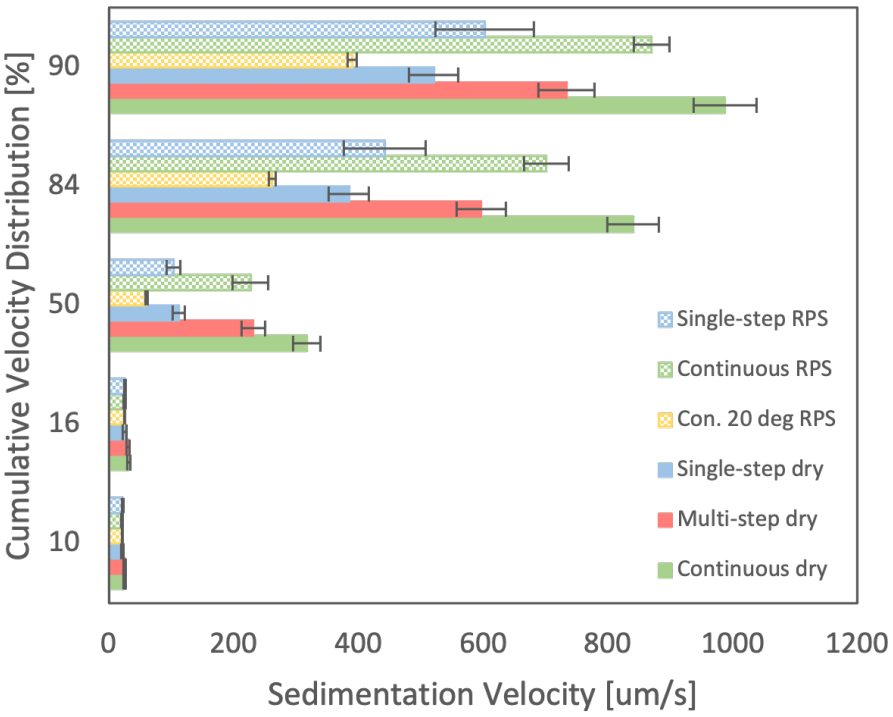

Figure 45: Comparison of cumulative velocity distribution of filtered and dried crystals between synthetic and real process solution studies. The distributions ranges like this example; 10% of distribution $\leq 23\mu$m/s etc.

Both synthetic and real process crystallization processes via single-step experiments show similar structures; sphere-like clusters with smaller clusters and individual crystals surrounding, shown in Figure 46 and 47. In the synthetic system there exist thinner plate-like crystals covering the clusters, and in the real process system, these plate-like crystals are thicker and have more brick-like structures. As seen in Figure 48 and 49 the continuous addition of the acid experiments in both systems show more elongated clusters with smaller crystals covering the surface, compared to the single-step experiments, and these elongated clusters seem to be more widespread in the real process system. More sphere-like cluster present in single-step addition of the acid experiments might indicate more pronounced spherulitic growth in single-step experiments, which correlates well with the high initial supersaturation in these experiments. The SEM images show similar trends in experiments from the same acid addition procedures, and support the trends in the filtration performance and size data. In the filtration and size data, it was also seen that the single-step and continuous real process experiments undergo smaller differences compared to the synthetic system. This is also supported by the SEM images as thicker plate-like and brick-like crystals are seen in both single-step and continuous addition of the acid experiments in RPS studies, while in SS studies brick-like crystals are not observed in single-step experiments, and these plate-like crystals look thinner. Additional SEM images can be found in Section I in the Appendix.

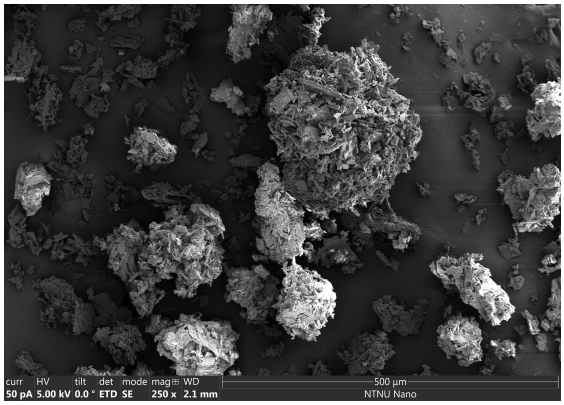

Figure 46: SEM image of final crystals from single-step addition of the acid, in the synthetic system.

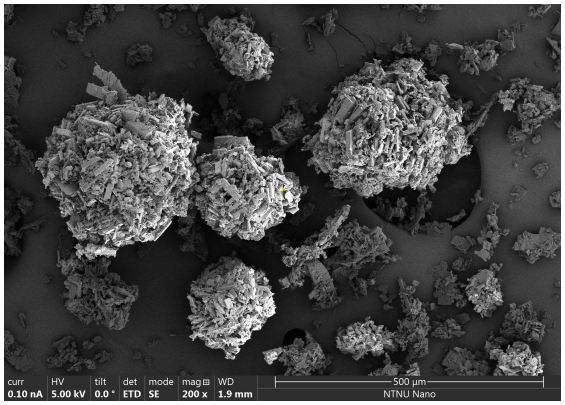

Figure 47: SEM image of final crystals from single-step addition of the acid, in the real process system.

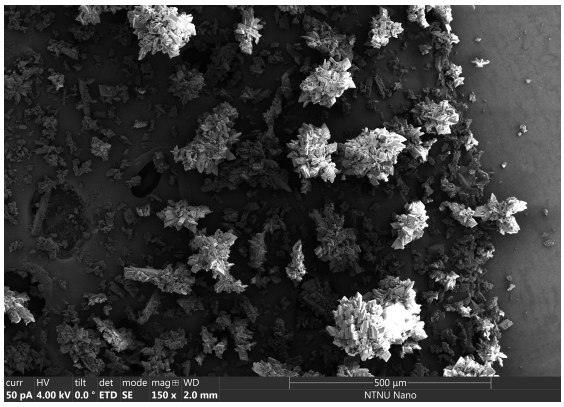

Figure 48: SEM image of final crystals from continuous addition of the acid, in the synthetic system.

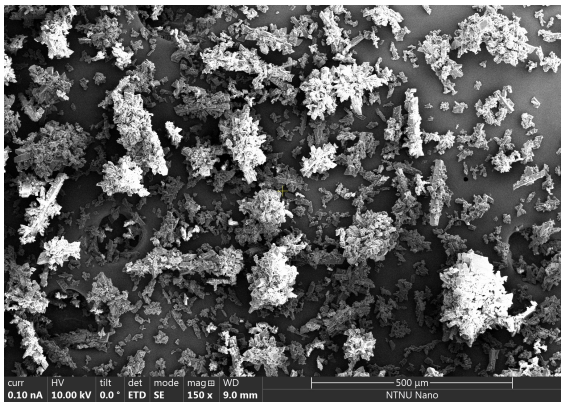

Figure 49: SEM image of final crystals from continuous addition of the acid, in the real process system.

5.3.3 Concluding Remarks

From a comparison of the synthetic system and real process system, trends and differences were determined in terms of the level of control in the systems, filtration performance, and crystal characteristics. The synthetic system possesses stricter control due to several optimization experiments, fewer preparation steps prior to crystallization, and control over the methanol-water solvent ratio. The real process system has impurities present, that might affect the crystal characteristics, and variations in impurity content and no optimization experiments could result in higher standard deviations and small batch-to-batch variations. However, both systems produced highly crystalline and pure products with high yields, fast filtration rates, and low standard deviations, indicating robust systems with consistent products. Filtration data showed similar trends in filterability, where semi-batch experiments showed improved filtration performance. This was supported by results from sedimentation velocities and similarities in structures from SEM images. Still, results from real process studies showed smaller differences in the filtration data and size data between single-step and continuous addition of the acid procedures. This was also supported by SEM images, with more similar crystal structures between the procedures in the real process system. SEM images revealed sphere-like clusters in all acid addition procedures, and it was indicated from a cross-section of a sphere-like

cluster that this could point towards spherulitic growth mechanisms. However, the crystals covering these sphere-like clusters have different structures, and continuous addition of the acid experiments in both systems showed both sphere-like clusters and several larger elongated crystals covered by smaller crystals. The supersaturation profiles dictate the final crystal characteristics, and in single-step addition of the acid experiments, a high initial supersaturation is generated resulting in smaller particles. In continuous addition of the acid experiments the supersaturation profile is generated at a lower level, indicating growth dominated-mechanisms producing larger crystals. These theories are in good agreement with results from filtration data, size data, and structures observed in SEM images.

Despite differences in the system setups, studies mark that both systems are robust and that the synthetic system is representable to the real process systems with the justification of similar trends. Investigations in this thesis revealed that semi-batch mode is advantageous to minimize energy demands in the filtration of slurry from crystallization of AA.

6 Conclusion

In this thesis, investigations regarding the crystallization and subsequent filtration process of AA were carried out. The crystallization process was achieved as a neutralization reaction followed by cooling crystallization. The effects of different acid addition procedures on filtration performance and final crystal characteristics were disclosed. Both synthetic and real process systems were investigated and compared to evaluate trends and differences. The main differences between the systems are the levels of control and the presence of impurities in the real process system. Strict control was established in the synthetic system, while the real process system possesses alleviated control confirmed by slightly higher standard deviations in results. Despite this, both systems showed low standard deviations, indicating reliable and consistent results. Highly crystalline and pure precipitates of AA were verified by FTIR, XRD, and HPLC analyses, whereas high yields and fast filtration rates, indicated robust systems. Filtration experiments showed similar trends in both systems; semi-batch experiments resulted in improved filterability in terms of specific cake resistance, and continuous addition of the acid experiments showed the best results. The moisture content was determined and exhibit values in the same range for both systems. Size data and morphology from SEM images were used to support the filtration data, and agreed well with filtration data. Continuous addition of the acid experiments showed higher sedimentation velocities, explained by larger particle sizes. From similar trends in filterability, size measurements, and morphologies, the synthetic system was assumed to be representable to the real process system, and can further be used for investigations and optimization. The different characteristics induced in both systems via variations in acid addition were less pronounced in real process system, which should be recognized in further investigations. A cross-section of a sphere-like cluster from the real process system via single-step addition of the acid was observed from a SEM image and could point towards spherulitic growth mechanisms via multidirectional growth. Precipitates via single-step experiments showed more pronounced sphere-like clusters, and are in good agreement with the high initial supersaturation levels that can induce spherulitic growth. Images from precipitates from continuous addition of the acid experiments revealed several

elongated brick-like crystals and some sphere-like clusters. A continuous addition of the acid experiment at 20°C from the real process system showed significantly higher specific cake resistance, with lower sedimentation velocities and significant differences in morphology, indicating that neutralization reaction of AA should be carried out at 50°C. Semi-batch procedures generate a gradual build-up of the supersaturation, indicating crystal growth as the dominating mechanism, resulting in larger particles that are easier to handle during filtration. Semi-batch acid addition procedures showed improved filterability and should be selected to minimize energy consumption in the filtration process.

7 Future Outlooks

The crystallization of AA provides opportunities for further optimization and investigations. In this section suggestions of future outlooks to advance the understanding and further control the system are outlined. It would be interesting to see where the limit of the number of steps in multi-step experiments is before results are similar to single-step experiments. In continuous addition of the acid experiments, it would be interesting to increase the feed rate of the acid to investigate its effects before unwanted results appear. Fewer steps in multi-step experiments and higher feed rates in continuous addition of the acid experiments could be advantageous in terms of batch cycle time. In the present studies, indications towards secondary nucleation mechanisms were suggested. This could stem from parent crystals present in suspension in combination with high supersaturation generated at additional acid portions. Also, a relatively high stirring rate is used in this work, and can also affect secondary nucleation mechanisms. Therefore, experiments with different stirring rates would be interesting to investigate the effect on secondary nucleation mechanisms. Initial analysis on sedimentation velocities of crystals directly from suspension was performed without optimization. It would be necessary to optimize the preparation and analysis methods to compare sizes prior to and after filtration and drying. The methanol-water solvent ratios are different in the synthetic and real process systems, and it could be useful to do experiments with other solvent ratios to point out the effects of for example higher water contents in the solvent. Seeding could be implemented to gain control over crystal sizes and CSD. Relatively high moisture contents are determined from this work, and studies to decrease the moisture contents would be necessary to decrease energy demands connected to drying. The long-term goal in the industrial production of AA may be to obtain a continuous process by using for example plug-flow reactor or a continuous stirred-tank reactor. Continuous processes can be advantageous in terms of more flexible operation, smaller facilities, decreased costs, high productivity and quality, and process automation [8]. Research in continuous reactor systems at lab-scale should be carried out before implementing a continuous process in a larger scale. Scale-up of this system to pilot scale would be of interest before scaling up to production scale.

Bibliography

[1] H.-H. Tung, E. Paul, M. Midler, and J. McCauley. *Crystallization of Organic Compounds: An Industrial Perspective*. Wiley, Canada, 2009.

[2] J. Chen, B. Sarma, J. M. B. Evans, and A. S. Myerson. Pharmaceutical crystallization. *Crystal Growth and Design*, pages 887–895, 2018.

[3] S. Teychené, I. Rodríguez-Ruiz, and R. K. Ramamoorthy. Reactive crystallization: from mixing to control of kinetics by additives. *Elsevier*, pages 1–19, 2020.

[4] R. Beck, A. Häkkinen, D. Malthe-Sørenssen, and J.-P. Andreassen. The effect of crystallization conditions, crystal morphology and size on pressure filtration of l-glutamic acid and an aromatic amine. *Elsevier*, pages 549–558, 2009.

[5] R. J. Wakeman. *Filtration : equipment selection, modelling and process simulation*. Elsevier Advanced Technology, Oxford, 1999.

[6] A. Meyerson. *Handbook of Industrial Crystallization, 2nd Edition*. ButterWorth-Heinemann, 2002.

[7] A. E. Lewis, M. Seckler, H. Kramer, and G. van Rosmalen. *Industrial Crystallization: Fundamentals and Applications*. Cambridge University Press, 2015. "`http://gen.lib.rus.ec/book/index.php?md5=3cb0ebaaa2f8aa2d4fd0bbec975ebb0c`".

[8] T. C. Lai, S. Ferguson, L. Palmer, B. L. Trout, and A. S. Myerson. Continuous crystallization and polymorph dynamics in the l-glutamic acid system. *ASCPublication*, pages 1382–1390, 2014.

[9] J. W. Mullin. *Crystallization*. Butterworth-Heinemann, Oxford, 4th ed. edition, 2001.

[10] K. M. Jim, K. J. Kim, and Y. N. Jang. Effect of supersaturation on the particle size of ammonium sulfate in semibatch evaporative crystallization. *Industrial and engineering chemistry research*, 52(32):11151–11158, 2013.

[11] M. A. McDonald, H. Salami, P. R. Harris, C. E. Lagerman, X. Yang, A. S. Bommarius, M. A. Grover, and R. W. Rousseau. Reactive crystallization: a review. *React. Chem. Eng.*, 6:364–400, 2021.

[12] J. Ulrich and C. Strege. Some aspects of the importance of metastable zone width and nucleation in industrial crystallizers. *Journal of Crystal Growth*, 237-239:2130–2135, 2002.

[13] K. Sangwal. Recent developments in understanding of the metastable zone width of different solutesolvent systems. *Journal of crystal growth*, 318(1):103–109, 2011.

[14] V. I. Kalikmanov. Nucleation theory, 2013.

[15] W. Beckmann. Crystallization: Basic concepts and industrial applications, 2013.

[16] S. S. Kadam, S. A. Kulkarni, R. Coloma Ribera, A. I. Stankiewicz, J. H. ter Horst, and H. J. M. Kramer. A new view on the metastable zone width during cooling crystallization. *Chemical engineering science*, 72:10–19, 2012.

[17] S. G. Agrawal and A. H. J. Paterson. Secondary nucleation: Mechanisms and models. *Chemical engineering communications*, 202(5):698–706, 2015.

[18] S. S. Kadam, H. J. M. Kramer, and J. H. ter Horst. Combination of a single primary nucleation event and secondary nucleation in crystallization processes. *Crystal growth and design*, 11(4):1271–1277, 2011.

[19] S. Xu, Z. Hou, and Y. Chuai, X.and Wang. Overview of secondary nucleation: From fundamentals to application. *Industrial and engineering chemistry research*, 59(41):18335–18356, 2020.

[20] I. Ådnebergli. Effects of variations in supersaturation build up on final crystal properties of an aromatic amine. *Chemical Engineering, NTNU*, 2020.

[21] M. Broby. Mineral scaling in natural gas processing : a classical crystal growth phenomenon, 2019.

[22] J.-P. Andreassen, R. Beck, and E. M. Flaten. Investigations of spherulitic growth in industrial crystallization, 2010.

[23] E. Ortega-Rivas. *Unit Operations of Particulate Solids : Theory and Practice (Edition 1)*. CRC Press, Baton Rouge, 2016.

[24] H. Wu, Z. Dong, H. Li, and M. Khan. An integrated process analytical technology (pat) approach for pharmaceutical crystallization process understanding to ensure product quality and safety: Fda scientist's perspective. *Organic process research and development*, 19(1):89–101, 2015.

[25] L. L. Simon and ... M. S. Chiu. Assessment of recent process analytical technology (pat) trends: A multiauthor review. *Organic process research and development*, 19(1):3–62, 2015.

[26] Z. Gao, S. Rohani, J. Gong, and J. Wang. Recent developments in the crystallization process: Torward the pharmaceutical industry. *Elsevier*, pages 343–353, 2017.

[27] Y. Gao, T. Zhang, Y. Ma, F. Xue, Z. Gao, B. Hou, and J. Gong. Application of pat-based feedback control approaches in pharmaceutical crystallization. *Crystals (Basel)*, 11(3):221, 2021.

[28] S. Yu, Y. Zhang, and X. Z. Wang. Improved understanding of cefixime trihydrate reactive crystallization and process scale-up with the aid of pat. 23(2):177–188, 2019.

[29] M. Trampuž, D. Teslić, and B. Likozar. Process analytical technology-based (pat) model simulations of a combined cooling, seeded and antisolvent crystallization of an active pharmaceutical ingredient (api). *Powder Technology*, 366:873–890, 2020.

[30] Department of Economic United Nations and Sustainable Development Social Affairs. *The 17 Goals [internet]*, "2021, (accesses 09/05/2021)". "`https://sdgs.un.org/goals`".

[31] P. T. Anastas. Green chemistry : theory and practice, 1998.

[32] W. McDonough, M. Braungart, P. T. Anastas, and J. B. Zimmerman. Applying the principles of green engineering to cradle-to-cradle design. *Environmental science and technology*, 37(23):434A–441A, 2003.

[33] A. Cote, D. Erdemir, K. P. Girard, D. A. Green, M. A. Lovette, E. Sirota, and N. K. Nere. Perspectives on the current state, challenges, and opportunities in pharmaceutical crystallization process development. *Crystal growth and design*, 20(12):7568–7581, 2020.

[34] S. Zhao, J. Gao, S. Ma, C. Li, Y. Ma, Y. He, J. Gong, F. Zhou, B. Zhang, and W. Tang. Mechanism and modelling of reactive crystallization process of lithium carbonate. *Processes*, 7(5), 2019.

[35] S. You, Y. Zhang, S. Cao, F. Chen, and Y. Zhang. Crystallization kinetics of monosodium aluminate hydrate in concentrated sodium aluminate solutions. *Industrial & Engineering Chemistry Research*, 51(22):7736–7741, 2012.

[36] W. Zhang, F. Zhang, L. Ma, J. Yang, J. Yang, and H. Xiang. Prediction of the crystal size distribution for reactive crystallization of barium carbonate under growth and nucleation mechanisms. *Crystal Growth & Design*, 19(7):3616–3625, 2019.

[37] C. Y. Tai and P.-C. Chen. Crystal growth and agglomeration of calcium sulfite hemihydrate crystals. *Industrial & Engineering Chemistry Research*, 34(4):1342–1351, 1995.

[38] E. L. Paul, H.-H. Tung, and M. Midler. Organic crystallization processes. *Powder technology*, 150(2):133–143, 2005.

[39] Advances in organic crystal chemistry : Comprehensive reviews 2015, 2015.

[40] Advances in organic crystal chemistry : Comprehensive reviews 2020, 2020.

[41] A. Dafnomilis, S. Diab, A. D. Rodman, A. G. Boudouvis, and D. I. Gerogiorgis. Multiobjective dynamic optimization of ampicillin batch crystallization: Sensitivity analysis of attainable performance vs product quality constraints. *Industrial and engineering chemistry research*, 58(40):18756–18771, 2019.

[42] M. Li, Z. Shang, and B. Hou. Optimizing the aspect ratio of cephalexin in reactive crystallization by controlling supersaturation and seeding policy. *Springer*, pages 348–356, 2019.

[43] H. P. Jones, R. J. Davey, and B. G. Cox. Crystallization of a salt of a weak organic acid and base: Solubility relations, supersaturation control and polymorphic behavior. *The journal of physical chemistry. B*, 109(11):5273–5278, 2005.

[44] R. Beck, R. Heskestad, D. Malthe-Sørenssen, A. Häkkinen, M. Louhi-Kultanen, and J.-P. Andreassen. Ageing of spherulites of an industrial relevant aromatic amine derivative. *Crystal research and technology (1979)*, 45(2):204–212, 2010.

[45] Å. Linga. Effects of seeding on the crystallization behaviour and filtration abilities of an aromatic amine. *Chemical Engineering, NTNU*, 2017.

[46] W. J. Liu, C. Y Ma, J. J. Liu, Y. Zhang, and X. Z. Wang. Continuous reactive crystallization of pharmaceuticals using impinging jet mixers. *AIChE journal*, 63(3):967–974, 2017.

[47] R. Zauner and A. G. Jones. Mixing effects on product particle characteristics from semi-batch crystal precipitation. *Chemical Engineering Research and Design*, 78(6):894–902, 2000. Process Design.

[48] Z. K. Nagy and E. Aamir. Systematic design of supersaturation controlled crystallization processes for shaping the crystal size distribution using an analytical estimator. *Chemical engineering science*, 84:656–670, 2012.

[49] N. C. S. Kee, R. B. H. Tan, and R. D. Braatz. Selective crystallization of the metastable α-form of l-glutamic acid using concentration feedback control. *Crystal growth & design*, 9(7):3044–3051, 2009.

[50] V. Liotta and V. Sabesan. Monitoring and feedback control of supersaturation using atr-ftir to produce an active pharmaceutical ingredient of a desired crystal size. *Organic process research and development*, 8(3):488–494, 2004.

[51] T. Zhang, B. Nagy, B. Szilágyi, J. Gong, and Z. K. Nagy. Simulation and experimental investigation of a novel supersaturation feedback control strategy for cooling crystallization in semi-batch implementation. *Chemical Engineering Science*, 225:115807, 2020.

[52] S. Khan, C. Y Ma, T. Mahmud, R. Y. Penchev, K. J. Roberts, J. Morris, L. Özkan, G. White, B. Grieve, A. Hall, P. Buser, N. Gibson, P. Keller, P. Shuttleworth, and C. J. Price. In-process monitoring and control of supersaturation in seeded batch cooling crystallisation of l-glutamic acid: From laboratory to industrial pilot plant. *Organic process research & development*, 15(3):540–555, 2011.

[53] F. Zhang, T. Liu, W. Chen, C. Y Ma, and X. Z. Wang. Seed recipe design for batch cooling crystallization with application to l-glutamic acid. *Industrial & engineering chemistry research*, 58(8):3175–3187, 2019.

[54] D. Acevedo, Y. Tandy, and Z. K. Nagy. Multiobjective optimization of an unseeded batch cooling crystallizer for shape and size manipulation. 54(7):2156–2166, 2015.

[55] T. Zhang, B. Szilágyi, J. Gong, and Z. K. Nagy. Novel semibatch supersaturation control approach for the cooling crystallization of heat-sensitive materials. *AIChE journal*, 66(6):n/a, 2020.

[56] K. Pal, Y. Yang, and Z. K. Nagy. Model-based optimization of cooling crystallization of active pharmaceutical ingredients undergoing thermal degradation. *Crystal growth & design*, 19(6):3417–3429, 2019.

[57] G. D. Dickey. *Filtration*. Reinhold Publishing Corporation, 1961.

[58] R. Wakeman. The influence of particle properties on filtration. *Separation and purification technology*, 58(2):234–241, 2007.

[59] R. Beck and J.-P. Andreassen. Influence of crystallization conditions on crystal morphology and size of caco3 and their effect on pressure filtration. *AIChE journal*, 58(1):107–121, 2012.

[60] D. Bourcier, J. P. Féraud, D. Colson, K. Mandrick, D. Ode, E. Brackx, and F. Puel. Influence of particle size and shape properties on cake resistance and compressibility during pressure filtration. *Chemical engineering science*, 144:176–187, 2016.

[61] C. Tien. Introduction to cake filtration : analyses, experiments and applications, 2006.

[62] C. L. Yaws. Handbook of viscosity : Vol. 1 : Organic compounds c_1 to c_4, 1995.

[63] E. Antonopoulou, C. F. Rohmann-Shaw, T. C. Sykes, O. J. Cayre, T. N. Hunter, and P. K. Jimack. Numerical and experimental analysis of the sedimentation of spherical colloidal suspensions under centrifugal force. *Physics of fluids (1994)*, 30(3):30702, 2018.

[64] A. De. *Sedimentation Process and Design of Settling Systems*. Springer India, 2017.

[65] LUM GmbH. The all-in-one dispersion analyser, "2020 (accessed 06.05.2021)". "`https://www.lum-gmbh.com/lumisizer_en.html`".

[66] M. Huttunen, L. Nygren, T. Kinnarinen, B. Ekberg, T. Lindh, V. Karvonen, J. Ahola, and A. Häkkinen. Real-time monitoring of the moisture content of filter cakes in vacuum filters by a novel soft sensor. *Separation and purification technology*, 223:282–291, 2019.

[67] I. B. Jenssen, S. Ucar, O. M. Dotterud, O. Bøckman, and J.-P. Andreassen. Investigating the effects of process parameters on the filtration performance of ferric hydroxide in a continuous msmpr reactor. *Hydrometallurgy*, 202:105594, 2021.

[68] S. Clercq, A. Mouahid, G. Pèpe, and E. Badens. Prediction of crystal–solvent interactions in a supercritical medium: A possible way to control crystal habit at high supersaturations with molecular modeling. *Crystal Growth & Design*, 20(10):6863–6876, 2020.

[69] M. Giulietti, M. M. Seckler, S. Derenzo, M. I. Ré, and E. Cekinski. Industrial crystallization one and precipitation from solutions: State of the technique. *Brazilian journal of chemical engineering*, 18(4):423–440, 2001.

[70] S. Bordawekar, Z. Kuvadia, P. Dandekar, S. Mukherjee, and M. Doherty. Interesting morphological behavior of organic salt choline fenofibrate: Effect of supersaturation and polymeric impurity. *Crystal growth & design*, 14(8):3800–3812, 2014.

[71] S. J. Urwin, G. Levilain, I. Marziano, J. M. Merritt, I. Houson, and J. H. Ter Horst. A structured approach to cope with impurities during industrial crystallization development. *Organic process research & development*, 24(8):1443–1456, 2020.

[72] I. Pritula and K. Sangwal. *Handbook of Crystal Growth: Fundamentals of Crystal Growth from Solutions (Second Edition).* Elsevier, 2015.

[73] T. M. Letcher. *Development and applications in solubility.* RSC Publications, 2007.

[74] Merck. *IR Spectrum Table and Chart [internet]*, "2020, (accessed 17.12.2020)". "`https://www.sigmaaldrich.com/technical-documents/articles/biology/ir-spectrum-table.html`".

Appendix

A Molar Mass of Compounds

The molar mass of compounds used in calculations is given in the table below.

Table 6: Molar mass used in calculations.

Compound	Mm [g/mol]
AA	363.8
NaOH	40.0
Tris buffer	121.1

B Calibration Curve for Experiments at NTNU

In previous work [20], a calibration curve was constructed. This was further used for concentration measurements in this thesis, and discussion on uncertainty in concentration measurements applies for synthetic solution experiments in this work.

B.1 Calculations

The calibration curve was constructed by measuring the absorbance of solutions with known concentrations by UV-Vis spectrometry. A 0.5L stock solution of AA at 0.1M was used, the amount of AA needed was calculated from the equations below.

$$n_{\mathrm{AA}} = c \cdot V = 0.1 mol/L \cdot 0.5 L = 0.01 mol \tag{B.1}$$

$$m_{\mathrm{AA}} = n \cdot Mm = 0.01 mol \cdot 363.8 g/mol = 3.638 g \tag{B.2}$$

Equivalent amount of NaOH was added, the amount needed was calculated from:

$$m_{\mathrm{NaOH}} = 0.01mol \cdot 40g/mol = 0.4g \tag{B.3}$$

Four additional solutions, with $V = 0.05$L, were made by diluting the stock solution with different dilution volumes, shown in the equation below.

$$V_{\mathrm{new}} = \frac{C_{\mathrm{new\ conc.}} \cdot V}{C_{\mathrm{stock}}} = \frac{0.08mol/L \cdot 0.05L}{0.1mol/L} = 0.04L \tag{B.4}$$

V_{new} is the volume withdrawn from the stock solution to prepare the new solution with concentration, $C_{\mathrm{new\ conc.}}$.

B.2 Establishment of Calibration Curve

10mM Tris buffer at pH 8 was prepared by dissolving the appropriate amount of Trizma base in water and adjusting the pH with 1M HCl. A stock solution of 0.1M AA was prepared by dissolving the salt in the presence of equivalent moles of NaOH. The stock solution was diluted with water to prepare four solutions at different concentrations, respectively 0.01M, 0.02M, 0.05M, and 0.08M. The four diluted solutions and the stock solution were then diluted in a 1:250 ratio of solution:Tris buffer. 4mL cuvettes were washed with the further measured solution and the absorbance was measured three times each to quantify the uncertainty of the measurements. The absorbance of the Tris buffer was also collected three times and subtracted from the measurements for blank correction.

The established calibration curve is shown in Figure B.1, with corresponding error bars from absorbance measurements. The concentration of AA was calculated by Equation B.5 and corresponds to the linear graph. C_{AA} was multiplied with the dilution factor d for measurements of diluted liquid samples. For the solutions prepared it would be ideal to use the same solvent as for the crystallization experiments, but using water instead was assumed to not affect the results. Water was used to not affect the results as the amount of methanol in the final measured solution would

be smaller than 1% due to dilution in 1:250 ratio with Tris buffer.

$$C_{\mathrm{AA}}[\mathrm{mol/L}] = \frac{Abs - 0.0006349}{9.9031746} \tag{B.5}$$

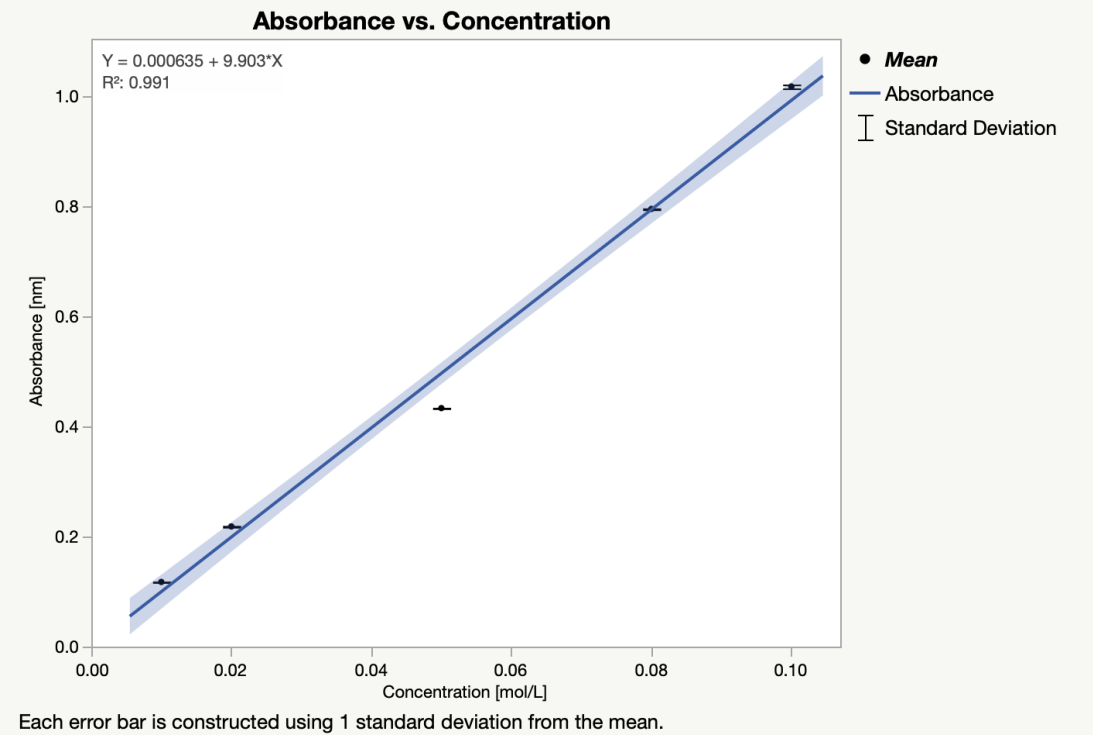

Figure B.1: The established calibration curve as a linear regression between the concentration of AA and absorbance. With corresponding error bars from absorbance measurements.

B.3 Concentration of AA in Reaction Solution

The concentration of AA in the liquid phase was determined by absorbance measurements with UV-Vis spectrophotometry. Liquid samples of 2-5mL from the batch reactor were withdrawn at different times after acid addition by a syringe coupled with a tube and filtered through a 0.22μm syringe filter (Millipore) to remove solid crystals. Samples with high concentrations were diluted to ensure sufficiently low and stable values of absorbance. 1mL of the collected sample was diluted in a 1:250 ratio of sample:Tris buffer. Before absorbance measurements, 4mL plastic cuvettes were rinsed with the sample. The absorbance values were measured from 3 parallels

for each sample and displayed with three digits. Tris buffer was freshly prepared before each experiment and its absorbance was measured for blank correction.

B.4 Discussion on Uncertainty in Concentration Measurements

The constructed calibration curve was used to calculate the concentration at initial, intermediates, and final steps during all the crystallization experiments. R^2 is the coefficient of determination, which ranges from 0 to 1. It is a statistical measure representing the proportion of the variance for the dependent variable, here concentration, predicted from the independent variable, here wavelength, from UV-Vis. From Figure B.1 the $R^2 = 0.991$, meaning that the curve shows high linearity, creating a good base for concentration measurements. In the curve, small standard deviations in each point are shown, these standard deviations are based on three UV-vis samples in each step. The blue area surrounding the curve is the 95% confidence interval, which defines the range of values that are believed to contain, with a 95% probability, the true value of the population mean. One thing to keep in mind is that the calibration curve is constructed from known concentrations, but there is uncertainty in these values connected to inaccuracies in the method solution preparation. Overall the established calibration curve shows good statistical data and the concentration measurements thus seem reasonable.

When withdrawing samples there was a risk that the methanol-water solvent contributed to deviations in the concentration measurements as it evaporates easily. Possible differences in evaporation rate with higher pressure of the solvent vapor over the solution, than that of the solute, could enable the solvent to evaporate[72]. Also, when samples were withdrawn there was a temperature difference between the sample and the surroundings, which might evoke cooling crystallization possibly resulting in a lower concentration than the actual one in the reactor. At higher concentrations, the solution was diluted twice to get adequate UV-Vis measurements, which increases the probability of inaccuracies and uncertainty in the resulting concentration value.

C Solubility Curve and Reaction Time of Neutrtralization Reaction of AA

In previous work [20], the solubility limits of the neutralization reaction of AA were determined by the solubility curve of AA at equivalents of acid, and are explained below. Here, Exp.0 and Exp.1 refer to single-step experiments, Exp.2 and Exp.4 refers to multi-step experiments. The initial concentration of the experiments is approximately 0.3M. The reaction time of the neutralization reaction of AA was also determined.

C.1 Discussion on Solubility Curve of AA

The solubility curve of AA at equivalent addition of HCl was constructed and is shown in Figure C.2. The figure shows decreasing solubility of AA with the addition of HCl, as expected. The curve is created by Exp.0 (single-step), Exp.1 (single-step), Exp.2 (multi-step), and Exp. 4 (multi-step) and gives information about the solubility limits of the neutralization reaction of AA. Exp.1, Exp.2, and Exp.4 give the solubility of AA at equivalents of HCl at 50°C, and the experiments show the same trend, especially for the endpoint at 1.1 equivalent HCl. In Exp.4 additional steps were performed to confirm that the equilibrium of the crystallization was reached. The endpoint was assumed reached due to similar concentrations for the three last steps, illustrated by the flat curve in the final steps.

In Exp.0 the temperature was decreased to 20°C after 1h crystallization, and left for the night, which gives the solubility of AA at 20°C at 100% neutralization. It shows a lower solubility than the same amount of HCl at 50°C, which is expected as the solubility in most cases decreases with decreasing temperatures. The decrease in kinetic energy that comes with lower temperatures makes the solvent molecules less effectively break apart the solute molecules that are held together by intermolecular attractions. Less heat into the system follows Le Chatlier's principle; the system adjusts to this defect heat energy by decreasing the precipitation reaction, thus decreasing the solubility [73]. From the graphs of Exp.2 and Exp.4, one can see that

the curves decrease more slowly between the two first points than for the rest of the curve. Because NaOH was added at 1.1 equivalents of the AA salt, the added strong acid will neutralize the excess strong base before precipitating crystals. The standard deviations in all experiments are from UV-Vis measurements and show small deviations. Exp.2 and Exp.4 were performed as parallels, but for the first two steps in Exp.4 samples were withdrawn every 20min to investigate the reaction time of crystallization. After 20min the reaction was not finished which gives reason for higher standard deviations in each point.

From the graphs of Exp.2 and Exp.4, one can see that the curves decrease more slowly between the two first points than for the rest of the curve. Because NaOH was added at 1.1 equivalents of the ABA-HCl salt, the added strong acid will neutralize the excess strong base before precipitating crystals.

The standard deviations in all experiments are from UV-Vis measurements and show small deviations. Exp.2 and Exp.4 were performed as parallels, but for the first two steps in Exp.4 samples were withdrawn every 20min to investigate the reaction time of crystallization. After 20min the reaction was not finished which gives reason for higher standard deviations at each point.

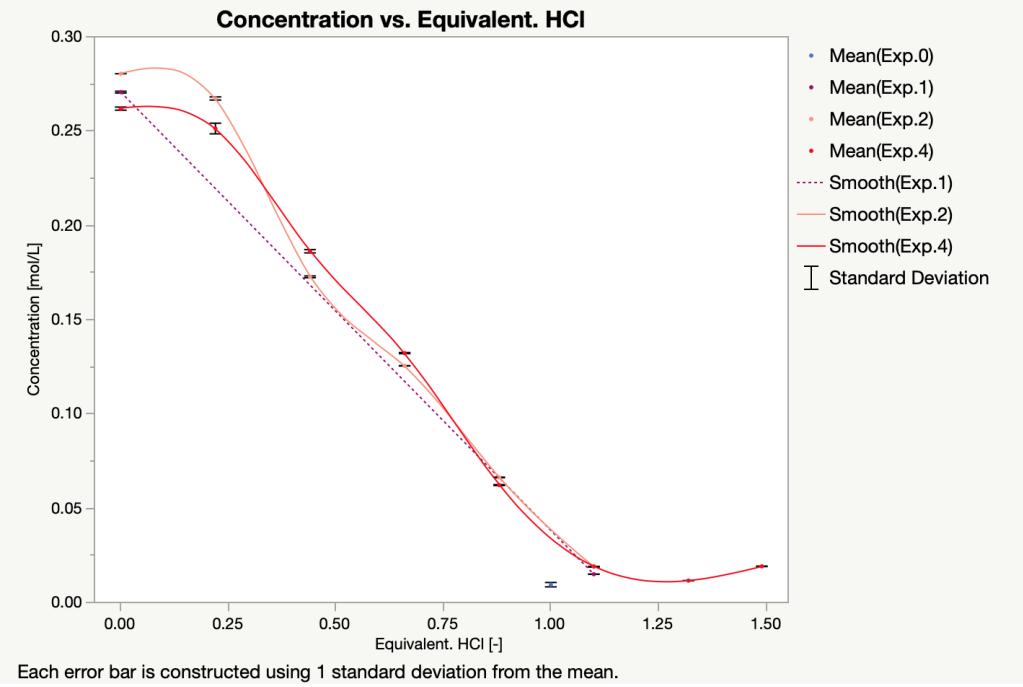

Figure C.2: The solubility of AA in equivalents amount of HCl, with corresponding standard deviations from UV-Vis measurements. The reddish points refer to the experiments performed at 50°C and the blue point at 20°C

C.2 Reaction Time of Neutralization Reaction of AA

The reaction time was investigated in Exp.0 and Exp.1. In Exp.0 the concentration was measured after 1h, then the temperature was decreased to 20°C and left for the night. The day after a new sample was withdrawn for concentration measurement and showed the same value. From this, the crystallization was assumed to be finished after 1h. In Exp.1 this was verified by taking samples after 1h and 5.5h at the same temperature and showed the same result. These observations of the reaction time give reason to assume that the crystallization was finished after 1h. In Exp.4 the reaction time was checked to see if it could be shorter than 1h. Samples were withdrawn every 20min in the first three acid addition steps. The concentrations from the samples showed that the reaction was done after 40min to 1h. In the first and third addition, the concentration was still decreasing from 40min to 1h, while in the second it was quite similar in this time range. Because of variations between the additions the reaction time was determined to be finished after 1h.

D FTIR Analysis

The results from FTIR analysis of single-step and multi-step experiments performed in previous work [20] are shown in Figure D.3. An analysis was performed to investigate the functional groups and fingerprint region in precipitates. The spectrum is divided into two regions: the functional group region from 4000-1500cm^{-1}, and the fingerprint region for the remaining part. The peaks of the spectra are numerated from 1-8 and explained below [74].

1. The broad peak seen Exp.2 experiment, which also appears for the Exp.0 and Exp.1. Broad peaks at 3230-3550cm^{-1} corresponds to **OH groups**. It could be NH-stretching of aniline, but then it should be closer to 3500cm^{-1}.

2. The narrow peak at 2970cm^{-1} corresponds to **CH**.

3. The peak at 2880cm^{-1} corresponds to **amine salt**, which usually is around 3000-2800cm^{-1}.

4. The peak at 1650cm^{-1} could be different functional groups. It could be NH from a primary amine, double bonding of carbon (C=C) from the aromatic amine, or secondary amide (C=O).

5. This peak could also correspond to the secondary amide (C=O).

6. The sixth and seventh peak could correspond to the amine, secondary or primary alcohol.

7. Mentioned above.

8. The peak at 880cm^{-1} could correspond to the CH out of plane bending vibration from the aromatic amine. It could also correspond to the NH wag from primary and secondary amines.

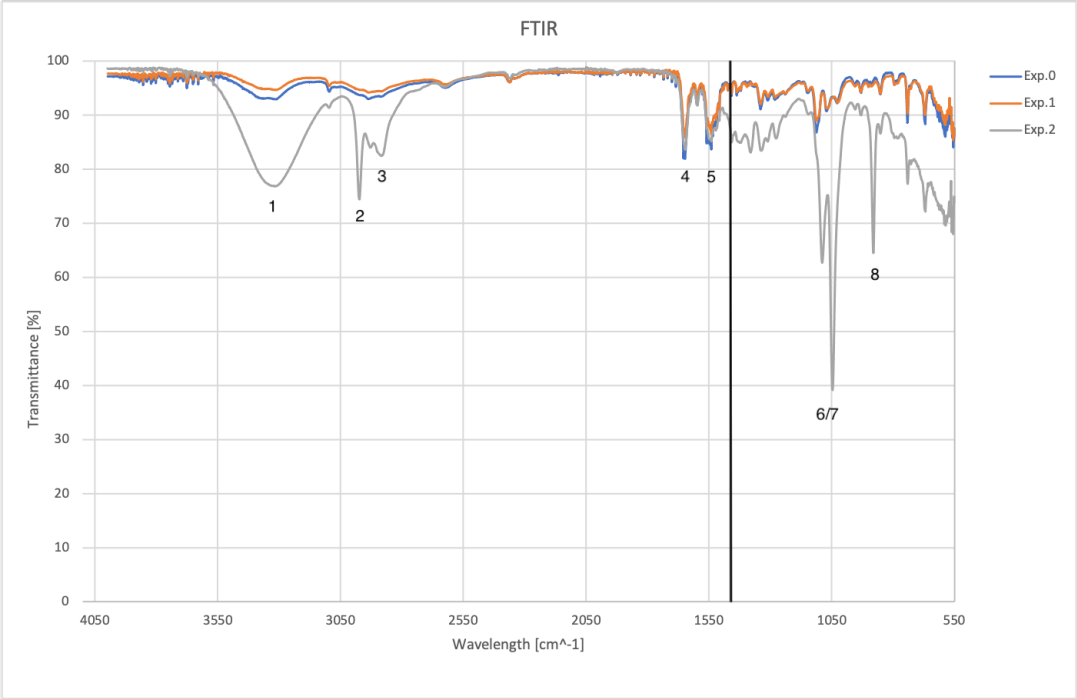

Figure D.3: FTIR spectrum of single-step and multi-step addition of the acid experiments, Exp.0 and Exp.1 are single-step experiments and Exp.2 is a multi-step experiment.

E Calculation of Moisture Content

The moisture content of filter cakes, M, is defined as the ratio of the mass of liquid in the cake to the total mass of the wet cake [5],

$$M[\text{wt}\%] = \frac{\text{evaporated liquid}}{\text{mass of wet cake}}. \tag{E.6}$$

F Calculation of Yield

Yield, Y, is a measure of the percentage AA recovered by crystallization. The yield of the experiments was calculated from the equation below. c_0 is the initial concentration of AA and c_f is the final concentration of AA.

$$Y[\%] = \frac{c_0 - c_f}{c_0} \cdot 100\%. \tag{F.7}$$

G Filtration Experiments and Calculations of Specific Filter Cake Resistance

Filtration experiments were performed by filtering the slurry of synthetic and real process solutions of AA. The filtration weight was recorded as a function of time with LABview and iPhone, for SS and RPS, respectively. The weight and time were further plotted, shown in the example in Figure G.4. Then, by using the density and mass of the filtrate, the volume was calculated from,

$$V = \frac{m}{\rho_l} \tag{G.8}$$

Further, the $\frac{t-t_0}{V-V_0}$ was plotted as a function of volume, and the linear part of the graph was found by obtaining a trend line equation, shown in the example in Figure G.5. The slope of the trend line was used to find the specific cake resistance, α, from $\frac{\alpha c \mu}{2A^2 \Delta p}$ in the equation;

$$\frac{t - t_0}{V - V_0} = \frac{\alpha c \mu}{2A^2 \Delta p} V + \frac{\mu R}{A \Delta p}. \tag{G.9}$$

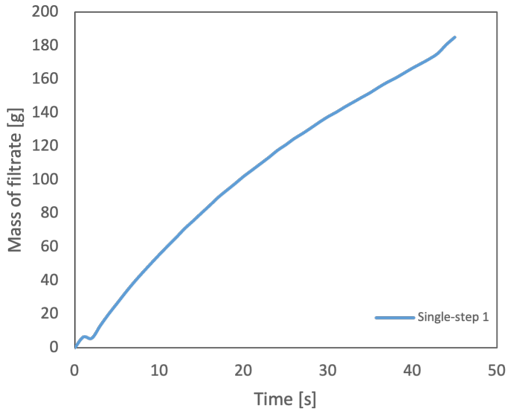

Figure G.4: Example of the recorded weight of filtrate as a function of time.

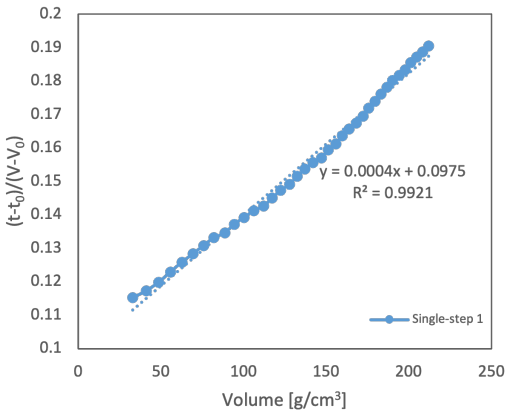

Figure G.5: Example of trend line from plotting $\frac{t-t_0}{V-V_0}$ as a function of volume.

In the figures below, all filtration curves and trend lines for different acid addition procedures in both synthetic and real process systems are shown. The trend lines are in the figures to the left, and the coefficients of determination, R^2, are given. Table 7 gives an overview of all R^2 values. Experiments from the synthetic system indicate high linearity, explained by high R^2 values. In the synthetic system, 300mL of the slurry was filtrated and give enough time to get data points to plot a linear curve. The experiments in the real process system show, in general, lower R^2 values, can be due to recording with an iPhone, where the time between each data point withdrawn might deviate from 1s. Overall, the established trend lines show good statistical data with R^2 from 0.830-0.997, and the calculated specific cake resistances from the trend lines seem reliable.

Table 7: An overview of R^2 from trend lines in filtration experiments.

Synthetic system	R^2	**Real process system**	R^2
Single-step 1	0.993	Single-step 1	0.971
Single-step 2	0.992	Single-step 2	0.916
Multi-step 1	0.996	Single-step 3	0.971
Multi-step 2	0.997	Continuous 1	0.895
Continuous 1	0.991	Continuous 2	0.830
Continuous 2	0.988	Continuous 20°C	0.997

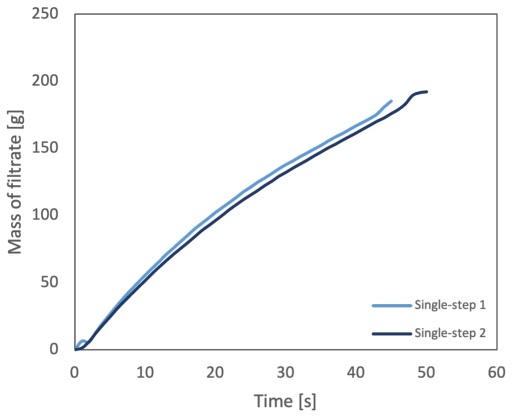

Figure G.6: Filtration curve from single-step experiments in synthetic system.

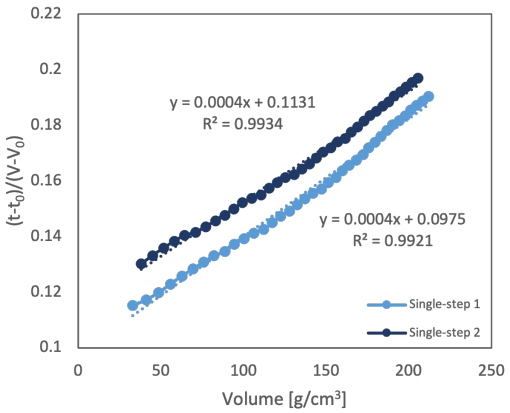

Figure G.7: Trend lines from single-step experiments in synthetic system.

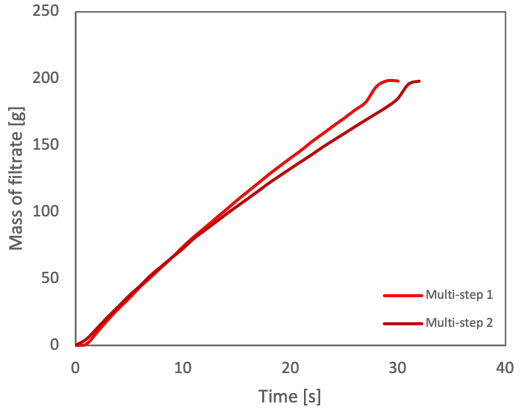

Figure G.8: Filtration curve from multi-step experiments in synthetic system.

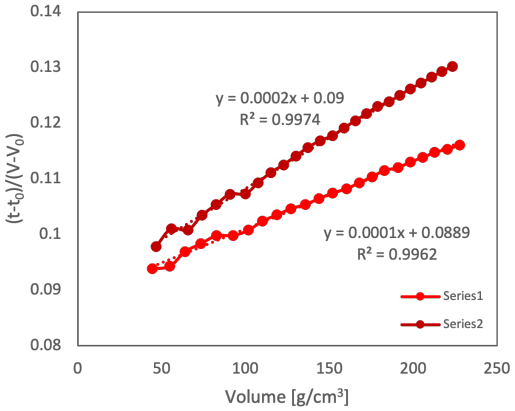

Figure G.9: Trend lines from multi-step experiments in synthetic system.

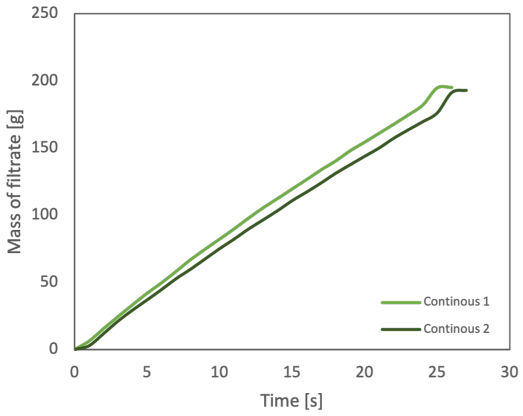

Figure G.10: Filtration curves from single-step experiments in synthetic system

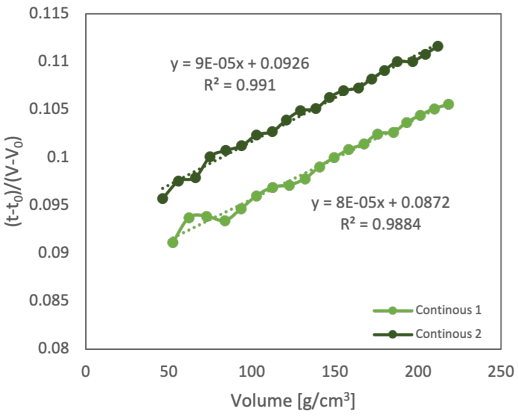

Figure G.11: Trend lines from single-step experiments in synthetic system.

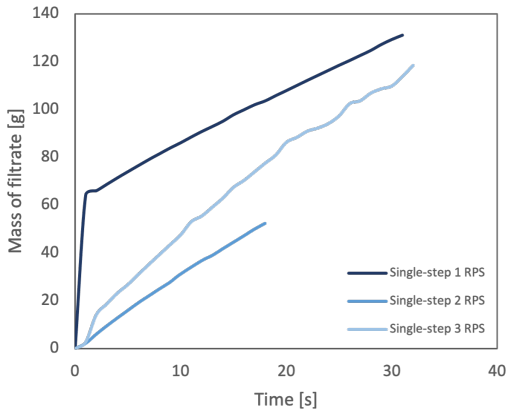

Figure G.12: Filtration curves from single-step experiments in real process system.

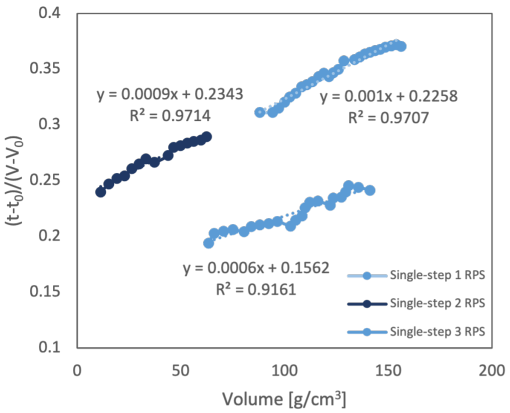

Figure G.13: Trend lines from single-step experiments in real process system.

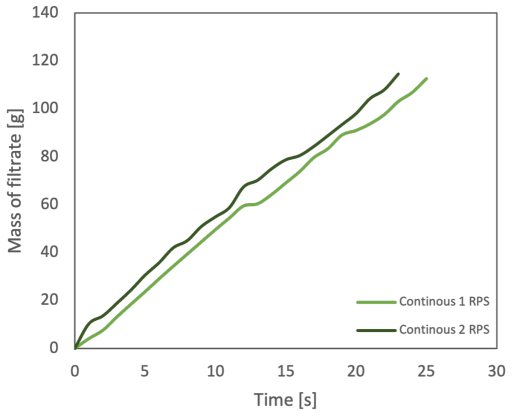

Figure G.14: Filtration curves from continuous addition of the experiments in real process system.

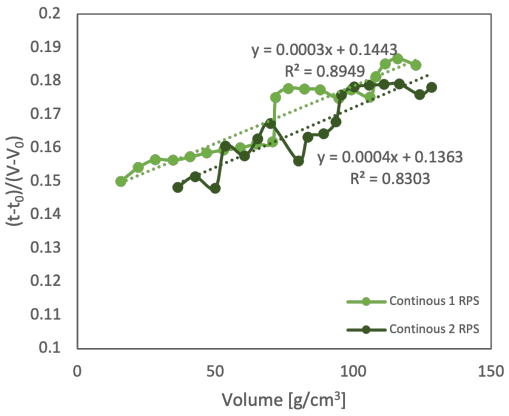

Figure G.15: Trend lines from continuous addition of the experiments in real process system.

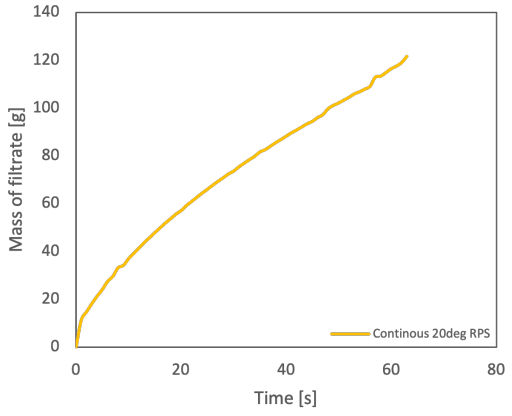

Figure G.16: Filtration curve from continuous addition of the experiment at 20°C in real process system.

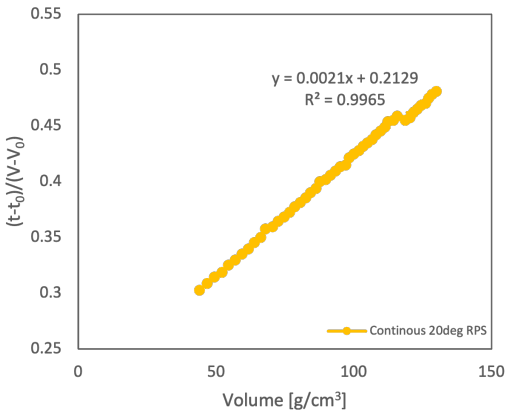

Figure G.17: Trend line from continuous addition of the experiment at 20°C in real process system.

H LUMiSizer

H.1 Analyses from Suspension of AA

In Figure H.18 the sedimentation velocity is analyzed directly from the suspension, prior to filtration and drying. The figure shows significantly lower sedimentation velocities with small variations between the acid addition procedures compared to

what was seen in analysis from filtered, dried, and redispersed crystals. When comparing with the figure of dry crystals it is shown that the single-step addition of the acid shows similar trends, while semi-batch experiments show significantly lower values. Also, the continuous addition of the acid shows the lowest values which is the opposite of what was seen for dry crystals. These differences from dry and solution sedimentation velocities could be explained by clustering occurring during filtration, but it is difficult to conclude something from the method of these analyses as they did not undergo an optimization procedure, like for the dry and redispersed samples. For example, the concentration of these analyses is not comparable. This is an important consideration as the sedimentation is affected by the traffic of particles in the samples giving the settling of collided particles rather than individual clusters or particles.

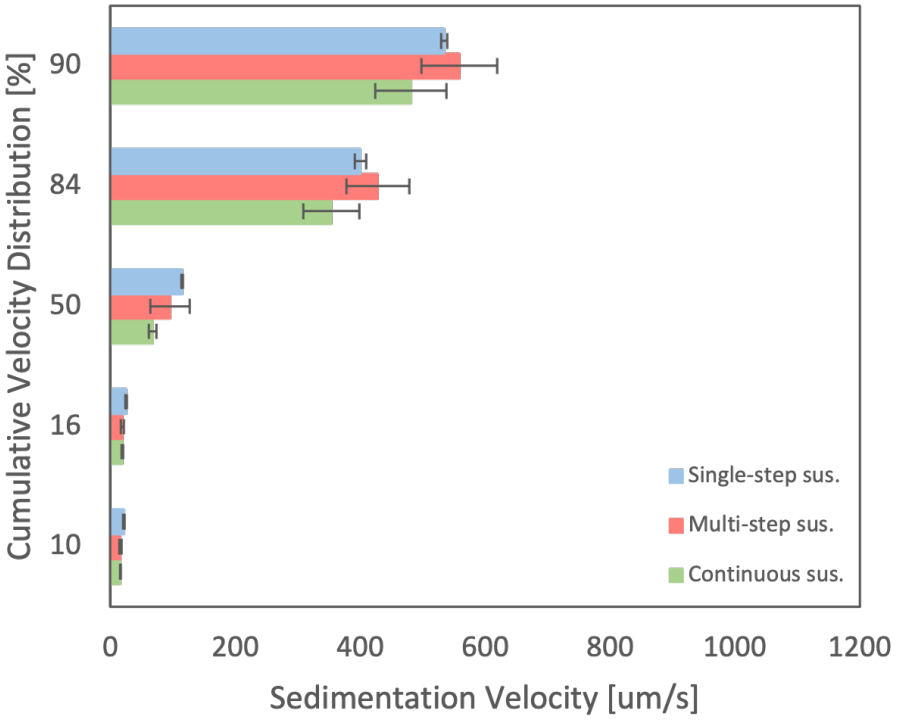

Figure H.18: Cumulative velocity distribution of suspension of SS. The distributions ranges like this; 10% of distribution $\leq 23\mu$m/s etc.

H.2 LUMiSizer Analysis for Each Experiment

In the figures below, the differences in LUMiSizer analysis between experiments of the same acid addition procedure are given. The standard deviations vary from experiment to experiment, but in general show small deviations, giving representable results at the given conditions.

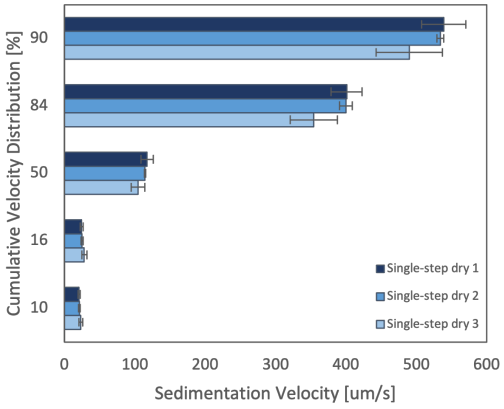

Figure H.19: Analysis of dry crystals re-dispersed in methanol, from single-step experiments in the synthetic system.

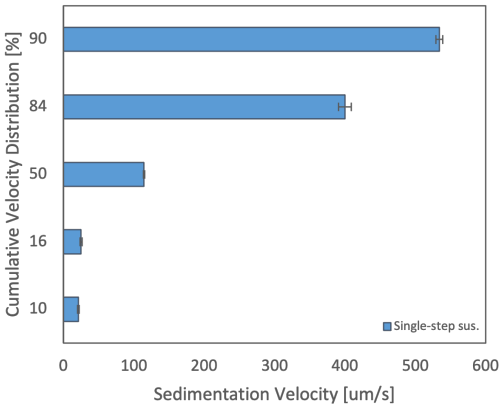

Figure H.20: Analysis of crystals directly from suspension and diluted with methanol, from a single-step experiment in the synthetic system.

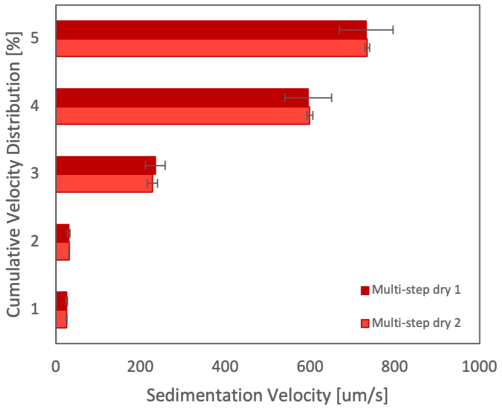

Figure H.21: Analysis of dry crystals re-dispersed in methanol, from multi-step experiments in the synthetic system.

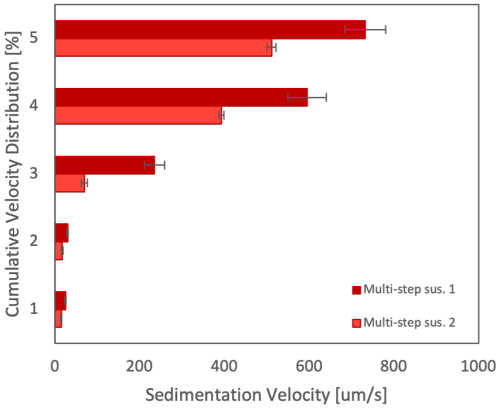

Figure H.22: Analysis of crystals directly from suspension and diluted with methanol, from multi-step experiments in the synthetic system.

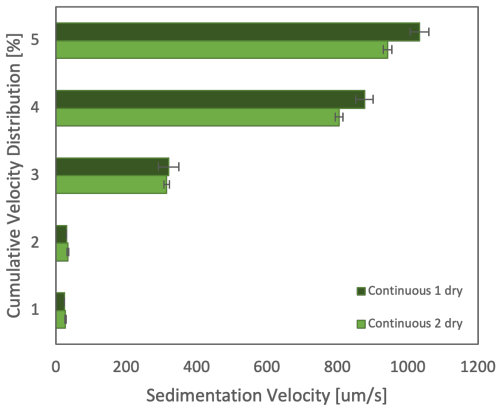

Figure H.23: Analysis of dry crystals re-dispersed in methanol, from continuous addition of the experiments in the synthetic system.

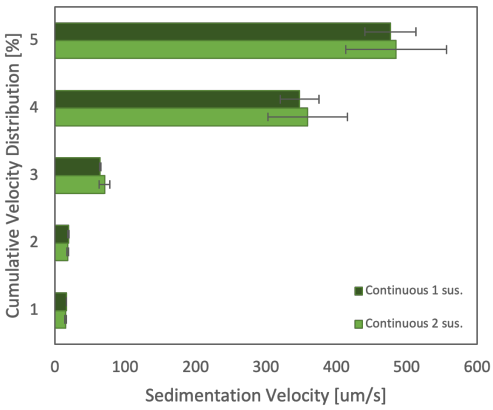

Figure H.24: Analysis of crystals directly from suspension and diluted with methanol, from continuous addition of the experiments in the synthetic system.

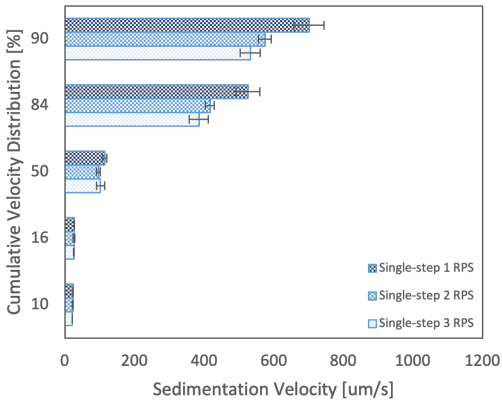

Figure H.25: Analysis of dry crystals re-dispersed in methanol, from single-step addition of the acid experiments in the real process system.

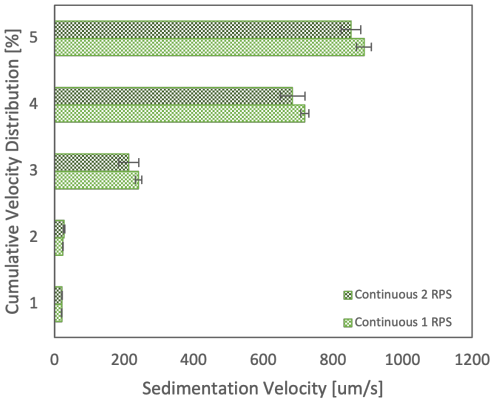

Figure H.26: Analysis of dry crystals re-dispersed in methanol, from continuous addition of the experiments in the real process system.

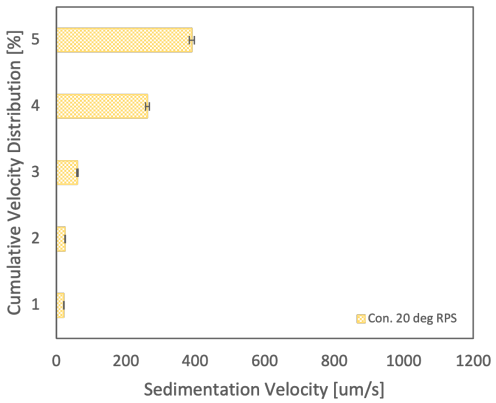

Figure H.27: Analysis of dry crystals re-dispersed in methanol, from continuous addition of the acid experiment at 20°Cin the real process system.

H.3 LUMiSizer - Analysis Summary

An example of one LUMiSizer analysis summary is shown on the next page. The SOP, transmission profile, and cumulative velocity distribution curve are given. In the end, the results of the average distribution are given, which are the data used to calculate size data.

Analysis Summary

Title of Analysis:	new_rps_3.2.1 20 deg
Saved:	20 May 2021 11:50:07
User:	NTNU user
Samples:	RPS_3.2.1 20 deg
Normalization:	Normalization applied, dynamic baseline correction
Smoothing:	Profiles: Moving Average (9 points) Results: Moving Average (3 points)
Distribution Type:	Velocity Distribution
Separation Type:	Sedimentation
Analysis Mode:	Constant Position
Reference Profile:	Sample's Last Profile
Notes:	

Data Range Analysed:

Sample Name	Start Point in mm	Range in mm	Nodes in mm	Profiles	Channel/ Wavelength
RPS_3.2.1 20 deg	108.69	1.000	120.9, 122.4, 124.1	All	4 410 nm

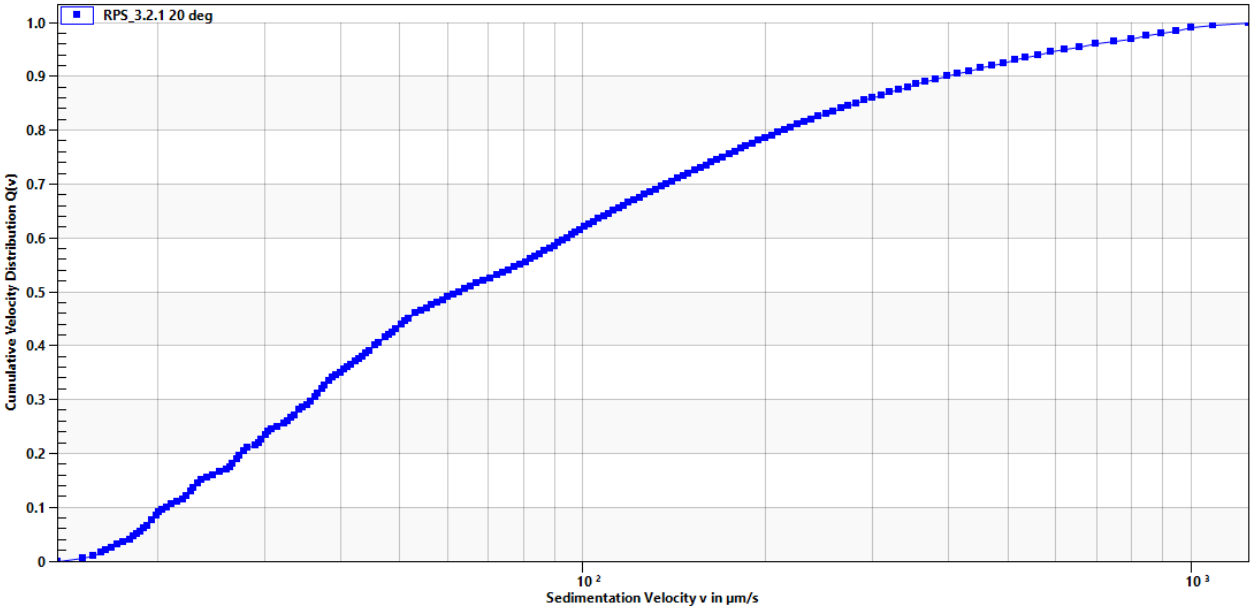

Results:

Sample Name	Median in µm/s	Harmonic Mean in µm/s	Std. Dev. in µm/s	Span (v90-v10)/v50	Mean RCA in g
RPS_3.2.1 20 deg	62.78	48.54	206.5	6.008	1,070

Sample Name	10% ≤ in µm/s	16% ≤ in µm/s	50% ≤ in µm/s	84% ≤ in µm/s	90% ≤ in µm/s
RPS_3.2.1 20 deg	20.75	24.67	62.78	265.9	397.9

Details for Sample: RPS_3.2.1 20 deg

Measurement Title: RPS_con 20210516 15:08:42

Sample Name: RPS_3.2.1 20 deg

Channel: 4

Wavelength: 410 nm

Sample GUID: {974D8437-A7F4-4117-B33F-AD2A010D88F5}

Measurement Date: 16 May 2021 15:08:42

Device: LUMiSizer 6514-122 (12 channels)

Sample Cell: [6] LUM 10mm, PC, Rect. Synthetic Cell (110-132xx)

Meniscus: 108.69 mm

Notes:

SOP

#	Profiles	Interval	Speed	Light Factor	Temperature
1	10	10s	200 RPM	1.00	25.0°C
2	10	10s	200 RPM	1.00	25.0°C
3	10	10s	200 RPM	1.00	25.0°C
4	10	10s	300 RPM	1.00	25.0°C
5	10	10s	450 RPM	1.00	25.0°C
6	10	10s	600 RPM	1.00	25.0°C
7	5	10s	750 RPM	1.00	25.0°C
8	5	10s	1,000 RPM	1.00	25.0°C
9	5	10s	1,300 RPM	1.00	25.0°C
10	5	10s	1,700 RPM	1.00	25.0°C
11	5	10s	2,200 RPM	1.00	25.0°C
12	50	10s	2,700 RPM	1.00	25.0°C
13	50	60s	3,200 RPM	1.00	25.0°C

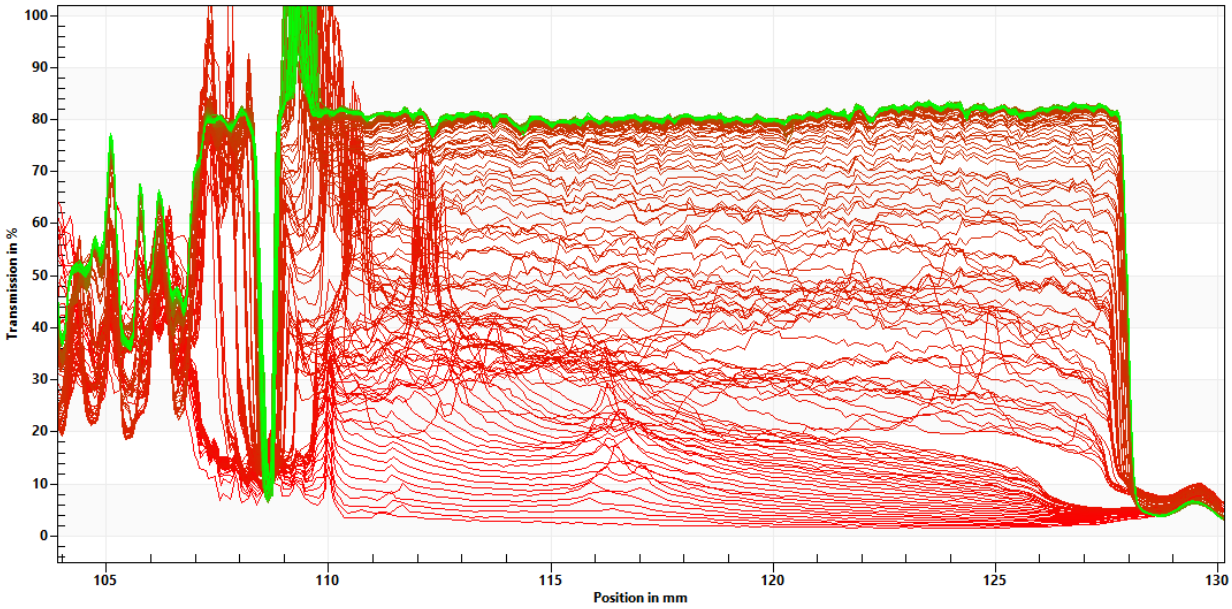

Analysis Settings:

Distribution Type	Velocity Distribution
Separation Type	Sedimentation
Analysis Mode	Constant Position (Profiles: All)
Analyze Positions	Span: 1.00mm, Nodes: 120.87mm, 122.40mm, 124.08mm
Reference Profile	Sample's Last Profile
Start Point	108.69
Device	LUMiSizer 6514-122 (12 channels), Wavelength: 410 nm

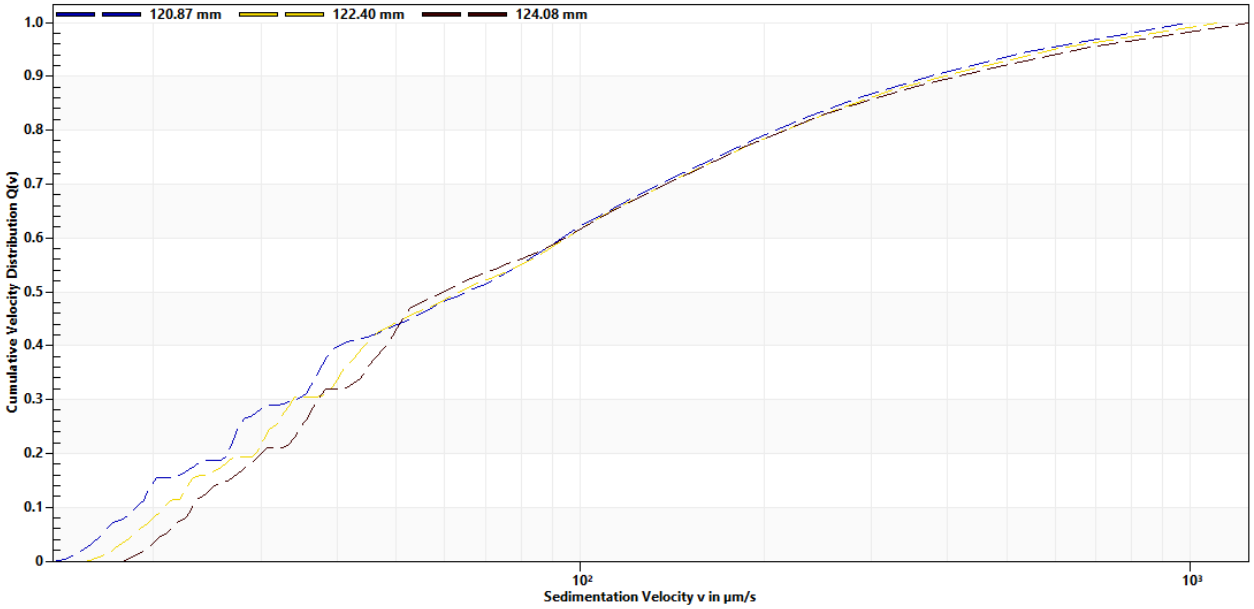

Results: Average Distribution

10% of Distribution ≤ 20.75 μm/s	Median v50: 62.78 μm/s
16% of Distribution ≤ 24.67 μm/s	Harmonic Mean: 48.54 μm/s
50% of Distribution ≤ 62.78 μm/s	Standard Deviation: 206.5 μm/s
84% of Distribution ≤ 265.9 μm/s	Span (v90-v10)/v50: 6.008
90% of Distribution ≤ 397.9 μm/s	Mode: 23.01 μm/s

I Additional SEM Images

In this section are additional SEM images from all acid addition procedures from both synthetic and real process systems.

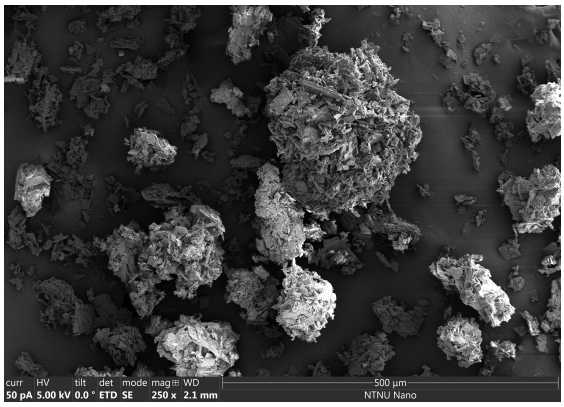

Figure I.28: SEM image of final crystals from single-step addition of the acid, in the synthetic system.

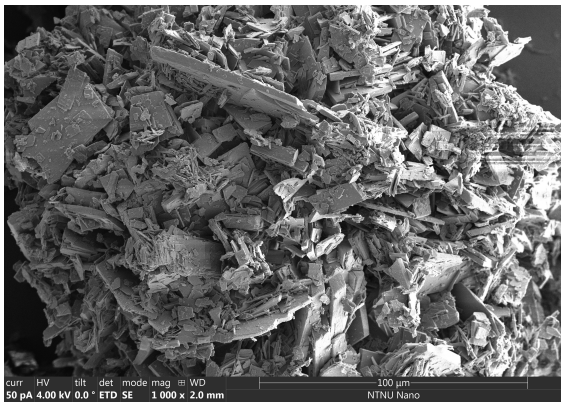

Figure I.29: SEM image of final crystals from single-step addition of the acid, in the synthetic system.

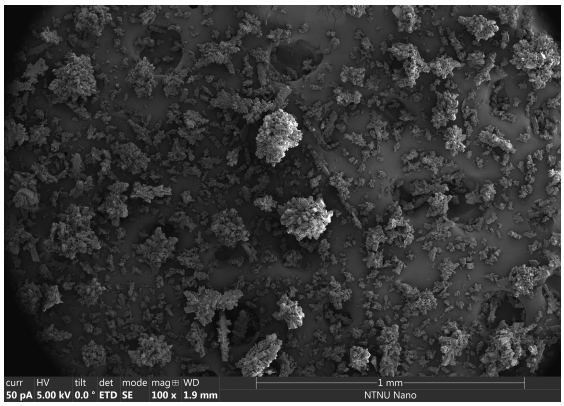

Figure I.30: SEM image of final crystals from multi-step addition of the acid, in the synthetic system.

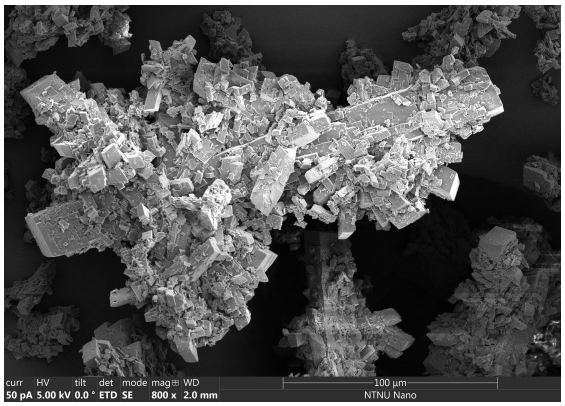

Figure I.31: SEM image of final crystals from multi-step addition of the acid, in the synthetic system.

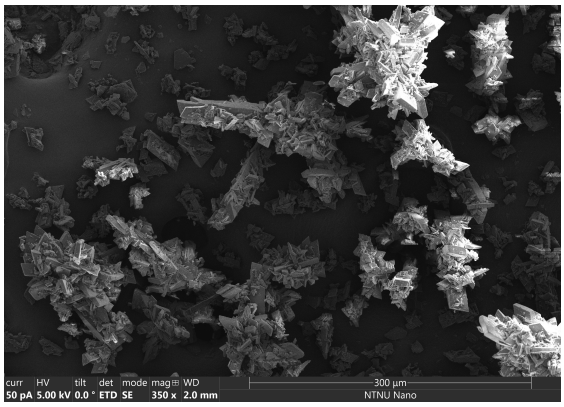

Figure I.32: SEM image of final crystals from continuous addition of the acid, in the synthetic system.

Figure I.33: SEM image of final crystals from continuous addition of the acid, in the synthetic system.

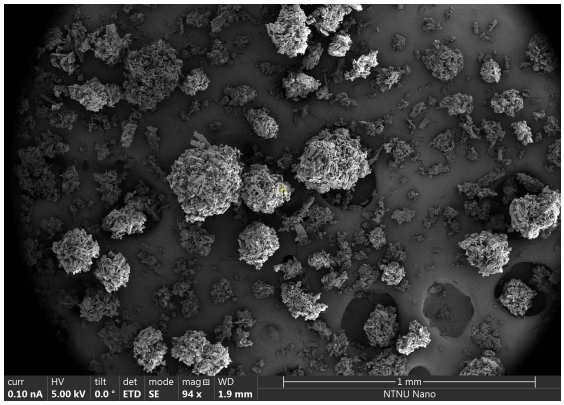

Figure I.34: SEM image of final crystals from single-step addition of the acid, in the real process system.

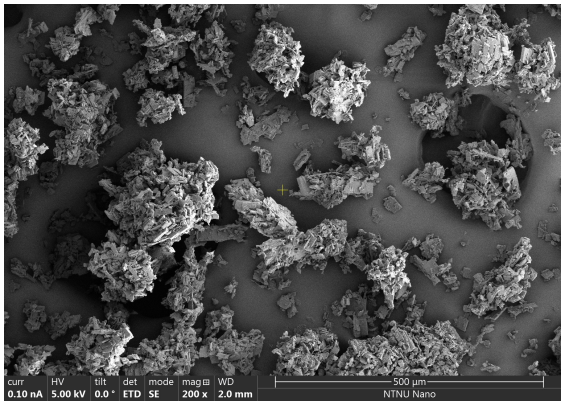

Figure I.35: SEM image of final crystals from single-step addition of the acid, in the real process system.

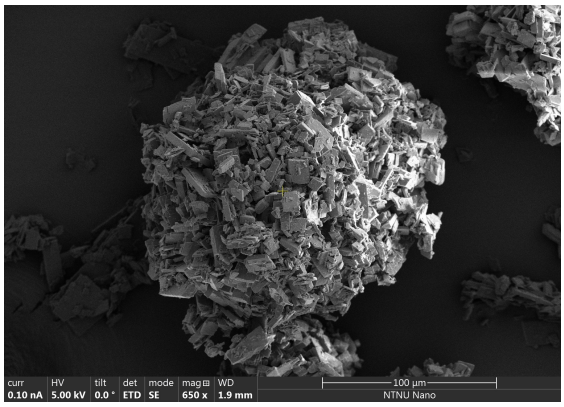

Figure I.36: SEM image of final crystals from single-step addition of the acid, in the real process system.

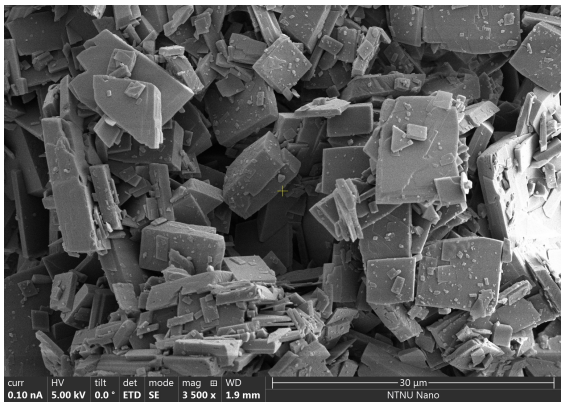

Figure I.37: SEM image of final crystals from single-step addition of the acid, in the real process system.

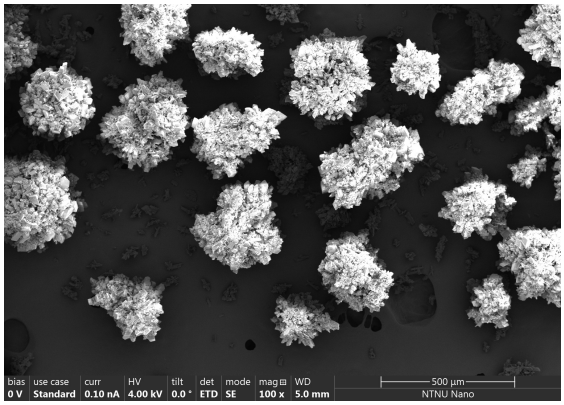

Figure I.38: SEM image from the same sample as cross-section image. Single-step experiment at uncertain conditions in real process system.

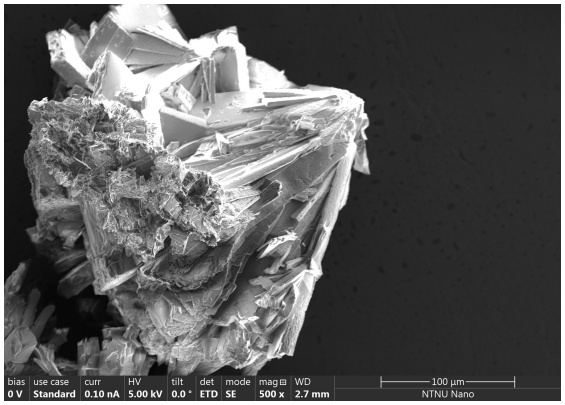

Figure I.39: SEM image from the same the sample as cross-section image. Single-step experiment at uncertain conditions in real process system.

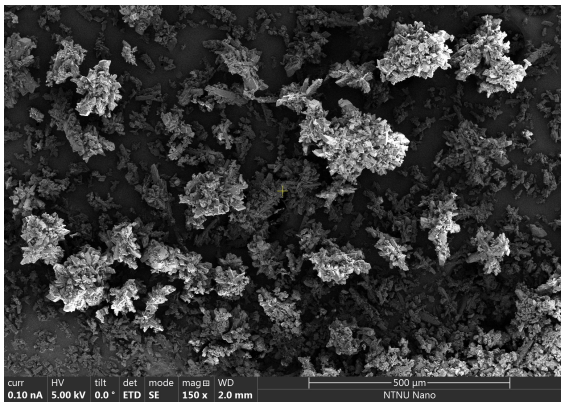

Figure I.40: SEM image of final crystals from continuous addition of the acid, in the real process system.

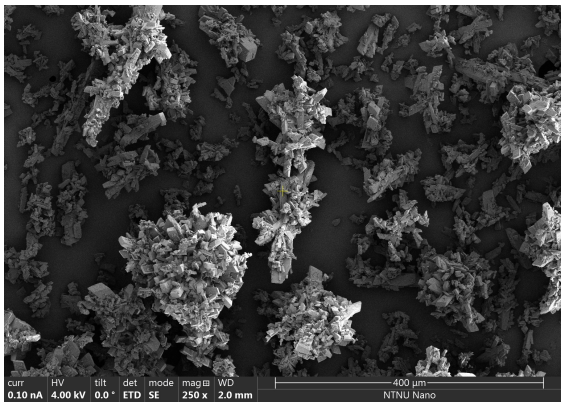

Figure I.41: SEM image of final crystals from continuous addition of the acid, in the real process system.

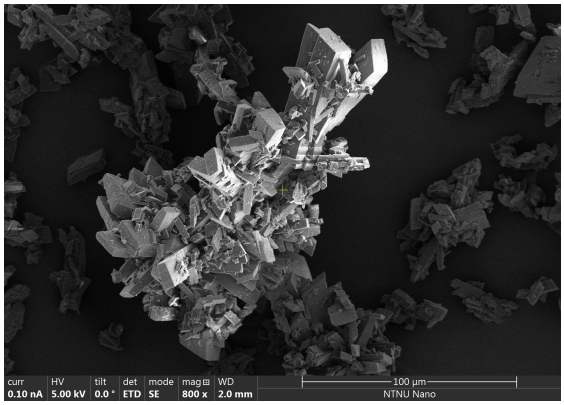

Figure I.42: SEM image of final crystals from continuous addition of the acid, in the real process system.

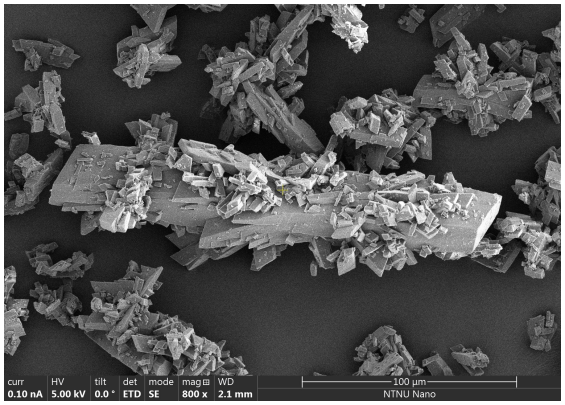

Figure I.43: SEM image of final crystals from continuous addition of the acid, in the real process system.

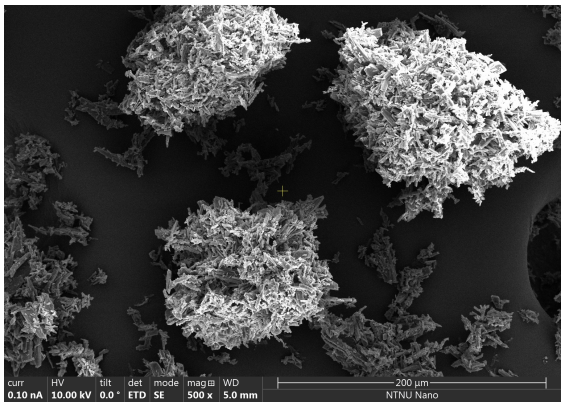

Figure I.44: SEM image of final crystals from continuous addition of the acid at 20°C, in the real process system.

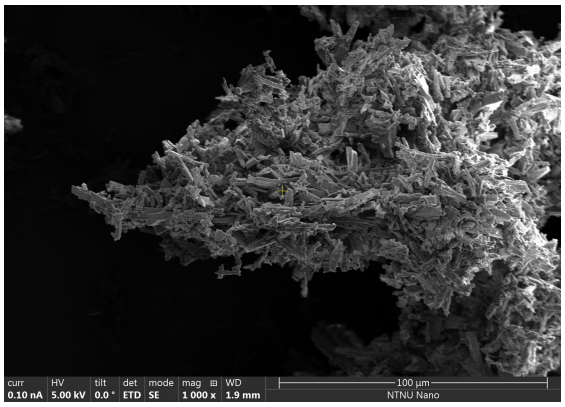

Figure I.45: SEM image of final crystals from continuous addition of the acid at 20°C, in the real process system.

J Additional LM Images

In this section are additional LM images from all acid addition procedures in the synthetic system presented. LM images from experiments conducted from the real process system are not added due to lack of scale-bars.

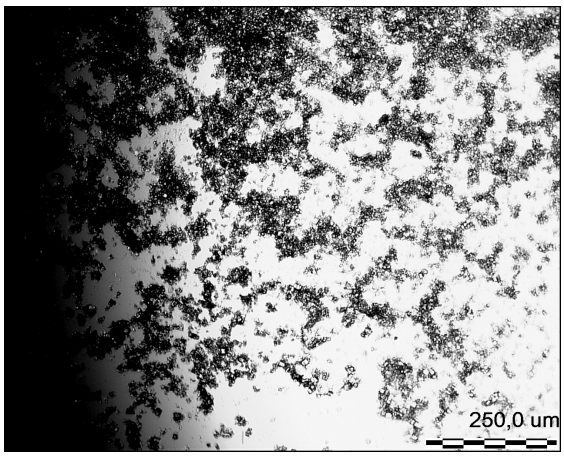

Figure J.46: LM image of crystals from endpoint of crystallization in single-step addition of the acid, in the synthetic system.

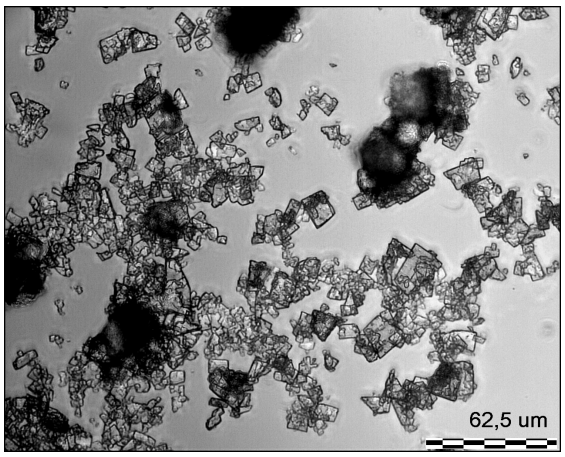

Figure J.47: LM image of crystals from endpoint of crystallization in single-step addition of the acid, in the synthetic system.

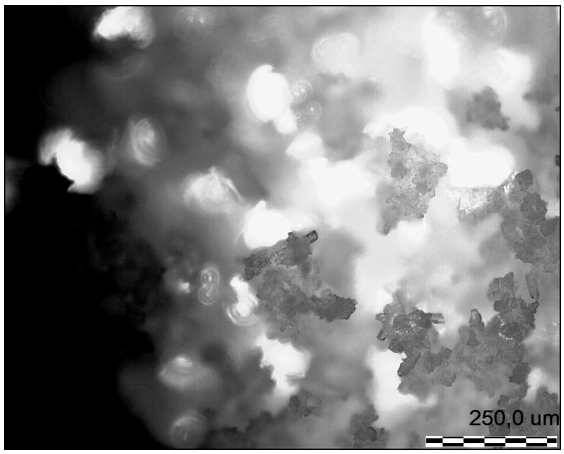

Figure J.48: LM image of crystals from endpoint of crystallization in multi-step addition of the acid, in the synthetic system.

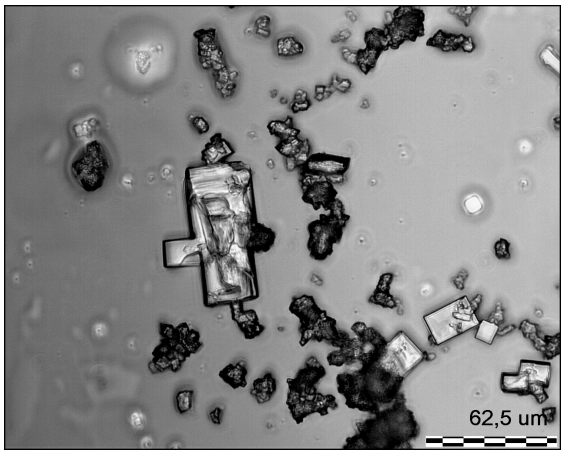

Figure J.49: LM image of crystals from endpoint of crystallization in multi-step addition of the acid, in the synthetic system.

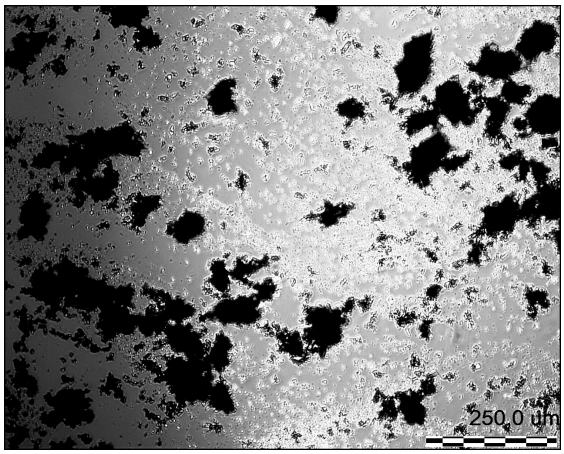

Figure J.50: LM image of crystals from endpoint of crystallization in continuous addition of the acid, in the synthetic system.

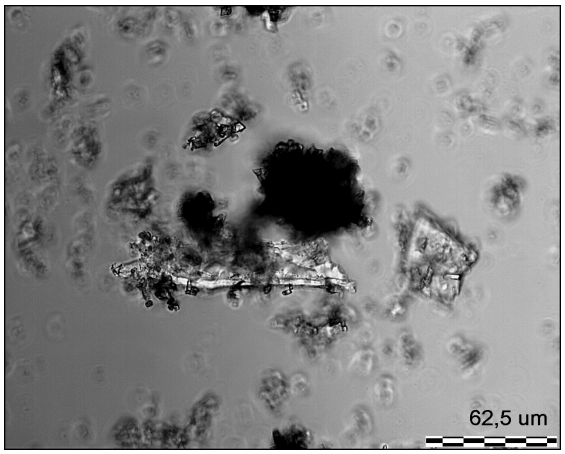

Figure J.51: LM image of crystals from endpoint of crystallization in continuous addition of the acid, in the synthetic system.

K HPLC Analyses of RPS Studies

HPLC analyses of the real process studies were performed by GE Healthcare Lindesnes, in order to determine the purity of initial suspension and final precipitate in experiments. Table 8 shows an overview of the initial and final purity of AA

and purification of the crystallization processes. In Table 9 the average purification from crystallization experiments via different acid addition procedures are given. Single-step experiments show higher average purification. However, it is difficult to conclude what acid addition procedure resulting in the highest purification, because the purification is dependent on the initial concentrations, which deviate from each other.

Table 8: An overview of HPLC analyses of the real process solution studies.

Experiment	AA_i [%]	AA_f [%]	Purification [%]
Single-step 1	96.69	98.07	1.41
Single-step 2	96.91	98.55	1.66
Single-step 3	98.02	99.07	1.06
Continuous 1	97.93	98.89	0.97
Continuous 2	98.43	98.99	0.57
Con. 20°C	98.41	99.21	0.81

Table 9: Purification of crystallization experiments with different acid addition procedures of real process solution studies.

Experiment	$\text{Purification}_{\text{avg.}}$ [%]
Single-step	1.38±0.30
Continuous	0.77±0.29
Con. 20°C	0.81

L In-situ Images with EasyViewer

An EasyViewer 100 was used in one experiment of real process solution with continuous addition of the acid at 20°C. With the EasyViewer in-situ images of the emergence of crystals in the solution was observed. Changes at the beginning of

precipitation were seen, but at some point, the suspension was too crowded to observe changes, and crystals covered the lens. Below are images from different time points of the crystallization. Crystals were observed after 10-13min of acid addition (Figure L.52). After approximately 50min a crowded suspension was observed (Figure L.53). How the crystals covering the lens looked like are shown in Figure L.54, this image was taken at the endpoint of crystallization.

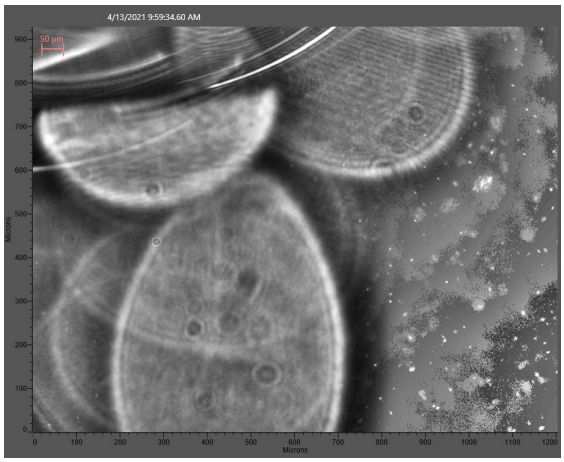

Figure L.52: Crystals were observed after 10-13min of the continuous addition of the acid experiment at 20°C (RPS).

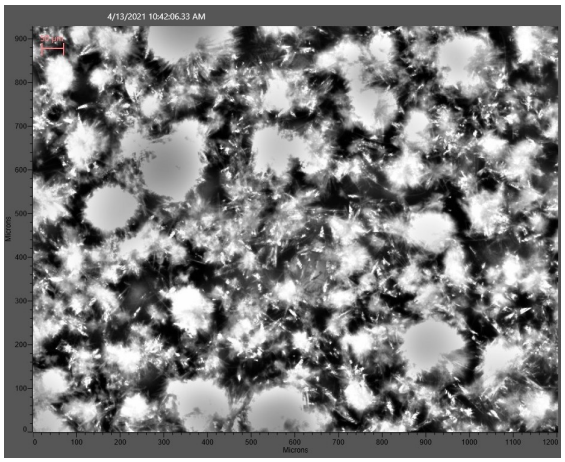

Figure L.53: Image of the suspension after approximately 50min of the continuous addition of the acid experiment at 20°C (RPS).

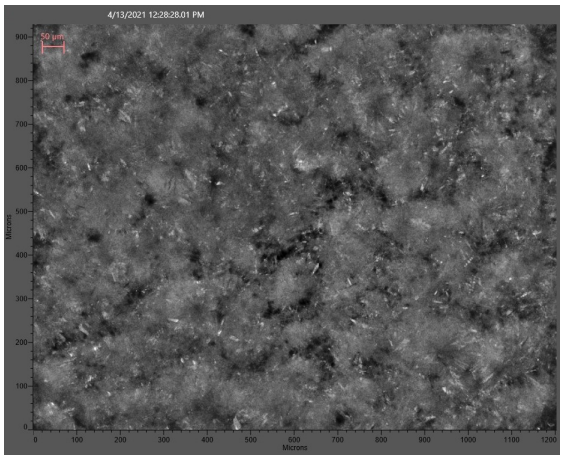

Figure L.54: Crystals covering the lens at endpoint of crystallization in the continuous addition of the acid experiment at 20°C (RPS).

Ida Adneberg

Effects of Supersaturation Build-Up on the Crystal Properties and Filtration Performance of an Aromatic Amine

NTNU
Norwegian University of
Science and Technology